ON THE NUMERICAL SIMULATION OF TURBULENT FLOWS IN COMPLEX GEOMETRIES

BY

WILLIAM KEVIN COPE

B.S., Michigan Technological University, 1989

THESIS

Submitted in partial fulfillment of the requirements
for the degree of Master of Science in Mechanical Engineering
in the Graduate College of the
University of Illinois at Urbana-Champaign, 1991

Urbana, Illinois

19981202 043

REPORT DOCUMENTATION PAGE

AFRL-SR-BL-TR-98-
0729

1. AGENCY USE ONLY (Leave Blank)	2. REPORT DATE July 1991	3. REPORT TYPE AND DATES COVERED Final

4. TITLE AND SUBTITLE
On the Numerical Simulation of Turbulent Flows in Complex Geometries

5. FUNDING NUMBERS

6. AUTHORS
William Kevin Cope

7. PERFORMING ORGANIZATION NAME(S) AND ADDRESS(ES)
University of Illinois at Urbana-Champaign

8. PERFORMING ORGANIZATION REPORT NUMBER

9. SPONSORING/MONITORING AGENCY NAME(S) AND ADDRESS(ES)
AFOSR/NI
4040 Fairfax Dr, Suite 500
Arlington, VA 22203-1613

10. SPONSORING/MONITORING AGENCY REPORT NUMBER

11. SUPPLEMENTARY NOTES

12a. DISTRIBUTION AVAILABILITY STATEMENT
Approved for Public Release

12b. DISTRIBUTION CODE

13. ABSTRACT *(Maximum 200 words)*
See attachment

14. SUBJECT TERMS

15. NUMBER OF PAGES

16. PRICE CODE

17. SECURITY CLASSIFICATION OF REPORT	18. SECURITY CLASSIFICATION OF THIS PAGE	19. SECURITY CLASSIFICATION OF ABSTRACT	20. LIMITATION OF ABSTRACT
Unclassified	Unclassified	Unclassified	UL

ON THE NUMERICAL SIMULATION OF TURBULENT FLOWS IN COMPLEX GEOMETRIES

BY

WILLIAM KEVIN COPE

B.S., Michigan Technological University, 1989

THESIS

Submitted in partial fulfillment of the requirements
for the degree of Master of Science in Mechanical Engineering
in the Graduate College of the
University of Illinois at Urbana-Champaign, 1991

Urbana, Illinois

UNIVERSITY OF ILLINOIS AT URBANA-CHAMPAIGN

THE GRADUATE COLLEGE

JULY, 1991

WE HEREBY RECOMMEND THAT THE THESIS BY

WILLIAM KEVIN COPE

ENTITLED ON THE NUMERICAL SIMULATION OF TURBULENT FLOWS IN

COMPLEX GEOMETRIES

BE ACCEPTED IN PARTIAL FULFILLMENT OF THE REQUIREMENTS FOR

THE DEGREE OF MASTER OF SCIENCE

_____
Director of Thesis Research

_____
Head of Department

Committee on Final Examination†

_____
Chairperson

_____

_____

_____

† Required for doctor's degree but not for master's.

O-517

ABSTRACT

A solution methodology for the numerical simulation of turbulent reacting flows in geometries described by general curvilinear coordinates has been developed. The method is based on the solution of Favre averaged variables. A k-ε turbulence model with wall functions has been used to close the governing equations. Models for turbulent diffusion and premixed flames have been incorporated into the solution method. The numerical solution of the governing equations is accomplished by solving for the Cartesian velocity components on a non-staggered grid. An evaluation of the solution methodology is presented.

" I am the resurrection, and the life: he that believeth in me, though he were dead, yet shall he live: And whosoever liveth and believeth in me shall never die. Believest thou this? "

John 11:25-26 (KJV)

In loving memory of my sister, Karen Joyce Cope (Nov. 22, 1971 - June 13, 1990).

" For what is your life? It is even a vapor, that appeareth for a little time, and then vanisheth away. "   James 4:14 (KJV)

ACKNOWLEDGEMENTS

TABLE OF CONTENTS

NOMENCLATURE

a_{11}	Transformation metric; $a_{11} = y_\eta$.
a_{12}	Transformation metric; $a_{12} = -x_\eta$.
a_{21}	Transformation metric; $a_{21} = -y_\xi$.
a_{22}	Transformation metric; $a_{22} = x_\xi$.
A_p, A_e, A_w	
A_n, A_s	Coefficients in the discrete equation for a given variable.
C	Molar concentration (mol/cm^3).
C_{EBU}	Constant in eddy break up model of turbulent combustion, 3.0.
C_μ	Turbulence constant, 0.09.
C_1	Turbulence constant, 1.44.
C_2	Turbulence constant, 1.92.
C_p	Constant pressure specific heat (J/kgK).
D	Diameter.
E	Constant in log-law relation, 9.025.
E_a	Activation energy (J/kmol).
f	Mixture fraction.
fx	Interpolation factor for ξ coordinate.
fy	Interpolation factor for η coordinate.
g	Concentration fluctuation.
h	Enthalpy (J/kg).
h_o	Stagnation enthalpy (J/kg).
J	Jacobian of the coordinate transformation.
k	Turbulent kinetic energy (m^2/s^2).
k_f	Reaction rate constant.

L_T	Length scale of turbulence.
nx	Number of cells in the ξ direction.
ny	Number of cells in the η direction.
P	Pressure (N/m^2).
P_k	Production of turbulent kinetic energy.
Pr	Prandtl number.
q_{11}, q_{12}	
q_{21}, q_{22}	Metrics of the coordinate transformation.
Q	Heat of reaction (J/kg).
r,z	Cartesian coordinates used to describe axisymmetric geometries.
R	Gas constant for a particular gas. Also, the radius of a pipe.
R_u	Universal gas constant, 8314.3 J/kmol K.
S	Designation given to a source term in the governing equations. Also constant in Sutherland's law expression for molecular viscosity.
Sc	Schmidt number.
t	Time (s).
T	Temperature (K).
u	Cartesian velocity component in the x (z) direction.
U	Contravariant velocity component perpendicular to lines of constant ξ.
v	Cartesian velocity component in the y (r) direction.
V	Contravariant velocity component perpendicular to lines of constant η.
w	Swirl velocity component.
W	Molecular weight (kg/kmol).
x,y	Cartesian coordinates.
Y	Mass fraction.

Greek Symbols

α	Variable used in turbulent diffusion flame model. Fraction of time spent in a particular state.
δ_{ij}	Kronecker delta function.
ε	Turbulent dissipation rate (m^2/s^3).
ϕ	General scalar variable. Also, the stoichiometric air to fuel ratio.
Γ	Diffusive exchange coefficient.
η	General curvilinear coordinate.
K	von Karman constant, 0.4.
μ	Dynamic molecular viscosity (kg/m s).
ν	Kinematic viscosity (m^2/s).
ρ	Density (kg/m^3).
τ	Stress acting on fluid (N/m^2).
ω	Relaxation factor.
$\dot{\omega}$	Reaction rate (kg/m^3 s).
ξ	General curvilinear coordinate.
Ψ	Schvab-Zeldovich variable.

Subscripts

ARR	Arrhenius rate expression.
EBU	Eddy break up expression.
e	Quantity corresponding to the east face of a control volume (identical to use of $i + 1/2$).
eff	Effective value of a quantity for a particular variable.

FU	Fuel variable.
i	Denotes a particular specie. Also the index in ξ direction.
IN	Refers to an inlet quantity.
j	Index in the η direction.
L	Denotes a laminar quantity.
n	Quantity corresponding to the north face of a control volume (identical to use of $j - 1/2$).
nb	Refers to neighbor quantities.
OX	Oxidant variable.
PR	Product variable.
s	Quantity corresponding to the south face of a control volume (identical to use of $j + 1/2$).
T	Denotes turbulence quantity.
TR	Denotes quantity arising from coordinate transformation.
w	Quantity corresponding to the west face of a control volume (identical to use of $i - 1/2$).

Superscripts

'	Denotes Reynolds average fluctuation. Also a correction quantity.
"	Denotes Favre average fluctuation.
+	Denotes a parameter non-dimensionalized with respect to friction velocity. Also denotes a quantity at the upper limit of turbulent fluctuation.
-	Denotes a Reynolds averaged quantity. Also denotes a quantity at the lower limit of turbulent fluctuation.

$\sim$ Denotes a Favre averaged quantity.

*   Denotes an estimated value of the prescribed quantity.

CHAPTER 1: INTRODUCTION

The ultimate goal in understanding combustion processes in practical devices is to relate the parameters in the control of the designer to the performance of the combustion system (Edelman and Harsha, 1978). Identification of the parameters which control the distribution and extent of heat release is important in the design of efficient combustion devices. It is also desirable to know how flow turbulence effects the mixing and combustion of fuel and air. The numerical simulation of turbulent reacting flows using computational fluid dynamics is useful in attaining these goals.

A complete simulation of a turbulent reacting flow requires the solution of the time dependent Navier-Stokes equations along with the governing equations for species and energy. Such a simulation is referred to as a direct numerical simulation (DNS) (Jou and Riley, 1989). A direct numerical simulation is capable of resolving the temporal and spatial dependencies of the turbulent flow field. However, the ability to resolve the significant time and length scales is achieved at the cost of computational effort. As an example, a fully turbulent isothermal channel flow calculation using a DNS required 250 hours of CPU time on a Cray X-MP supercomputer (Moin and Kim, 1982). At the present time, DNS is not a viable option for the solution of practical flow fields (Pope, 1990).

In an attempt to circumvent the problem of large computational times for solution, a large eddy simulation (LES) may be performed (Tafti and Vanka, 1990). The use of LES in simulating turbulent reacting flow has been undertaken by some researchers (Menon and Jou, 1991). This method appears to be quite promising but computational times are still quite large.

The solution of time or mass averaged equations is currently the most widely used means of simulating a turbulent reacting flow (Jou and Riley, 1989). In solving a set of averaged equations, a temporally and spatially resolved solution is replaced by a stochastic

1

description of the flow. The dependent variables of the governing equations are time or mass averaged quantities.

The solution of averaged equations is obtained only after certain closure hypotheses have been invoked. The closure hypotheses or turbulence models relate the mean fluctuations (Reynolds stresses) to the time or mass averaged flow variables. The degree of sophistication of this closure is somewhat dependent on the flowfields which are to be studied. A descriptive review of the various models which are in use for predicting internal flows is given by Nallasamy, 1987. For wall bounded flows, Patel et. al., 1985 give and analysis of various low Reynolds number k-ϵ turbulence models. A review of Reynolds stress models is given by Speziale, 1991. A turbulence model of some kind must be used if a solution of the averaged flow variables is sought.

In simulating turbulent reacting flows, a combustion model must also be used. The objective of the combustion model is to relate the time mean reaction rate to the mean flow variables. In general, different combustion models are used depending on whether a premixed or non-premixed combustion process is to be studied (Lockwood, 1977).

For the simulation of diffusion or non-premixed flames, it has become common to assume infinitely fast kinetics and equal specie diffusivities, whence the thermochemical state of the mixture at any point and time is only dependent on the mixture fraction (Bilger, 1989). The averaged species, temperature, and density are determined either by assuming a probability density function (pdf) (Bilger, 1980) or by solving an equation for the pdf (Pope, 1990). As was the case for turbulence models, different levels of complexity exist among the many models for diffusion flames. Reviews by Spalding, 1976 and by Jones and Whitelaw, 1982 present some of the various aspects relevant to modelling a turbulent diffusion flame.

Simulation of turbulent premixed flames has proven to be more difficult than the simulation of diffusion flames (Pope, 1990). A currently used model for premixed flames

2

is the eddy break up model of Spalding, 1976. Various forms of this model have been proposed and are in use (Magnussen and Hjertager, 1976; Lockwood, 1977). Another method for modelling turbulent premixed flames involves solving for a reaction progress variable. Details of this method are given by Bray, 1980.

Once the governing equations and closure models have been specified, the task becomes one of solving a coupled set of partial differential equations. A closed form analytical solution is not known except for very simple cases, therefore an approximate solution based on numerical methods is sought.

A variety of methods are available for solving the equations which govern a turbulent reacting flow. Since most combustion devices operate at low subsonic speeds, the numerical method used must be capable of solving nearly incompressible flows. Therefore, methods which are based on solving density as a primary dependent variable are not appropriate. The most widely used methods for solving such flows are pressure based algorithms which have their basis in the SIMPLE algorithm of Patankar and Spalding, 1972.

The simulation of turbulent reacting flows in practical combustion devices requires use of a coordinate system which is aligned with the physical geometry of the device. The governing equations are therefore written in terms of general curvilinear coordinates (Thompson, et. al., 1974).

In solving the flow equations in curvilinear coordinates, one can solve for the staggered Cartesian velocity components as was done in the original SIMPLE algorithm. Various researchers have used this method with some success (Shyy, Tong, and Correa, 1985; Correa and Shyy, 1987; Shyy and Braaten, 1988). It has recently been learned however, that the convergence rate of such methods diminishes as the grid lines increasingly deviate from a Cartesian like coordinate system (Vanka, et. al., 1989). Thus, the solution of the flow in such devices as reverse flow annular combustors would not be well convergent.

Other methods applicable for solving the flow in complex geometries have been developed. Maliska and Raithby, 1984 proposed a method whereby both Cartesian velocity components are stored on each face. The convergence problems for reverse flow geometries are eliminated but more variables must be stored and more equations must be solved.

Several researchers have proposed methods which solve grid oriented velocities as the dependent variables of the momentum equations. Karki and Patankar, 1988 proposed a method for solving covariant velocity components (velocities which are parallel to the general curvilinear coordinates). The algorithm involved a decoupled solution procedure in which the continuity equation was replaced with a pressure correction equation. The SIMPLER algorithm (Patankar, 1980) was used to correct pressure and a SIMPLE like correction equation was used to correct the covariant velocities. Joshi and Vanka, 1990 proposed a method based on contravariant velocities as the dependent variables (velocities which are perpendicular to the coordinate lines). The method did not employ a pressure correction equation, but rather retained the continuity equation in its primitive variable form. A coupled solution of the momentum and continuity equations (Vanka, 1986) was used to solve for contravariant velocities and pressure. Demirdzic, et. al., 1990 also proposed a method based on contravariant velocities as dependent variables. The method involved a decoupled solution procedure and employed a pressure correction equation to correct for the contravariant velocities and pressure. One drawback to procedures which are based on solving for grid oriented velocities is that they require the calculation of grid sensitive curvature terms (Peric, et. al., 1988). Also, since the methods employ a staggered grid, more than one set of control volumes must be used in the discretization of the governing equations.

Recent research in solving for the flow in complex geometries has led many researchers to consider non-staggered or collocated grids for velocities and pressure. Rhie and Chow,

4

1983 developed a method appropriate for solving the flow equations on a non-staggered grid. A method which avoided the well known checkerboard split in the pressure field. This method has since been extended to solve for much more complex flows (Rhie and Stowers, 1988; Rhie and Stowers, 1989; Rhie and Syed, 1990). Further work by Majumdar, 1988 and Acharya and Moukalled, 1989 have eliminated some early problems with the original method proposed by Rhie. These problems involved relaxation dependencies and failure to satisfy integral mass conservation. Further research in this area has been conducted by Miller and Schmidt, 1988, Thiart, 1990, and Kobayashi and Pereira, 1991.

In the present work, a computer program appropriate for the numerical simulation of turbulent reacting flow has been developed. The simulation is based on the solution of mass averaged equations on a non-staggered grid. Suitable models for turbulence and combustion have been incorporated into the numerical method proposed by Rodi, Majumdar, and Schonung, 1987.

In the following report, the governing equations for a turbulent reacting flow are first treated. The presentation of the k-ε turbulence model is followed by a description of models for diffusion and premixed flames. The numerical method is next described and is followed by an evaluation in several different flows. Finally, a summary of the work done is given along with conclusions and recommendations for the use of the presently proposed solution algorithm.

CHAPTER 2: GOVERNING EQUATIONS

The fundamental equations which govern the distribution of flow describing variables are based on the conservation laws for mass, momentum, and energy. The present model of turbulent reacting flow seeks to obtain a solution of the time mean steady form of these equations.

2.1 Laminar Flow Equations

The flow of a laminar, Newtonian fluid is governed by the familiar Navier-Stokes equations. In Cartesian x-y coordinates, these equations are given as follows:

$$\frac{\partial}{\partial x}(\rho u) + \frac{\partial}{\partial y}(\rho v) = 0 \tag{2.1}$$

$$\frac{\partial}{\partial x}(\rho uu) + \frac{\partial}{\partial y}(\rho uv) = -\frac{\partial P}{\partial x} + \frac{\partial \tau_{xx}}{\partial x} + \frac{\partial \tau_{yx}}{\partial y} \tag{2.2}$$

$$\frac{\partial}{\partial x}(\rho uv) + \frac{\partial}{\partial y}(\rho vv) = -\frac{\partial P}{\partial y} + \frac{\partial \tau_{xy}}{\partial x} + \frac{\partial \tau_{yy}}{\partial y} \tag{2.3}$$

$$\tau_{xx} = \frac{2}{3}\mu\left[2\frac{\partial u}{\partial x} - \frac{\partial v}{\partial y}\right] \tag{2.4}$$

$$\tau_{yy} = \frac{2}{3}\mu\left[2\frac{\partial v}{\partial y} - \frac{\partial u}{\partial x}\right] \tag{2.5}$$

$$\tau_{xy} = \tau_{yx} = \mu\left[\frac{\partial u}{\partial y} + \frac{\partial v}{\partial x}\right] \tag{2.6}$$

$$\frac{\partial}{\partial x}(\rho u h_0) + \frac{\partial}{\partial y}(\rho v h_0) = \frac{\partial}{\partial x}\left[\frac{\mu}{Pr}\frac{\partial h_0}{\partial x}\right] + \frac{\partial}{\partial y}\left[\frac{\mu}{Pr}\frac{\partial h_0}{\partial y}\right] - \sum_{i=1}^{N}\dot{\omega}_i h_i^o \tag{2.7}$$

6

$$h_o = \int_{T_o}^{T} C_p \, dT + \frac{1}{2} \left| \vec{V} \right|^2 \tag{2.8}$$

$$\frac{\partial}{\partial x}(\rho u Y_i) + \frac{\partial}{\partial y}(\rho v Y_i) = \frac{\partial}{\partial x}\left[\frac{\mu}{Sc}\frac{\partial Y_i}{\partial x}\right] + \frac{\partial}{\partial y}\left[\frac{\mu}{Sc}\frac{\partial Y_i}{\partial y}\right] + \dot{\omega}_i \tag{2.9}$$

The present model is also applicable for axisymmetric flows. The governing equations in r-z coordinates are given in appendix A. A detailed derivation of the above equations may be found in Burmeister, 1983 or in Kuo, 1986.

The present model assumes that Fourier's law of heat conduction is valid and that specie concentrations are sufficiently dilute such that Fick's law of mass diffusion may be used. The transport properties which these laws introduce into the model are taken to be isotropic. There is thus no preferred direction for diffusive processes.

It is assumed that Soret and Dufour effects are not present in the flowfield (Libby and Williams, 1980). Also, viscous heating and radiation effects are assumed to be negligible. The former assumption is valid provided that the flow Mach number is not large.

The solution of the above equations is valid only for laminar flows. Due to the random and highly fluctuating nature of a turbulent flow, a time dependent spatially resolved solution of the flowfield (direct numerical simulation) becomes difficult to obtain since the length and time scales of the turbulence are extremely small. Such a direct numerical simulation would require an exorbitant amount of effort for even geometrically simple flows (Moin and Kim, 1982). A stochastic description of the flow is thus sought. Rather than seek a solution of the time dependent properties describing a turbulent flow, the averaged flow variables are the desired result in a stochastic description of a turbulent flow.

7

2.2 Turbulent Flow Equations

The equations which govern the distribution of flow properties in a turbulent flow are obtained by an averaging process. Both Reynolds averaging and Favre averaging have been used in the description of turbulent flows. The present model of turbulent reacting flow employs Favre averaging.

2.2.1 Favre Averaging

Favre averaging or mass weighted averaging is recommended for variable density flows (Bilger, 1975). Such an averaging process involves decomposing the flow variables into a suitable mean and fluctuating component:

$$\phi = \tilde{\phi} + \phi'' \qquad (2.10)$$

where,

$$\tilde{\phi} = \frac{\int_{t}^{t+\Delta t} \rho \phi \, dt}{\int_{t}^{t+\Delta t} \rho \, dt} \qquad (2.11)$$

and ϕ is any flow variable except pressure, viscosity, or density. In using mass weighted averaging, the pressure and density are decomposed into time mean and fluctuating quantities, e.g.,

$$P = \overline{P} + P' \qquad (2.12)$$

where,

$$\overline{P} = \frac{\int_{t}^{t+\Delta t} P\, dt}{\Delta t} \tag{2.13}$$

The fluctuations in molecular viscosity are neglected. After decomposing each flow variable into its appropriate mean and fluctuating component, the governing equations are time averaged. The equations which govern the distribution of the mean flow variables are thus given as follows (Anderson, et.al., 1984):

$$\frac{\partial}{\partial x}(\bar{\rho}\tilde{u}) + \frac{\partial}{\partial y}(\bar{\rho}\tilde{v}) = 0 \tag{2.14}$$

$$\frac{\partial}{\partial x}(\bar{\rho}\tilde{u}\tilde{u}) + \frac{\partial}{\partial y}(\bar{\rho}\tilde{v}\tilde{u}) = -\frac{\partial\bar{P}}{\partial x} + \frac{\partial}{\partial x}(\bar{\tau}_{xx} - \overline{\rho u''u''}) + \frac{\partial}{\partial y}(\bar{\tau}_{yx} - \overline{\rho u''v''}) \tag{2.15}$$

$$\frac{\partial}{\partial x}(\bar{\rho}\tilde{u}\tilde{v}) + \frac{\partial}{\partial y}(\bar{\rho}\tilde{v}\tilde{v}) = -\frac{\partial\bar{P}}{\partial y} + \frac{\partial}{\partial x}(\bar{\tau}_{xy} - \overline{\rho u''v''}) + \frac{\partial}{\partial y}(\bar{\tau}_{yy} - \overline{\rho v''v''}) \tag{2.16}$$

$$\bar{\tau}_{xx} = \frac{2}{3}\mu\left[2\frac{\partial\tilde{u}}{\partial x} - \frac{\partial\tilde{v}}{\partial y}\right] + \frac{2}{3}\mu\left[2\frac{\partial\overline{u''}}{\partial x} - \frac{\partial\overline{v''}}{\partial y}\right] \tag{2.17}$$

$$\bar{\tau}_{yy} = \frac{2}{3}\mu\left[2\frac{\partial\tilde{v}}{\partial y} - \frac{\partial\tilde{u}}{\partial x}\right] + \frac{2}{3}\mu\left[2\frac{\partial\overline{v''}}{\partial y} - \frac{\partial\overline{u''}}{\partial x}\right] \tag{2.18}$$

$$\bar{\tau}_{xy} = \bar{\tau}_{yx} = \mu\left[\frac{\partial\tilde{u}}{\partial y} + \frac{\partial\tilde{v}}{\partial x}\right] + \mu\left[\frac{\partial\overline{u''}}{\partial y} + \frac{\partial\overline{v''}}{\partial x}\right] \tag{2.19}$$

$$\frac{\partial}{\partial x}(\bar{\rho}\tilde{u}\tilde{h}_o) + \frac{\partial}{\partial y}(\bar{\rho}\tilde{v}\tilde{h}_o) = \frac{\partial}{\partial x}\left[\frac{\mu}{Pr}\frac{\partial}{\partial x}(\tilde{h}_o + \overline{h''_o})\right] \tag{2.20}$$

$$+ \frac{\partial}{\partial y}\left[\frac{\mu}{Pr}\frac{\partial}{\partial y}(\tilde{h}_o + \overline{h''_o})\right] - \frac{\partial}{\partial x}(\overline{\rho u''h''_o}) - \frac{\partial}{\partial y}(\overline{\rho v''h''_o}) - \sum_{i=1}^{N}\overline{\dot\omega}_i h_i^o$$

$$\frac{\partial}{\partial x}(\bar{\rho}\tilde{u}\tilde{Y}_i) + \frac{\partial}{\partial y}(\bar{\rho}\tilde{v}\tilde{Y}_i) = \frac{\partial}{\partial x}\left[\frac{\mu}{Sc}\frac{\partial}{\partial x}(\tilde{Y}_i + \overline{Y''_i})\right] \tag{2.21}$$

9

$$+ \frac{\partial}{\partial y}\left[\frac{\mu}{Sc}\frac{\partial}{\partial y}(\tilde{Y}_i + \overline{Y_i''})\right] - \frac{\partial}{\partial x}(\overline{\rho u''Y_i''}) - \frac{\partial}{\partial y}(\overline{\rho v''Y_i''}) + \overline{\dot{\omega}_i}$$

The use of mass weighted averaging instead of Reynolds averaging for variable density flows results in fewer fluctuation terms (e.g. - $\overline{\rho u'' u''}$) and makes the continuity equation exact (i.e. no terms involving fluctuating quantities). Use of mass weighted averaging does however give rise to some additional terms that would not be present for Reynolds averaging. The mean of the fluctuations such as in equation 2.17 are present because the fluctuation is not one in time only, but is rather a mass weighted fluctuation:

$$\overline{\phi''} = \frac{- \overline{\rho' \phi'}}{\bar{\rho}} \tag{2.22}$$

These terms are small based on an order of magnitude analysis (Anderson, et.al., 1984) and are neglected in the present model.

An important consequence of the use of a statistical description of the flow is that the averaged equations are not closed. There are more unknowns than equations. The averaged equations govern the distribution of the mean flow variables ($\tilde{u}$, $\tilde{v}$, P, $\bar{\rho}$, etc.). No equations are available which govern the distribution of the mean fluctuations (e. g. $\overline{\rho u'' u''}$, $\overline{\rho u'' v''}$, etc.). Such a dilemna is known as the turbulence closure problem.

A description of the mean fluctuations in terms of the mean flow variables is known as a turbulence model. Many turbulence models are available for the closure of the governing equations. All of the turbulence models developed to date lack universal generality. A turbulence model which exhibits generality would be equally applicable for a broad range of flows (e.g., a free shear flow as well as a confined recirculating flow). The available turbulence models differ in their complexity as well as in their generality. The simplest but more restrictive turbulence models are the so called zero equation models (Anderson, et.al.,

10

1984). Prandtl's mixing length model is one of the most successful of the zero equation models. At the other end of the spectrum are the Reynolds stress models which solve partial differential equations for the mean fluctuations (also called Reynolds stresses) (Speziale, 1991).

The turbulence model used in the present study is the standard k-ε turbulence model. The k-ε model is based on the concept of an eddy viscosity. The governing equations are closed by describing the mean fluctuations in terms of the gradients in the mean flow field.

2.2.2. Boussinesq Approximation

The Boussinesq approximation (Anderson, et. al., 1984) is invoked to relate the Reynolds stresses to the gradients of the mean flow field:

$$ - \overline{\rho u_i'' u_j''} = \mu_T \left[\frac{\partial \tilde{u}_i}{\partial x_j} + \frac{\partial \tilde{u}_j}{\partial x_i} \right] - \frac{2}{3} \delta_{ij} \left[\mu_T \frac{\partial \tilde{u}_k}{\partial x_k} + \rho \bar{k} \right] \tag{2.23} $$

Similar expressions are used for the other turbulent fluxes (e.g. $\overline{\rho u'' Y_{FU}''}$, etc.). Use of the Boussinesq approximation is analogous to the manner in which the viscous stresses in a laminar flow were related to the velocity gradients. The quantity μ_T is referred to as the turbulent or eddy viscosity, it is determined in accordance with the standard k-ε turbulence model,

$$ \mu_T = \frac{C_\mu \rho k^2}{\varepsilon} \tag{2.24} $$

11

where k is the turbulent kinetic energy and ε the turbulent dissipation rate. The details of the turbulence model are treated in the next chapter.

With the incorporation of the Boussinesq approximation and the determination of the eddy viscosity through knowledge of k and ε, the equations are thus closed.

$$\frac{\partial}{\partial x}(\bar{\rho}\tilde{u}) + \frac{\partial}{\partial y}(\bar{\rho}\tilde{v}) = 0 \qquad (2.25)$$

$$\frac{\partial}{\partial x}(\bar{\rho}\tilde{u}\tilde{u}) + \frac{\partial}{\partial y}(\bar{\rho}\tilde{v}\tilde{u}) = -\frac{\partial P}{\partial x} + \frac{\partial}{\partial x}\left[\Gamma_{eff}\frac{\partial \tilde{u}}{\partial x}\right] + \frac{\partial}{\partial y}\left[\Gamma_{eff}\frac{\partial \tilde{u}}{\partial y}\right] \qquad (2.26)$$

$$\frac{\partial}{\partial x}(\bar{\rho}\tilde{u}\tilde{v}) + \frac{\partial}{\partial y}(\bar{\rho}\tilde{v}\tilde{v}) = -\frac{\partial P}{\partial y} + \frac{\partial}{\partial x}\left[\Gamma_{eff}\frac{\partial \tilde{v}}{\partial x}\right] + \frac{\partial}{\partial y}\left[\Gamma_{eff}\frac{\partial \tilde{v}}{\partial y}\right] \qquad (2.27)$$

$$\frac{\partial}{\partial x}(\bar{\rho}\tilde{u}\tilde{h}_o) + \frac{\partial}{\partial y}(\bar{\rho}\tilde{v}\tilde{h}_o) = \frac{\partial}{\partial x}\left[\frac{\Gamma_{eff}}{Pr_T}\frac{\partial \tilde{h}_o}{\partial x}\right]$$
$$+ \frac{\partial}{\partial y}\left[\frac{\Gamma_{eff}}{Pr_T}\frac{\partial \tilde{h}_o}{\partial y}\right] - \sum_{i=1}^{N}\overline{\dot{\omega}_i\, h_i^o} \qquad (2.28)$$

$$\frac{\partial}{\partial x}(\bar{\rho}\tilde{u}\tilde{Y}_i) + \frac{\partial}{\partial y}(\bar{\rho}\tilde{v}\tilde{Y}_i) = \frac{\partial}{\partial x}\left[\frac{\Gamma_{eff}}{Sc_T}\frac{\partial \tilde{Y}_i}{\partial x}\right] + \frac{\partial}{\partial y}\left[\frac{\Gamma_{eff}}{Sc_T}\frac{\partial \tilde{Y}_i}{\partial y}\right] + \overline{\dot{\omega}_i} \qquad (2.29)$$

The turblent flow equations for axisymmetric geometries are given in appendix B. The above equations are used in the present study to model turbulent reacting flows. It has been assumed that the cross derivative terms in the momentum equations (e.g. $\frac{\partial}{\partial x}\left[\Gamma_{eff}\frac{\partial \tilde{u}}{\partial y}\right]$, etc.) are negligible. Such terms are not present for uniform viscosity, incompressible flow and are here assumed to be small. Also, the turbulent Prandtl and Schmidt numbers are assumed constant. Recent work by Sturgess et. al., 1984 has revealed that better results may be obtained by allowing these quantities to vary. However, the functional relations for these quantities are not certain and are seemingly problem dependent.

12

2.3. General Conservation Principle

All of the governing equations presented follow a general conservation principle. Three physical processes are responsible for distributing the flow variables throughout the domain of interest: convection, diffusion, and generation/depletion through a source or sink. The general conservation equation which accounts for these processes is as follows:

$$\frac{\partial}{\partial x}(\rho \tilde{u} \tilde{\phi}) + \frac{\partial}{\partial y}(\rho \tilde{v} \tilde{\phi}) = \frac{\partial}{\partial x}\left[\Gamma_{eff}\frac{\partial \tilde{\phi}}{\partial x}\right] + \frac{\partial}{\partial y}\left[\Gamma_{eff}\frac{\partial \tilde{\phi}}{\partial y}\right] + S^{\phi}(x,y) \qquad (2.\ 30)$$

$$\Gamma_{eff} = \frac{\mu}{Pr_L^{\phi}} + \frac{\mu_T}{Pr_T^{\phi}} \qquad (2.\ 31)$$

where Pr_L^{ϕ} and Pr_T^{ϕ} are laminar and turbulent Prandtl numbers of the variable ϕ. The governing equations for the various flow variables are thus seen to differ only in the values of diffusive exchange coefficient (Γ_{eff}) and source term (S^{ϕ}).

2.4. Coordinate Transformation

The equations which govern the distribution of the flow variables are transformed to a general curvilinear coordinate system so as to facilitate study of flows in complex geometries. The coordinate transformation involves changing the independent variables of the governing equations. Rather than describing the flow geometry in x-y coordinates, it is described in general coordinates (ξ,η). Figure 1 is an example of how the general coordinate system (ξ,η) would appear in the Cartesian coordinate system (x,y).

The geometries of practical combustion systems are such that they are not readily described by a Cartesian coordinate system. To avoid use of a " stair-stepping " procedure

13

(Rhode, et. al., 1982), a coordinate transformation is invoked such that the coordinates of the computational grid are coincident with the physical boundaries of the given geometry. Use of a coordinate transformation greatly enhances the accuracy of the boundary condition specification in comparison with the alternative, i.e. stair-stepping. The latter procedure requires the boundary conditions to be interpolated to appropriate grid points. If the gradients of the dependent variables are large in the vicinity of a boundary which is defined via the stair-stepping procedure, the boundary conditions are particularly inaccurate (Thompson, et. al., 1974).

The transformation of coordinates is implemented by considering that the Cartesian coordinates (x,y) are functions of the general curvilinear coordinates (ξ,η), whence,

$$x = f_1(\xi,\eta)$$

$$y = f_2(\xi,\eta)$$

The transformation must be one to one. A given point (x,y) can correspond to only one point in the transformed plane (ξ,η) (Fletcher, 1988b). All derivatives in x,y are subsequently expanded as functions of ξ,η through use of the chain rule of calculus:

$$\frac{\partial \phi}{\partial x} = \left[\frac{\partial \phi}{\partial \xi} y_\eta - \frac{\partial \phi}{\partial \eta} y_\xi\right]\frac{1}{J} \qquad (2.\ 32)$$

$$\frac{\partial \phi}{\partial y} = \left[-\frac{\partial \phi}{\partial \xi} x_\eta + \frac{\partial \phi}{\partial \eta} x_\xi\right]\frac{1}{J} \qquad (2.\ 33)$$

where $J = x_\xi y_\eta - x_\eta y_\xi$.

The transformation enforced in the present method is such that the size of a cell in the transformed plane is unity ($\Delta\xi = \Delta\eta = 1$). In general, an analytical expression is not available for determining the transformation and so it is determined numerically

(Thompson, et. al., 1974). The present method is appropriate for use with algebraic and differential equation methods of defining the transformation (grid generation).

Upon expanding all the derivatives as functions of ξ and η and by rearranging, the general conservation equation may be written as follows:

$$\frac{\partial}{\partial \xi}(\rho U\phi) + \frac{\partial}{\partial \eta}(\rho V\phi) = \frac{\partial}{\partial \xi}\left[\Gamma\, q_{11}\, \frac{\partial \phi}{\partial \xi}\right] + \frac{\partial}{\partial \eta}\left[\Gamma\, q_{22}\, \frac{\partial \phi}{\partial \eta}\right]$$

$$+ \frac{\partial}{\partial \xi}\left[\Gamma\, q_{12}\, \frac{\partial \phi}{\partial \eta}\right] + \frac{\partial}{\partial \eta}\left[\Gamma\, q_{21}\, \frac{\partial \phi}{\partial \xi}\right]$$

$$+ |J|\, S^\phi (\xi,\eta) \tag{2.34}$$

$$U = u y_\eta - v x_\eta \tag{2.35}$$

$$V = v x_\xi - u y_\xi \tag{2.36}$$

$$q_{11} = \frac{1}{|J|}\left(y_\eta{}^2 + x_\eta{}^2\right) \tag{2.37}$$

$$q_{22} = \frac{1}{|J|}\left(y_\xi{}^2 + x_\xi{}^2\right) \tag{2.38}$$

$$q_{21} = q_{12} = -\frac{1}{|J|}\left(y_\xi y_\eta + x_\xi x_\eta\right) \tag{2.39}$$

$$|J| = \left(x_\xi y_\eta - x_\eta y_\xi\right) \tag{2.40}$$

The quantities U and V are contravariant velocities. The contravariant velocity U is perpendicular to coordinate lines of constant ξ and is actually a volume flow rate. The contravariant velocity V is perpendicular to coordinate lines of constant η and is also a volumetric flow rate. For an incompressible flow, these quantities are conserved. The transformation metrics corresponding to a transformation from r,z to ξ,η coordinates are different than those given above. These transformation metrics are given in appendix C.

The governing equations in the transformed space may be written in several different forms. The governing equations have been written in conservation law form in the present

15

implementation since this form leads naturally to conservative discretizations (Anderson, et. al., 1984).

2.5. Boundary Conditions

The prescription of a well posed mathematical problem requires specification of appropriate boundary conditions. Since the governing equations are written as functions of the independent variables ξ and η, the boundary conditions are imposed in the transformed plane. In the present method, four types of boundary conditions have been utilized: wall, symmetry, inlet, and outlet.

2.5.1. Wall Boundary Condition

All solid boundaries are treated as no slip, no penetration boundaries. The contravariant velocities (U and V) as well as the Cartesian velocities are equal to zero at the walls.

The walls are also treated as being adiabatic. The derivative of the stagnation enthalpy in the direction perpendicular to the wall is equal to zero. For example, if a wall lies along a coordinate of constant η, then the following is specified,

$$\frac{\partial h}{\partial \eta} = 0 \qquad (2.\,41)$$

Such a boundary condition is only true if the grid is orthogonal at the boundary. If not, some error is introduced at the boundary. The error will be proportional to the extent of non-orthogonality at the wall. Thompson gives a boundary condition implementation which is appropriate for boundary non-orthogonal grids (Thompson, et. al., 1974).

16

A similar treatment is used for the fuel fraction at a wall, thus treating all solid boundaries as non-catalytic. The boundary conditions for the turbulence quantities k and ε are imposed by wall functions. Details of the wall function implementation are given in the next chapter.

2.5.2. Symmetry Boundary Condition

A zero first derivative is specified perpendicular to any boundary designated as a symmetry boundary. The zero derivative is specified for the Cartesian velocity components as well as the scalar quantities. The contravariant velocities perpendicular to any symmetry boundary are specified as zero. The contravariant velocities parallel to a symmetry are treated in the same manner as scalar quantities.

2.5.3. Inflow Boundary Condition

The present model of turbulent reacting flow treats the inlet as a Dirichlet boundary condition. Values of velocities and scalars are specified at the inlet. A uniform distribution of the flow variables is taken as the default specification. Parabolic and other non-uniform distributions of flow variables can also be used. Currently, the model does not account for pressure boundary conditions, thus phenomena such as choking cannot be treated. The inlet specification is best suited for incompressible and subsonic compressible flows.

2.5.4. Outflow Boundary Condition

A fully developed flow condition is specified for all variables at any boundary that is designated as an outflow. If an outflow lies along a coordinate line of constant ξ, then the following would be specified at the outflow plane:

$$\frac{\partial \phi}{\partial \xi} = 0 \qquad (2.42)$$

The contravariant velocities parallel to the outflow plane are additionally specified as being equal to zero. The outflow boundary condition has no affect on the solution domain if the outflow plane is properly specified. With the given discretization scheme (see Ch. 4), all information at the outlet plane is cut off from the rest of the domain when the cell Peclet number is greater than two (Patankar, 1980). Thus, the outflow plane is properly specified if the flow in that region is expected to be locally "one-way" (i.e. no recirculation) and if the convective effects are dominant ($Pe_{cell} > 2$).

2.6. Thermodynamic and Transport Properties

The prescription of thermodynamic and transport properties is required to close the system of equations governing the flow. The specific heat, molecular weight, molecular viscosity, specific heat ratio, and density all need to be related to the primary dependent variables (u, v, P, h_o, Y_{FU}, etc.)

The fluid density is determined via the equation of state. It is assumed that the fluid obeys the ideal gas law, hence:

$$\rho = \frac{PW}{R_u T} \qquad (2.43)$$

where W is the mixture molecular weight and R_u is the universal gas constant.

The molecular weight is a function of the specie mass fractions. If Dalton's model of partial pressures is taken to describe the reacting mixture, then the mixture molecular weight is given as follows:

$$\frac{1}{W_{mix}} = \sum_{i=1}^{N} \left[\frac{Y_i}{W_i} \right] \qquad (2.44)$$

The constant pressure specific heat is determined by the specie mass fractions and by the temperature. Following the treatment used in the NASA thermochemistry code (Gordon and McBride, 1976), the specific heat for a particular specie is given by the following:

$$C_{pi} = \frac{R_u}{W_i} (a_1 + a_2 T + a_3 T^2) \qquad (2.45)$$

The mixture specific heat is defined as a mass weighted average of the specie mass fractions:

$$C_{pmix} = \sum_{i=1}^{N} Y_i C_{pi} \qquad (2.46)$$

The specific heat ratio is taken to be a constant in the present model. The specific heat ratio for air ($\gamma=1.4$) is assumed to be an accurate representation of the actual value of the gas mixture.

19

In the present model for turbulent reacting flow, the molecular viscosity is assumed to be a function of only temperature. The molecular viscosity is determined from the Sutherland's law expression for air (White, 1974):

$$\frac{\mu}{\mu_o} = \left[\frac{T}{T_o}\right]^{3/2} \frac{T_o + S}{T + S} \tag{2.47}$$

A more rigorous treatment of the molecular viscosity would treat the various species present in the flow. Such a detailed treatment of the molecular viscosity is not considered necessary since the turbulent "eddy" viscosity is much larger (Bilger, 1980). The exchange coefficient appearing in the governing equations is thus primarily determined by the turbulent viscosity. For the calculation of laminar reacting flows, a more detailed treatment of the molecular viscosity would be beneficial.

CHAPTER 3: TURBULENCE AND COMBUSTION MODELS

" Mathematical models are tools used in engineering and science to predict functional relationships between certain input and output functionals." (Magnussen and Hjertager, 1976). In simulating turbulent reacting flows, mathematical models are employed in order to close the system of equations which governs the mean flowfield. The desired " output " of these models are Reynolds stresses ($-\overline{\rho u''v''}$, etc.), turbulent fluxes of scalar quantities (e.g. $\overline{\rho u''Y''_{FU}}$), and mean chemical reaction rates ($\dot{\omega}$). The input variables of the models are properties of the mean flowfield (i.e. $\tilde{u}$, $\tilde{v}$, $\tilde{Y}_{FU}$, etc.). The mean properties are governed by the fundamental conservation laws. The turbulence and combustion models thus relate the turbulent fluctuation quantities to the primary dependent variables.

The present simulation of turbulent reacting flows uses the standard k-ε turbulence model with wall functions to facilitate closure of the governing equations (Launder and Spalding, 1974). Two simple models of combustion are given in the present simulation: a turbulent premixed flame model and a diffusion flame model. The turbulent premixed flame simulation is based on an EBU model proposed by Magnussen and Hjertager, 1976. The diffusion flame model is based on the assumption of infinitely fast kinetics and is of the assumed pdf variety.

3.1. Turbulence Model

The objective of the turbulence model is to relate the turbulent fluxes (e.g. $-\overline{\rho u''v''}$, etc.) to the mean flow variables ($\tilde{u}$, $\tilde{v}$, $\tilde{Y}_{FU}$, etc.). As was stated in the previous chapter, there are in existence numerous procedures for obtaining turbulence closure. The various methods range from the simple mixing length models to the more complex Reynolds stress

models. The available turbulence models all differ in their complexity and generality. For the present effort, it was desired to use a computationally efficient turbulence model. A model which exhibited reasonable generality without requiring an exhaustive computational effort. The standard two equation k-ε turbulence model with wall functions is used in the present simulation.

The standard k-ε model is based on the concept of a turbulent or "eddy" viscosity. The Reynolds stresses are written in terms of the mean flow gradients by invoking the Boussinesq assumption:

$$- \overline{\rho u_i'' u_j''} = \mu_T \left[\frac{\partial \tilde{u}_i}{\partial x_j} + \frac{\partial \tilde{u}_j}{\partial x_i} \right] - \frac{2}{3} \delta_{ij} \left[\mu_T \frac{\partial \tilde{u}_k}{\partial x_k} + \rho \bar{k} \right] \qquad (3.1)$$

A similar relation is used for expression of other turbulent fluxes. The use of the Boussinesq approximation shifts the burden of closure from one of describing $- \overline{\rho u'' v''}$, to one of determining the eddy viscosity μ_T. The modelling of the eddy viscosity is achieved by analogy with the kinetic theory of gases.

The expression for the viscosity of a gas as obtained from kinetic theory is as follows (Burmeister, 1983):

$$\mu = \frac{\bar{v} \lambda m n}{3} \qquad (3.2)$$

where,

$$\bar{v} = \text{average particle velocity}$$

$$\lambda = \text{mean free path of particles}$$

$$m = \text{particle mass}$$

$$n = \text{number of particles per unit volume}$$

In an analogous manner, the eddy viscosity is taken to be directly proportional to turbulent length and velocity scales,

$$\mu_T \sim \rho V_T L_T \tag{3.3}$$

The k-ε model uses the square root of turbulent kinetic energy ($k^{1/2}$) as the characteristic velocity. The turbulent length scale, L_T is determined as a function of the turbulent dissipation rate, ε (Launder and Spalding, 1974):

$$L_T = \frac{C_D k^{3/2}}{\varepsilon} \tag{3.4}$$

The resulting expression for the eddy viscosity is therefore:

$$\mu_T = \frac{\rho C_\mu k^2}{\varepsilon} \tag{3.5}$$

The k-ε turbulence model determines both the turbulent velocity and length scales from transport equations:

$$
\frac{\partial}{\partial \xi}(\rho U k) + \frac{\partial}{\partial \eta}(\rho V k) = \frac{\partial}{\partial \xi}\left[\Gamma_k q_{11} \frac{\partial k}{\partial \xi}\right] + \frac{\partial}{\partial \eta}\left[\Gamma_k q_{22} \frac{\partial k}{\partial \eta}\right]
$$
$$
+ \frac{\partial}{\partial \xi}\left[\Gamma_k q_{12} \frac{\partial k}{\partial \eta}\right] + \frac{\partial}{\partial \eta}\left[\Gamma_k q_{21} \frac{\partial k}{\partial \xi}\right] \tag{3.6}
$$
$$
+ |J| P_k - \rho \varepsilon |J|
$$

$$
\frac{\partial}{\partial \xi}(\rho U \varepsilon) + \frac{\partial}{\partial \eta}(\rho V \varepsilon) = \frac{\partial}{\partial \xi}\left[\Gamma_\varepsilon q_{11} \frac{\partial \varepsilon}{\partial \xi}\right] + \frac{\partial}{\partial \eta}\left[\Gamma_\varepsilon q_{22} \frac{\partial \varepsilon}{\partial \eta}\right]
$$

23

$$+ \frac{\partial}{\partial \xi} \left[\Gamma_\varepsilon \, q_{12} \frac{\partial \varepsilon}{\partial \eta} \right] + \frac{\partial}{\partial \eta} \left[\Gamma_\varepsilon \, q_{21} \frac{\partial \varepsilon}{\partial \xi} \right] \qquad (3.7)$$

$$+ |J| \frac{C_1 P_k \varepsilon}{k} - |J| \frac{C_2 \rho \varepsilon^2}{k}$$

$$P_k = \mu_T \left\{ 2 \left[\frac{\partial \tilde{u}}{\partial x} \right]^2 + 2 \left[\frac{\partial \tilde{v}}{\partial y} \right]^2 + \left[\frac{\partial \tilde{u}}{\partial y} + \frac{\partial \tilde{v}}{\partial x} \right]^2 \right\} \qquad (3.8)$$

It is evident from the expression for eddy viscosity that it is a property of the flow and not the fluid. Different flow geometries and inlet conditions produce varied distributions of k and ε and thus μ_T.

The k-ε model is a reasonably simple means of closure as regards computational effort. Only two additional differential equations are introduced into the solution procedure. The price paid for the simplicity is lack of universality. The k-ε model treats the turbulence as having only a single characteristic velocity and length scale respectively. Such a description is not valid for all flows (Burmeister, 1983). Two additional constraining assumptions incorporated into the k-ε turbulence model are that the model is based on local isotropy and the presence of fully developed turbulence. The latter assumption requires near wall regions to be treated in a special manner since the flow in the immediate vicinity of a solid boundary is not fully turbulent (Schlichting, 1979). The near wall region may be treated by employing an alternate form of the k-ε model known as a low Reynolds number k-ε model (Patel, et. al., 1985). The low Reynolds number k-ε models employ suitable modifications of the transport equations for k and ε in near wall regions. In using these models it is necessary to resolve the near wall region with the chosen computational grid. An alternative procedure is to use wall functions as a means of linking the near wall flow to the fully turbulent core (Launder and Spalding, 1974).

Wall functions assume that the flow near a solid boundary is locally a Couette flow (Burmeister, 1983). With this assumption, the component of velocity parallel to the wall is described by a logarithmic profile (Schlichting, 1979):

$$u^+ = \frac{1}{K} \ln (Ey^+) \qquad (3.9)$$

$$K = 0.4$$

$$E = 9.025$$

It is further assumed that the production and dissipation of turbulent kinetic energy are equal in the near wall region (Hwang and Liou, 1991), thus implying the following:

$$k = \frac{C_\mu^{-1/2} \tau_w}{\rho} \qquad (3.10)$$

The logarithmic velocity profile is thus expressed as follows:

$$\tilde{u} = \frac{C_\mu^{1/4} k^{1/2}}{K} \ln \left[\frac{EyC_\mu^{1/4} k^{1/2} \rho}{\mu} \right] \qquad (3.11)$$

A straightforward manner of implementing the wall functions for velocity is to replace the near wall velocity with that obtained from the log-law profile. (This is done computationally through suitable source term linearization (Patankar, 1980)). In the context of a geometry described by general curvilinear coordinates, this can be a tedious process since the log-law profile is utilized for the component of velocity which is parallel to the wall. In general curvilinear coordinates, this velocity will be comprised of both Cartesian velocity components. Rather than forcing the near wall velocity to be equal to the

25

log-law value as proposed above, the near wall eddy viscosity is suitably modified so as to reflect the resulting turbulent shear stress,

$$\mu_T = \frac{\rho K C_\mu^{1/4} k^{1/2} y_p}{\ln\left[\dfrac{E C_\mu^{1/4} k^{1/2} \rho y_p}{\mu}\right]} \qquad (3.\ 12)$$

where y_p is the distance from the wall to the center of the cell nearest the wall. In using the wall function method, it is important to note that the cell nearest the wall must be such that y_p lies within the fully turbulent core.

The near wall affect on turbulent kinetic energy is enforced by writing the production and dissipation terms in the k transport equation in their integrated form according to the log-law velocity profile. Therefore,

$$P_k = \tau_w \left(\frac{\partial \tilde{u}}{\partial y}\right) = \frac{\rho (\tilde{u})^2 K C_\mu^{1/4} k^{1/2}}{\ln\left[\dfrac{E C_\mu^{1/4} k^{1/2} \rho y_p}{\mu}\right] y_p} \qquad (3.\ 13)$$

$$\begin{aligned}
\bar{\varepsilon} &= \iint \varepsilon \, dx \, dy \\
&= \frac{C_\mu^{3/4}}{K y_p} k^{3/2} \ln\left[\frac{E C_\mu^{1/4} k^{1/2} \rho y_p}{\mu}\right]
\end{aligned} \qquad (3.\ 14)$$

The transport equation for k is solved at the near wall cell but the production and dissipation terms are modified as given above (Launder and Spalding, 1974).

The near wall effect on the turbulent dissipation rate, ε is implemented in the present method by fixing the near wall value of ε. Given the definition of the turbulent dissipation rate (Launder and Spalding, 1974),

26

$$\varepsilon = \nu \; \overline{\frac{\partial u'_i}{\partial x_k} \frac{\partial u'_i}{\partial x_k}} \qquad (3.\,15)$$

the following approximation is made in the near wall, locally Couette flow, region:

$$\varepsilon = \frac{\tau_w}{\rho} \left| \frac{\partial \tilde{u}}{\partial y} \right| \qquad (3.\,16)$$

where y is the direction normal to the wall and $\tilde{u}$ is the velocity parallel to the wall. Since the mean velocity in the near wall region is taken to be governed by a log-law, the value of the turbulent dissipation rate at the point nearest the wall is given as follows:

$$\varepsilon_p = \frac{C_\mu^{3/4} k_p^{3/2}}{K y_p} \qquad (3.\,17)$$

3.2. Premixed Flame Model

The purpose of the turbulent premixed flame model is to provide a functional relation for the determination of the mean reaction rates of all relevant species. A complete description of hydrocarbon combustion can require the consideration of as many as 83 chemical reactions with 27 participating chemical species (Jachimowski, 1984). Therefore, 27 expressions for $\dot{\omega}_i$ would be required, one for each specie.

In order to keep the overall flowfield simulation computationally tractable, a simple one-step description of the combustion process is considered. The one-step mechanism of C_3H_8 chemistry proposed by Westbrook and Dryer, 1981 is used in the present simulation:

$$C_3H_8 + 5(\,O_2 + 3.76\,N_2\,) \;\text{-----> } 3\,CO_2 + 4\,H_2O + 18.8\,N_2 \qquad (3.\,18)$$

27
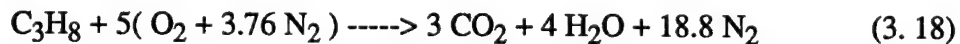
$$\frac{dC_{FU}}{dt} = k_f [C_{FU}]^{0.1} [C_{OX}]^{1.65} \qquad (3.19)$$

$$k_f = 8.6(10^{11})\exp\left[\frac{-30}{R_u T}\right] \qquad (3.20)$$

Reaction rate expressions for the other species (O_2, CO_2, etc.) are not needed, since the mass fractions of species other than fuel are determined from the law of conservation of atoms. The number of carbon atoms entering the reaction is the same as the number of carbon atoms after reaction (a statement of mass conservation), therefore an expression for the mass fraction of CO_2 can be determined:

$$Y_{CO_2} = \frac{3\ W_{CO_2}}{W_{FU}} (f - Y_{FU}) \qquad (3.21)$$

Similar expressions exist for H_2O and O_2:

$$Y_{H_2O} = \frac{4\ W_{H_2O}}{W_{FU}} (f - Y_{FU}) \qquad (3.22)$$

$$Y_{O_2} = 0.2331 (1 - f) - (f - Y_{FU}) \frac{5\ W_{O_2}}{W_{FU}} \qquad (3.23)$$

The mass fraction of nitrogen is calculated from the sum of all mass fractions being equal to unity, therefore:

$$Y_{N_2} = 1 - Y_{FU} - Y_{O_2} - Y_{H_2O} - Y_{CO_2} \qquad (3.24)$$

28

In describing the mean reaction rate ($\overline{\dot{\omega}}$) it is not sufficient to simply substitute mean values of flow variables into the reaction rate expression. Such a procedure neglects turbulent fluctuations of specie concentrations and temperature and will lead to errors of typically an order of magnitude (Jones and Whitelaw, 1982).

The present model of turbulent premixed flames determines the mean reaction rate as being the smaller of two limiting cases. The first limiting case involves a kinetically limited flame for which the decay rate of turbulent concentration fluctuations is much greater than the instantaneous rate at which the reaction proceeds (Libby and Williams, 1980). For this limit, the mean reaction rate does equal the expression given above (Zhou, 1989):

$$\overline{\dot{\omega}}_{ARR} = - \overline{k}_f \, \overline{\rho}^{(a+b)} \, \widetilde{Y}^a_{FU} \, \widetilde{Y}^b_{O_2} \tag{3.25}$$

$$\overline{k}_f = B \, \overline{\exp\left[\frac{-E_a}{R_u T}\right]} \tag{3.26}$$

The expression for the mean reaction rate constant ($\overline{k}_f$) is further simplified in the present model:

$$\overline{k}_f = B \, \exp\left[\frac{-E_a}{R_u \widetilde{T}}\right] \tag{3.27}$$

This expression assumes that the decay rate of temperature fluctuations is also much greater than the instantaneous reaction rate.

The other limiting case involves combustion in which the instantaneous chemical reaction occurs so fast that only the turbulent mixing limits the combustion process. The chemical reaction rate is much greater than the decay rate of turbulent fluctuations. This

29

limit corresponds to a physically controlled turbulent flame where the chemical kinetics do not effect the flame shape and length. An expression for the mean reaction rate for this limit is given by Magnussen and Hjertager, 1976:

$$\overline{\dot{\omega}}_{EBU} = - C_{EBU}\,\overline{\rho}\,\tilde{Y}_{FU}\,\frac{\varepsilon}{k} \qquad (3.28)$$

Two different expressions are available for the determination of the mean reaction rate. In the simulation of turbulent premixed flames, the mean reaction rate is taken as equal to the smaller of the two limiting cases given. Therefore,

$$\overline{\dot{\omega}}_{FU} = - \min\{\,|\,\overline{\dot{\omega}}_{ARR}\,|\,,\,|\,\overline{\dot{\omega}}_{EBU}\,|\,\} \qquad (3.29)$$

3.3. Diffusion Flame Model

The present simulation of turbulent reacting flow considers two models for diffusion flames. The first model is for a laminar flame. The second model is applicable for turbulent diffusion flames and is based on the fundamental concepts of the laminar flame model.

3.3.1. Laminar Flame Model

A model for laminar flames is not required as regards obtaining a closure of equations. Since an averaging process is not used, no turbulent fluxes or mean reaction rates are present in the governing equations. However, a model is incorporated in the present simulation so as to simplify the prediction of laminar diffusion flames.

30

The quantities of interest in the description of a reacting flow are specie mass fractions and the temperature. Rather than solve the governing differential equations, it is assumed that the chemical reactions occur at an infinitely fast rate. This assumption obviates one from having to solve all the differential equations which govern the distributions of mass fractions and temperature. Instead, the knowledge of the mixture fraction is sufficient for the determination of mass fractions and temperature.

The present model assumes that the reaction of fuel and oxidant occurs irreversibly in one step:

$$\text{Fuel + Oxidizer ----> Product} \tag{3.30}$$
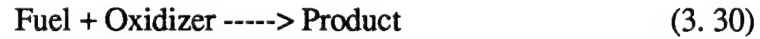
Given this, knowledge of only three mass fractions is required: fuel, oxidizer, and product.

In the present model for laminar diffusion flames, it is assumed that the reaction occurs only when the fuel and oxidizer are in stoichiometric proportions, thus:

$$\text{1 kg Fuel} + \phi \text{ kg Oxidizer ------>} (1 + \phi) \text{ kg Product} \tag{3.31}$$
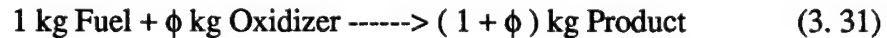
where ϕ is the stoichiometric air to fuel ratio based on mass. With the further assumption that the diffusivities of fuel and oxidizer are equal, the differential equations governing the distributions of fuel and oxidizer mass fractions can be linearly combined to yield an equation for the Schvab-Zeldovich variable Ψ (Bilger, 1980):

$$\frac{\partial}{\partial \xi}(\rho U \Psi) + \frac{\partial}{\partial \eta}(\rho V \Psi) = \frac{\partial}{\partial \xi}\left[\Gamma \, q_{11} \frac{\partial \Psi}{\partial \xi}\right] + \frac{\partial}{\partial \eta}\left[\Gamma \, q_{22} \frac{\partial \Psi}{\partial \eta}\right]$$
$$+ \frac{\partial}{\partial \xi}\left[\Gamma \, q_{12} \frac{\partial \Psi}{\partial \eta}\right] + \frac{\partial}{\partial \eta}\left[\Gamma \, q_{21} \frac{\partial \Psi}{\partial \xi}\right] \tag{3.32}$$

31

$$\Psi = Y_{FU} - Y_{OX}/\phi \qquad (3.33)$$

The normalization of the conserved variable Ψ yields a relation for the mixture fraction f:

$$f = \frac{\Psi - \Psi_{OX}}{\Psi_{FU} - \Psi_{OX}} \qquad (3.34)$$

where $\Psi_{OX} = -1/\phi$ and $\Psi_{FU} = 1$ if no diluent is present in either stream. The mixture fraction is also a conserved variable and is thus governed by the following equation:

$$\frac{\partial}{\partial \xi}(\rho U f) + \frac{\partial}{\partial \eta}(\rho V f) = \frac{\partial}{\partial \xi}\left[\Gamma \, q_{11} \frac{\partial f}{\partial \xi}\right] + \frac{\partial}{\partial \eta}\left[\Gamma \, q_{22} \frac{\partial f}{\partial \eta}\right]$$
$$+ \frac{\partial}{\partial \xi}\left[\Gamma \, q_{12} \frac{\partial f}{\partial \eta}\right] + \frac{\partial}{\partial \eta}\left[\Gamma \, q_{21} \frac{\partial f}{\partial \xi}\right] \qquad (3.35)$$

The assumption of infinitely fast chemistry implies that fuel and oxidizer cannot exist at the same point and time in the flowfield. Therefore if the conserved variable Ψ is calculated to be positive (implying fuel rich) then only fuel and product exist at that point. Alternately, if Ψ is negative (fuel lean condition) then only oxidizer and product are present.

$$\Psi > 0 \quad Y_{FU} = \Psi \quad Y_{OX} = 0 \quad Y_{PR} = 1 - Y_{FU} \qquad (3.36)$$

$$\Psi < 0 \quad Y_{FU} = 0 \quad Y_{OX} = -\phi\Psi \quad Y_{PR} = 1 - Y_{OX} \qquad (3.37)$$

$$\Psi = 0 \quad Y_{FU} = 0 \quad Y_{OX} = 0 \quad Y_{PR} = 1 \qquad (3.38)$$

32

Note that $\Psi = 0$ corresponds to the stoichiometric condition and hence the location of the flame surface. In the present model, the differential equation for Ψ is not solved, rather, the mixture fraction is solved from which Ψ is determined according to the above relations.

It is assumed in the present model that the Lewis number is unity (Pr = Sc) and therefore the governing equation for enthalpy is free of a source term (Libby and Williams, 1980). It is also assumed that the combustion process occurs adiabatically. The enthalpy can therefore be determined as a function of the mixture fraction:

$$h = f\, h_{FUEL} + (1 - f)\, h_{OX} \tag{3.39}$$

where h_{FUEL} and h_{OX} are the enthalpies of the fuel and oxidant streams respectively. The mixture temperature is determined from knowledge of the enthalpy:

$$T = \frac{h - Y_{FU}\, Q}{C_{pmix}} \tag{3.40}$$

where Q is the heat of combustion.

3.3.2. Turbulent Flame Model

The model for turbulent diffusion flames assumes that the reactions occur infinitely fast, just as in the laminar case. In the case of a turbulent flow, the quantities to be calculated by the combustion model are averaged quantities: $\tilde{Y}_{FU}$, $\tilde{Y}_{OX}$, $\tilde{Y}_{PR}$, $\tilde{T}$. For the purpose of simplicity, a one-step irreversible reaction is again assumed to describe the kinetics. If the mean quantities are determined in a manner identical to that for a laminar flame, significant error results. To do so would be to neglect the presence of turbulent fluctuations in the flow variables. Such a treatment of combustion would assume that the

33

averaged fuel and oxidizer mass fractions cannot exist at the same point. This is not observed experimentally (Bilger, 1980). In order to determine the mean flow variables, the definition of an average is used (Hogg, et. al., 1987):

$$\bar{\phi} = \int_0^1 \phi \, P(f) \, df \qquad (3.41)$$

where $P(f)$ is the probability density function.

The quantities to be determined are mass averaged values and therefore a Favre pdf (Bilger, 1980) defines the mean quantities:

$$\tilde{Y}_{FU} = \int_0^1 Y_{FU}(f) \, \tilde{P}(f;\bar{x}) \, df \qquad (3.42)$$

$$\tilde{Y}_{OX} = \int_0^1 Y_{OX}(f) \, \tilde{P}(f;\bar{x}) \, df \qquad (3.43)$$

$$\tilde{Y}_{PR} = \int_0^1 Y_{PR}(f) \, \tilde{P}(f;\bar{x}) \, df \qquad (3.44)$$

$$\tilde{h} = \int_0^1 h(f) \, \tilde{P}(f;\bar{x}) \, df \qquad (3.45)$$

where $\tilde{P}(f;\bar{x})$ is the Favre pdf. The probability density function used in the present simulation is a double delta function pdf (Jones and Whitelaw, 1982).

34

$$\tilde{P}(f:\bar{x}) = \alpha \, \delta(f - f^+) + (1 - \alpha) \, \delta(f - f^-) \qquad (3.46)$$

$$\alpha = \frac{\tilde{f} - f^-}{f^+ - f^-} \qquad (3.47)$$

Other researchers have used a clipped Gaussian pdf (Lockwood and Naguib, 1975), a beta function pdf (Lentini, 1990), and a 10 points pdf (Chen, et. al., 1991).

The probability density function is spatially dependent and methods have been used which solve for the pdf prior to determining the means of the other flow variables (Pope, 1990). The model used in the current simulation of turbulent reacting flow is an assumed shape pdf model (Kuo, 1986).

The double delta function is specified by the fluctuation limits f^+ and f^- :

$$f^+ = \tilde{f} + \sqrt{g} \qquad (3.48)$$

$$f^- = \tilde{f} - \sqrt{g} \qquad (3.49)$$

The concentration fluctuation g (where $g = \overline{f'^2}$), is determined from the modelled equation given by Spalding, 1971:

$$\begin{aligned}
\frac{\partial}{\partial \xi} (\rho U g) + \frac{\partial}{\partial \eta} (\rho V g) = & \frac{\partial}{\partial \xi}\left[\Gamma \, q_{11} \frac{\partial g}{\partial \xi}\right] + \frac{\partial}{\partial \eta}\left[\Gamma \, q_{22} \frac{\partial g}{\partial \eta}\right] \\
& + \frac{\partial}{\partial \xi}\left[\Gamma \, q_{12} \frac{\partial g}{\partial \eta}\right] + \frac{\partial}{\partial \eta}\left[\Gamma \, q_{21} \frac{\partial g}{\partial \xi}\right] \\
& + \left\{\frac{2\mu_T P_g \, |J|}{Pr_T^g}\right\} - \left\{\frac{2 \, |J| \, \rho \varepsilon g}{k}\right\}
\end{aligned} \qquad (3.50)$$

$$P_g = \left[\frac{\partial \tilde{f}}{\partial x}\right]^2 + \left[\frac{\partial \tilde{f}}{\partial y}\right]^2 \qquad (3.51)$$

With the use of a double delta function pdf, a numerical integration is not required in determining mean quantities. The determination of mean flow variables which describe a reacting flow are calculated based on a knowledge of α:

$$\tilde{Y}_{FU} = \alpha Y_{FU}^+ + (1 - \alpha) Y_{FU}^- \tag{3.52}$$

$$\tilde{Y}_{OX} = \alpha Y_{OX}^+ + (1 - \alpha) Y_{OX}^- \tag{3.53}$$

$$\tilde{Y}_{PR} = \alpha Y_{PR}^+ + (1 - \alpha) Y_{PR}^- \tag{3.54}$$

$$\tilde{h} = \alpha\, h^+ + (1 - \alpha)\, h^- \tag{3.55}$$

where Y_{FU}^+, Y_{OX}^+, etc. are the quantities which correspond to the mixture fraction at the extreme upper limit of fluctuation (f^+). The values Y_{FU}^-, Y_{OX}^-, etc. are the property

fluctuations corresponding to the lower limit of the mixture fraction fluctuation (f^-). The limit values are determined in a manner identical to that for a laminar flame except they are based on a mixture fraction fluctuation (f^+ or f^-). The mean temperature is determined from the mean enthalpy as follows:

$$\tilde{T} = \frac{\tilde{h} - \tilde{Y}_{FU}\, Q}{\bar{C}_{pmix}} \tag{3.56}$$

In using a pdf method, the effects of concentration fluctuation are accounted for to some extent. The ramification of pdf shape on the results has been studied by various

36

researchers (e.g. Chen, et. al., 1991). They concluded that the shape of the pdf does not greatly affect the flowfield except when a double delta function pdf is used. The use of a more descriptive yet computationally tractable pdf is thus desired.

CHAPTER 4: SOLUTION PROCEDURE

To facilitate the study of phenomena relevant to turbulent reacting flows, the governing conservation equations must be solved. These equations are highly nonlinear and are strongly coupled, thus precluding the determination of a closed form analytic solution. Rather than solve for continuous functions of the flow variables, the equations are discretized and values of the flow variables at only certain points are sought. The discretization process simplifies the problem from one of solving partial differential equations to one of solving algebraic equations. The nonlinearity of the algebraic equations as well as the inter-equation coupling is treated by the process of iteration. In general, the equations are solved in a sequential fashion. While one flow variable is solved, the others are held constant. By solving each equation in turn, one iteration is completed. Numerous iterations are required before a converged solution is obtained. Convergence is obtained when each flow variable satisfies its discretized equation and when the flow variables no longer change from one iteration to the next.

A solution procedure employing this sequential technique is referred to as a segregated or decoupled solution procedure. Coupled solution procedures have also been developed (Vanka, 1986; Galpin et.al., 1985). The coupling of all equations is usually not undertaken however. Coupled solution procedures normally couple only the momentum and continuity equations, with the various scalar equations being solved in a sequential decoupled framework.

The present solution procedure employs a decoupled solution technique. The momentum equations are solved first, followed by a pressure correction to satisfy the continuity constraint. The scalar equations for turbulent kinetic energy, turbulent dissipation rate, etc. are solved next, with an update of thermodynamic properties

(ρ,T,etc.) and transport coefficients (Γ) completing one iteration. In the discussion which follows, the discretization of the momentum equations will be treated. The use of a collocated grid for velocities and pressure and its ramification on the discretized momentum equations will be discussed. The pressure correction procedure employed will be described followed by the solution of the scalar equations. Lastly, a synopsis of the entire solution procedure will be presented.

4.1. Momentum Equations

The momentum equations are discretized in accordance with a finite volume method. The finite volume method has been chosen because of the conservative nature of the discretization obtained (Anderson, et.al., 1984; Fletcher, 1988a). In discretizing the momentum equations using a finite volume method, the computational domain is first subdivided into finite control volumes (see Figure 2). The Gauss divergence theorem is then used to integrate the partial differential equation over a given finite control volume. The resulting discrete forms of the u and v momentum equations are given as follows:

$$
\begin{aligned}
[\,(\rho U u)_{i+1/2,j} - (\rho U u)_{i-1/2,j}\,]\,\Delta\eta &+ [\,(\rho V u)_{i,j+1/2} - (\rho V u)_{i,j-1/2}\,]\,\Delta\xi = \\
&[\,(\Gamma q_{11}\tfrac{\partial u}{\partial\xi})_{i+1/2,j} - (\Gamma q_{11}\tfrac{\partial u}{\partial\xi})_{i-1/2,j}\,]\,\Delta\eta + \\
&[\,(\Gamma q_{22}\tfrac{\partial u}{\partial\eta})_{i,j+1/2} - (\Gamma q_{22}\tfrac{\partial u}{\partial\eta})_{i,j-1/2}\,]\,\Delta\xi + \\
&S^u_{TR} + S^u(\xi,\eta)
\end{aligned}
\tag{4.1}
$$

$$
\begin{aligned}
[\,(\rho U v)_{i+1/2,j} - (\rho U v)_{i-1/2,j}\,]\,\Delta\eta &+ [\,(\rho V v)_{i,j+1/2} - (\rho V v)_{i,j-1/2}\,]\,\Delta\xi = \\
&[\,(\Gamma q_{11}\tfrac{\partial v}{\partial\xi})_{i+1/2,j} - (\Gamma q_{11}\tfrac{\partial v}{\partial\xi})_{i-1/2,j}\,]\,\Delta\eta + \\
&[\,(\Gamma q_{22}\tfrac{\partial v}{\partial\eta})_{i,j+1/2} - (\Gamma q_{22}\tfrac{\partial v}{\partial\eta})_{i,j-1/2}\,]\,\Delta\xi +
\end{aligned}
\tag{4.2}
$$

39

$$S_{TR}^{v} + S^{v}(\xi, \eta)$$

where the coordinate transformation employed is such that $\Delta\xi = \Delta\eta = 1$.

The discrete form of the equations governing u and v requires knowledge of fluxes, exchange coefficients, and dependent variables at the cell faces. Values of the transformation metrics are also required at the cell faces. In the present solution procedure, some of the transformation metrics are considered as being stored at the cell faces and therefore no special treatment is required. For the determination of exchange coefficients, fluxes, and dependent variables, various interpolation techniques have been utilized.

In calculating the exchange coefficient at a particular cell face, a harmonic mean has been used (Patankar, 1980). The exchange coefficient at the i+1/2 face (see Figure 3) is thus determined as follows:

$$\Gamma_{i+1/2,j} = \frac{\Gamma_{ij}\,\Gamma_{i+1j}}{fx_{i+1/2j}\,\Gamma_{i+1j} + (1-fx_{i+1/2j})\,\Gamma_{ij}} \tag{4.3}$$

where $fx_{i+1/2,j}$ is the ξ coordinate interpolation factor at the i+1/2 face of the finite control volume. The harmonic mean has been used instead of linear interpolation because of the former's ability to handle abrupt changes in the distribution of the exchange coefficient. Such a characteristic was found by Nallasamy and Chen, 1985 to be crucial in obtaining physically realistic distributions of some flow field variables.

The value of the Cartesian velocity components at a cell face is obtained by assuming a piecewise linear distribution in the physical space. Such a procedure is consistent with a central differencing scheme. For large values of cell Peclet number (Pe > 2) a central differencing scheme becomes unstable and thus the cell face value is taken to be equal to the velocity of the upstream neighbor value. The use of central differencing for low Peclet number and upwinding for large Peclet number is known as hybrid differencing (Patankar,

1980). Various assumptions can be made as regards the piecewise distribution of the flow variables. Numerous studies have been made to ascertain the efficiency of some of these differencing schemes (Shyy and Correa, 1985; Pollard and Siu, 1982). Some of the more popular are skew upwind differencing (Raithby, 1976), quadratic upstream interpolation for convective kinematics, QUICK (Leonard, 1979), and second order upwind differencing.

The hybrid differencing scheme is formally only first order accurate and is thus questionable as regards grid independent solutions. More significant than the formal order of accuracy is the false diffusion which upwinding introduces into the calculation (Patankar, 1980). However, from a practical point of view, the computational efficiency of a solution procedure is more important than accuracy alone (Fletcher, 1988a). The accuracy of even a formally low order solution may be improved by refining the grid. Also, procedures such as Richardson extrapolation can be employed to improve solution accuracy (Fletcher, 1988a). The hybrid differencing scheme has been emplemented in the present solution procedure because it is unconditionally stable.

The values of the fluxes at the cell faces are not determined by a simple linear interpolation. In the context of a collocated grid for velocities and pressure, such a practice would invariably lead to a checkerboard split in the pressure field (Patankar, 1980). The proper treatment of the cell face fluxes is crucial for the development of a convergent and accurate numerical procedure. The cell face fluxes are ultimately written in terms of the discretized momentum equations. Therefore, a detailed exposition of the interpolation practice used for cell face fluxes is deferred until the final forms of the discretized momentum equations are obtained.

Given the interpolation practices for the various cell face quantities, the discretized equations for u and v are given as follows:

41

$$A_p \, u_{i,j} = A_e \, u_{i+1,j} + A_w \, u_{i-1,j} + A_n \, u_{i,j+1} + A_s \, u_{i,j-1} + S_{TR}^u + S^u(\xi,\eta) \qquad (4.4)$$

$$A_p \, v_{i,j} = A_e \, v_{i+1,j} + A_w \, v_{i-1,j} + A_n \, v_{i,j+1} + A_s \, v_{i,j-1} + S_{TR}^v + S^v(\xi,\eta) \qquad (4.5)$$

$$A_e = \text{amax1}(\, 0.0, \ -(\rho U)_{i+1/2,j}, \ -(\rho U)_{i+1/2,j} \, fx_{i+1/2,j} + (q_{11})_{i+1/2,j} \, \Gamma_{i+1/2,j} \,) \quad (4.6)$$

$$A_w = \text{amax1}(\, 0.0, \ (\rho U)_{i-1/2,j}, \ \ (\rho U)_{i-1/2,j} \, (1\text{-}fx_{i-1/2,j}) + (q_{11})_{i-1/2,j} \, \Gamma_{i-1/2,j} \,) \quad (4.7)$$

$$A_n = \text{amax1}(\, 0.0, \ -(\rho V)_{i,j+1/2}, \ -(\rho V)_{i,j+1/2} \, fy_{i,j+1/2} + (q_{22})_{i,j+1/2} \, \Gamma_{i,j+1/2} \,) \quad (4.8)$$

$$A_s = \text{amax1}(\, 0.0, \ (\rho V)_{i,j-1/2}, \ (\rho V)_{i,j-1/2} \, (1 - fy_{i,j-1/2}) + (q_{22})_{i,j-1/2} \, \Gamma_{i,j-1/2} \,) \quad (4.9)$$

$$A_p = A_e + A_w + A_n + A_s \qquad (4.10)$$

$$S^u(\xi,\eta) = - \left(a_{11} \frac{\partial P}{\partial \xi} + a_{21} \frac{\partial P}{\partial \eta} \right) \qquad (4.11)$$

$$S^v(\xi,\eta) = - \left(a_{12} \frac{\partial P}{\partial \xi} + a_{22} \frac{\partial P}{\partial \eta} \right) \qquad (4.12)$$

$$S_{TR}^u = \frac{\partial}{\partial \xi} \left(\Gamma q_{12} \frac{\partial u}{\partial \eta} \right) + \frac{\partial}{\partial \eta} \left(\Gamma q_{21} \frac{\partial u}{\partial \xi} \right) \qquad (4.13)$$

$$S_{TR}^v = \frac{\partial}{\partial \xi} \left(\Gamma q_{12} \frac{\partial v}{\partial \eta} \right) + \frac{\partial}{\partial \eta} \left(\Gamma q_{21} \frac{\partial v}{\partial \xi} \right) \qquad (4.14)$$

where amax1 is a fortran supplied function which is used in implementing the hybrid differencing procedure. It is important to note here that the coefficients for u and v are identical. The coefficients for u also serve as the coefficients for v. This occurs since a

collocated grid is used. If a staggered were used, then the coefficients of u and v would be different. Indeed, the coefficients of the discretized equations for all flow variables (k, ε, h_o, etc.) are the same. Therefore, the same routine can be used for the calculation of the coefficients of any flow variable.

In looking at the coefficients of the discretized equations for u and v, it is evident that all of the coefficients are positive. This is necessary for the numerical procedure to remain stable. Also, both the convective and diffusive fluxes at a given cell face are not ascribed to a particular cell. The cell face fluxes are not calculated as though they belong to any given cell. This quality ensures that inconsistencies do not arise in the discretized equations for adjacent control volumes. The flux leaving one control volume is assured of being the flux which enters the neighboring control volume. Finally, the central coefficient (A_p) is seen to be equal to the sum of the neighboring coefficients:

$$A_p = A_e + A_w + A_n + A_s + \{ (\rho U)_{i+1/2,j} - (\rho U)_{i-1/2,j} + (\rho V)_{i,j+1/2} - (\rho V)_{i,j-1/2} \} \quad (4.15)$$

$$====> A_p = \Sigma A_{nb} \quad (4.16)$$

where the term enclosed in brackets is the discretized continuity equation and is equal to zero. This condition is considered necessary for situations in which the differential equation is satisfied even if a constant were to be added to the dependent variable (Patankar, 1980).

When solving for u or v (or any flow variable) in an iterative manner, underrelaxation is employed in order to maintain stability of the numerical procedure. If underrelaxation is not employed, the scheme can become unstable since the coupled nonlinear equations are treated in a decoupled, linear fashion. In the present solution procedure, the underrelaxation is implemented in an implicit manner (Patankar, 1980). The final form of

43

the discretized equations for u and v as used in the present solution procedure are thus given as follows:

$$A_p\, u_{i,j} = A_e\, u_{i+1,j} + A_w\, u_{i-1,j} + A_n\, u_{i,j+1} + A_s\, u_{i,j-1} + S^u_{TR} + S^u(\xi,\eta) \qquad (4.\,17)$$

$$A_p\, v_{i,j} = A_e\, v_{i+1,j} + A_w\, v_{i-1,j} + A_n\, v_{i,j+1} + A_s\, v_{i,j-1} + S^v_{TR} + S^v(\xi,\eta) \qquad (4.\,18)$$

$$A_e = \mathrm{amax1}(\,0.0,\ -(\rho U)_{i+1/2,j},\ -(\rho U)_{i+1/2,j}\, fx_{i+1/2,j} + (q_{11})_{i+1/2,j}\, \Gamma_{i+1/2,j}\,) \qquad (4.\,19)$$

$$A_w = \mathrm{amax1}(\,0.0,\ (\rho U)_{i-1/2,j},\ (\rho U)_{i-1/2,j}\,(1\text{-}fx_{i-1/2,j}) + (q_{11})_{i-1/2,j}\, \Gamma_{i-1/2,j}\,) \qquad (4.\,20)$$

$$A_n = \mathrm{amax1}(\,0.0,\ -(\rho V)_{i,j+1/2},\ -(\rho V)_{i,j+1/2}\, fy_{i,j+1/2} + (q_{22})_{i,j+1/2}\, \Gamma_{i,j+1/2}\,) \qquad (4.\,21)$$

$$A_s = \mathrm{amax1}(\,0.0,\ (\rho V)_{i,j-1/2},\ (\rho V)_{i,j-1/2}\,(1 - fy_{i,j-1/2}) + (q_{22})_{i,j-1/2}\, \Gamma_{i,j-1/2}\,) \qquad (4.\,22)$$

$$A_p = \left[\frac{\Sigma A_{nb}}{\omega}\right] \qquad (4.\,23)$$

$$S^u(\xi,\eta) = -\left(a_{11}\frac{\partial P}{\partial \xi} + a_{21}\frac{\partial P}{\partial \eta}\right) + A_p\,(1-\omega)\,u^{old}_{ij} \qquad (4.\,24)$$

$$S^v(\xi,\eta) = -\left(a_{12}\frac{\partial P}{\partial \xi} + a_{22}\frac{\partial P}{\partial \eta}\right) + A_p\,(1-\omega)\,v^{old}_{ij} \qquad (4.\,25)$$

$$S^u_{TR} = \frac{\partial}{\partial \xi}\left(\Gamma q_{12}\frac{\partial u}{\partial \eta}\right) + \frac{\partial}{\partial \eta}\left(\Gamma q_{21}\frac{\partial u}{\partial \xi}\right) \qquad (4.\,26)$$

$$S^v_{TR} = \frac{\partial}{\partial \xi}\left(\Gamma q_{12}\frac{\partial v}{\partial \eta}\right) + \frac{\partial}{\partial \eta}\left(\Gamma q_{21}\frac{\partial v}{\partial \xi}\right) \qquad (4.\,27)$$

44

In the present solution procedure, the method of Rodi, Majumdar, and Schonung, 1987 has been used to determine the cell face values of the convective flux. Various methods exist for the treatment of collocated or non-staggered grids (Rhie and Chow, 1983; Thiart, 1990; Acharya and Moukalled, 1989; Miller and Schmidt, 1988). The present method is similar to that employed by Rhie and Chow. It differs from their method in that it is not relaxation dependent (Majumdar, 1988). Also, Acharya and Moukalled, 1989 found that the method proposed by Rhie and Chow did not satisfy integral mass conservation because of the flux correction which is employed in that method. The primary concept of the method proposed by Rhie and Chow was that pressure oscillations should not be allowed to occur as evidenced by physical reasoning. This feature is retained in the present solution procedure.

Following Majumdar (Majumdar, 1988) the values of the Cartesian velocities at the cell faces are written in terms of the interpolated discretized equations for the adjacent cell center velocities. For example, if a staggered grid were being used, the values of u_e and v_e would be written as follows:

$$u_e = \left\{ \frac{(\Sigma A_{nb} u_{nb})_e}{A_{pe}^u} \right\} - \left\{ \frac{1}{A_{pe}^u} \right\} (a_{11} \frac{\partial P}{\partial \xi} + a_{21} \frac{\partial P}{\partial \eta})_e + \left\{ \frac{1}{A_{pe}^u} S^u(\xi,\eta) \right\} + (1 - \omega) u_e^{old} \quad (4.\,28)$$

$$v_e = \left\{ \frac{(\Sigma A_{nb} v_{nb})_e}{A_{pe}^v} \right\} - \left\{ \frac{1}{A_{pe}^v} \right\} (a_{12} \frac{\partial P}{\partial \xi} + a_{22} \frac{\partial P}{\partial \eta})_e + \left\{ \frac{1}{A_{pe}^v} S^v(\xi,\eta) \right\} + (1 - \omega) v_e^{old} \quad (4.\,29)$$

where $S^u(\xi,\eta)$ and $S^v(\xi,\eta)$ obviously do not contain the source term due to pressure or relaxation. Now, a staggered is not being used and so quantities such as A_p and $\Sigma A_{nb} u_{nb}$ are not known at the cell faces. To determine these quantities, linear interpolation in the

45

physical space is used. In particular, only those terms surrounded by braces are interpolated. The pressure terms and relaxation terms are not interpolated. The cell face contravariant velocity in terms of u_e and v_e is as follows:

$$U_e = u_e \, a_{11} + v_e \, a_{12} \tag{4.30}$$

where a_{11} and a_{12} have been calculated at the cell face (east in this case). With the interpolation of the various terms in u_e and v_e included, the cell face contravariant velocity is thus expressed in terms of cell center quantities:

$$U_e = a_{11} \left(\overline{\frac{\Sigma A_{nb} u_{nb} + S^u(\xi,\eta)}{A_p^u}} \right) - a_{11} \left(\overline{\frac{1}{A_p^u}} \right) (a_{11} \frac{\partial P}{\partial \xi} + \overline{a_{21}} \frac{\partial P}{\partial \eta})_e + a_{11} (1 - \omega) u_e{}^{old}$$

$$+ a_{12} \left(\overline{\frac{\Sigma A_{nb} v_{nb} + S^v(\xi,\eta)}{A_p^v}} \right) - a_{12} \left(\overline{\frac{1}{A_p^v}} \right) (a_{12} \frac{\partial P}{\partial \xi} + \overline{a_{22}} \frac{\partial P}{\partial \eta})_e$$

$$+ a_{12} (1 - \omega) v_e{}^{old} \tag{4.31}$$

where the overbar indicates that a linear interpolation in the physical space has been used to obtain that quantity. If the terms involving u_e and v_e are grouped together, the resulting expression for U_e shows that it will be independent of the relaxation factor when a converged solution is obtained:

$$U_e = \omega \, U_e{}^{new} + (1 - \omega) \, U_e{}^{old} \tag{4.32}$$

The expressions for U_w, V_n, and V_s follow a similar logic. This procedure for determining cell face velocities has been referred to as momentum interpolation (Majumdar, 1988).

The cell face value of the contravariant velocity has been represented in terms of cell center values but nothing has been mentioned as regards density. The value of the cell face density is obtained by a strict upwinding procedure (Issa and Lockwood, 1977). In the present method then, the cell face flux is not treated as one entity. The cell face flux is determined by the product of the upwind density and the contravariant velocity as obtained from momentum interpolation.

4.2. Continuity Equation

In the present procedure, mass conservation is satisfied by applying corrections to the velocities (contravariant and Cartesian). The discretized form of the mass conservation statement serves as the basis for the development of a suitable correction equation.

$$(\rho U)_{i+1/2,j} - (\rho U)_{i-1/2,j} + (\rho V)_{i,j+1/2} - (\rho V)_{i,j-1/2} = 0 \tag{4.33}$$

The velocities, density, and pressure are written as the sum of their estimated values and a suitable correction.

$$\rho = \rho^* + \rho' \tag{4.34}$$

$$P = P^* + P' \tag{4.35}$$

$$U = U^* + U' \tag{4.36}$$

$$V = V^* + V' \tag{4.37}$$

47

Upon substitution into the discretized continuity equation, the following is obtained:

$$(\rho^*U' + \rho'U^*)_{i+1/2,j} - (\rho^*U' + \rho'U^*)_{i-1/2,j} + (\rho^*V' + \rho'V^*)_{i,j+1/2} - (\rho^*V' + \rho'V^*)_{i,j-1/2}$$

$$= -[(\rho^*U^*)_{i+1/2,j} - (\rho^*U^*)_{i-1/2,j} + (\rho^*V^*)_{i,j+1/2} - (\rho^*V^*)_{i,j-1/2}] \qquad (4.38)$$

It has been assumed that the nonlinear compressibility terms ($\rho'U'$, $\rho'V'$) are negligible. In the work of Shyy and Braaten, 1988 these terms were included in the pressure correction equation as an explicit source. It was found that inclusion of these terms was useful in preventing early divergence of the numerical procedure for the calculation of supersonic flows. The present method is envisioned for use in calculating subsonic compressible flows and so the nonlinear terms were not considered necessary. When incompressible or low mach number flows are calculated, the density corrections are removed altogether.

The right hand side of the above correction equation represents a mass source. When a converged solution is obtained, the velocities as calculated from the momentum equations, together with the density, will be such that this mass source is zero. Since corrections are not applied to the converged result from the momentum equations, the correction equation does not effect the formal accuracy of the procedure. The correction equation does however affect the convergence rate of the overall numerical procedure. It is therefore vitally important to utilize a correction equation which is convergent. The issue of a convergent correction equation arises when considering the form taken by the corrections in a non-orthogonal coordinate system.

Each of the velocity and density corrections is written in terms of a pressure correction. In this way the discretized continuity equation becomes a pressure correction equation. The mass source in the equation serves to drive these pressure corrections and thus satisfy continuity.

48

The density correction as a function of pressure is obtained from the isentropic speed of sound for an ideal gas:

$$\frac{\partial P}{\partial \rho} = \gamma RT \tag{4.39}$$

therefore,

$$\rho' = \frac{1}{\gamma RT} P' \tag{4.40}$$

Other researchers (Shyy and Braaten, 1988; Issa and Lockwood, 1977; Demirdzic, et.al., 1990) have obtained the expression for ρ' from the ideal gas law, hence

$$\rho' = \frac{1}{RT} P' \tag{4.41}$$

The use of the isentropic sound speed in expressing ρ' is thus seen to be merely an underrelaxed version of the expression obtained from the ideal gas law. The specific heat ratio (γ) ensures that ρ' as obtained from the sound speed definition will be less than the ρ' obtained from the ideal gas law.

The corrections to the contravariant velocities (U' and V') are obtained from the definitions of the contravariant velocities and from the momentum equations.

$$U' = a_{11} u' + a_{12} v' \tag{4.42}$$

$$V' = a_{21} u' + a_{22} v' \tag{4.43}$$

49

As an example, consider the form of the correction for the contravariant velocity at the east face of a control volume ($U'_{i+1/2,j}$).

$$U'_{i+1/2,j} = a_{11} u'_{i+1/2,j} + a_{12} v'_{i+1/2,j} \qquad (4.44)$$

The transformation metrics a_{11} and a_{12} are stored at the cell faces corresponding to lines of constant ξ. In this way, no averaging need be performed in order to express these quantities at the east or west face of a finite control volume. The values of u' and v' are determined from the momentum equations in a manner consistent with the SIMPLEC method suggested by VanDoormaal and Raithby, 1984. Consider the form of the discretized equations for the estimated velocities (u* and v*) at the east face of a control volume:

$$\left[A_p^u\right]_e u^*_e = \left[\Sigma A_{nb} u^*_{nb}\right]_e - \left(a_{11} \frac{\partial P^*}{\partial \xi} + a_{21} \frac{\partial P^*}{\partial \eta} \right)_e$$
$$+ \left[S_{TR}^u\right]_e + \left[A_p^u\right]_e (1 - \omega) u_e^{old} \qquad (4.45)$$

$$\left[A_p^v\right]_e v^*_e = \left[\Sigma A_{nb} v^*_{nb}\right]_e - \left(a_{12} \frac{\partial P^*}{\partial \xi} + a_{22} \frac{\partial P^*}{\partial \eta} \right)_e$$
$$+ \left[S_{TR}^v\right]_e + \left[A_p^v\right]_e (1 - \omega) v_e^{old} \qquad (4.46)$$

Since a collocated grid is being used, the coefficients (A_p, A_{nb}) are not defined at cell faces. These coefficients are obtained by linear interpolation of the cell center quantities as mentioned previously. If these equations for u^*_e and v^*_e are subtracted from the corresponding equations for u_e and v_e (eqns. 4.28 and 4.29), then the following equations for u'_e and v'_e are obtained.

$$\left[A_p^u \right]_e u'_e = \left[\Sigma A_{nb} u'_{nb} \right]_e - \left(a_{11} \frac{\partial P'}{\partial \xi} + a_{21} \frac{\partial P'}{\partial \eta} \right)_e \qquad (4.\,47)$$

$$\left[A_p^v \right]_e v'_e = \left[\Sigma A_{nb} v'_{nb} \right]_e - \left(a_{12} \frac{\partial P'}{\partial \xi} + a_{22} \frac{\partial P'}{\partial \eta} \right)_e \qquad (4.\,48)$$

In accordance with the SIMPLEC method, the quantity $(\Sigma A_{nb}^u) u'_e$ is subtracted from both sides of the equation for u'_e and $(\Sigma A_{nb}^v) v'_e$ is subtracted from both sides of the equation for v'_e. The final expressions for u'_e and v'_e are obtained by disregarding the terms involving the neighbor coefficients (VanDoormaal and Raithby, 1984). The form of the equation for u'_e and v'_e is therefore,

$$u'_e = \frac{1}{(A_p - \Sigma A_{nb})} \left(- a_{11} \frac{\partial P'}{\partial \xi} - a_{21} \frac{\partial P'}{\partial \eta} \right) \qquad (4.\,49)$$

$$v'_e = \frac{1}{(A_p - \Sigma A_{nb})} \left(- a_{12} \frac{\partial P'}{\partial \xi} - a_{22} \frac{\partial P'}{\partial \eta} \right) \qquad (4.\,50)$$

where the coefficients (A_p, A_{nb}) are obtained from a linear interpolation of cell center values. It is to be realized that the removal of the neighbor coefficient terms from the equations for u'_e and v'_e is a legitimate procedure. In the converged state, all pressure corrections will be zero since the mass source is zero. The converged solution is then uninfluenced by the form of the pressure correction equation since it is not used in the final iteration (Patankar, 1980). The form of the correction which is applied to U'_e is obtained then by substitution of u'_e and v'_e into equation 4.44:

$$U'_e = \left(\frac{1}{(A_p - \Sigma A_{nb})} \right)_e (a_{11}^2 + a_{12}^2)_e (P'_{i,j} - P'_{i+1,j})$$

$$+ \left(\cfrac{1}{(A_p - \Sigma A_{nb})} \right)_e (a_{11} \, \overline{a_{21}} + a_{12} \, \overline{a_{22}})_e \left(- \cfrac{\partial P'}{\partial \eta} \right)_e \qquad (4.51)$$

where the overbar denotes an interpolated quantity. The expressions for U'_w, V'_n, and V'_s are obtained in an analogous manner.

Note in the above expression for U'_e that two pressure gradients are present, one in the ξ coordinate direction and one in the η direction. The pressure gradient in the η direction in the above expression for U'_e is zero for an orthogonal grid. It is only present when non-orthogonal grids are used. This fact has led some researchers (Rhie and Chow, 1983; Acharya and Moukalled, 1989) to neglect these terms, thus assuming near orthogonality. As noted above, the assumptions made in deriving the pressure correction equation do not effect the final solution, only the rate of convergence of the solution procedure. Neglecting these non-orthogonal terms is thus a legitimate procedure. However, Peric, 1990 has found that the applicability of a solution procedure which incorporates the near orthogonal simplification is severely restricted when the grid becomes non-orthogonal. For this reason, the present solution procedure retains these non-orthogonal terms in the pressure correction equation. The inclusion of the non-orthogonal terms results in a nine point computational molecule for the pressure correction equation. Rather than use a more complex solver, the non-orthogonal terms have been included as explicit source terms, thus allowing the use of only a five point computational molecule. Therefore, the final form of the pressure correction equation as used in the present procedure is as follows:

$$A_p^p \, P'_{i,j} = A_e^p \, P'_{i+1,j} + A_w^p \, P'_{i-1,j} + A_n^p \, P'_{i,j+1} + A_s^p \, P'_{i,j-1} + S^M + S^{NO} \qquad (4.52)$$

$$A_e^p = \left[\cfrac{1}{(A_p - \Sigma A_{nb})} \right]_{i+1/2,j} (a_{11}^2 + a_{12}^2)_{i+1/2,j} \, \rho_{i+1/2,j}$$

$$- \; U^*_{i+1/2,j} \, fx_{i+1/2,j} \left(\frac{1}{\gamma RT}\right)_{i+1,j} \tag{4.53}$$

$$A^p_w = \left[\frac{1}{\overline{(\,A_p\text{-}\Sigma A_{nb}\,)}}\right]_{i\text{-}1/2,j} (\,a^2_{11} + a^2_{12}\,)_{i\text{-}1/2,j} \; \rho_{i\text{-}1/2,j}$$
$$+ \; U^*_{i\text{-}1/2,j} (\,1 - fx_{i\text{-}1/2,j}\,) \left(\frac{1}{\gamma RT}\right)_{i\text{-}1,j} \tag{4.54}$$

$$A^p_n = \left[\frac{1}{\overline{(\,A_p\text{-}\Sigma A_{nb}\,)}}\right]_{i,j+1/2} (\,a^2_{21} + a^2_{22}\,)_{i,j+1/2} \; \rho_{i,j+1/2}$$
$$- \; V^*_{i,j+1/2} \, fy_{i,j+1/2} \left(\frac{1}{\gamma RT}\right)_{i,j+1} \tag{4.55}$$

$$A^p_s = \left[\frac{1}{\overline{(\,A_p\text{-}\Sigma A_{nb}\,)}}\right]_{i,j\text{-}1/2} (\,a^2_{21} + a^2_{22}\,)_{i,j\text{-}1/2} \; \rho_{i,j\text{-}1/2}$$
$$+ \; V^*_{i,j\text{-}1/2} (\,1 - fy_{i,j\text{-}1/2}\,) \left(\frac{1}{\gamma RT}\right)_{i,j\text{-}1} \tag{4.56}$$

$$A^p_p = \left[\frac{1}{\overline{(\,A_p\text{-}\Sigma A_{nb}\,)}}\right]_{i+1/2,j} (\,a^2_{11} + a^2_{12}\,)_{i+1/2,j} \; \rho_{i+1/2,j}$$
$$+ \left[\frac{1}{\overline{(\,A_p\text{-}\Sigma A_{nb}\,)}}\right]_{i\text{-}1/2,j} (\,a^2_{11} + a^2_{12}\,)_{i\text{-}1/2,j} \; \rho_{i\text{-}1/2,j}$$
$$+ \left[\frac{1}{\overline{(\,A_p\text{-}\Sigma A_{nb}\,)}}\right]_{i,j+1/2} (\,a^2_{21} + a^2_{22}\,)_{i,j+1/2} \; \rho_{i,j+1/2}$$
$$+ \left[\frac{1}{\overline{(\,A_p\text{-}\Sigma A_{nb}\,)}}\right]_{i,j\text{-}1/2} (\,a^2_{21} + a^2_{22}\,)_{i,j\text{-}1/2} \; \rho_{i,j\text{-}1/2}$$
$$+ \; U^*_{i+1/2,j} (\,1 - fx_{i+1/2,j}\,) \left(\frac{1}{\gamma RT}\right)_{i,j} \; - \; U^*_{i\text{-}1/2,j} \, fx_{i\text{-}1/2,j} \left(\frac{1}{\gamma RT}\right)_{i,j}$$
$$+ \; V^*_{i,j+1/2} (\,1 - fy_{i,j+1/2}\,) \left(\frac{1}{\gamma RT}\right)_{i,j} \; - \; V^*_{i,j\text{-}1/2} \, fy_{i,j\text{-}1/2} \left(\frac{1}{\gamma RT}\right)_{i,j} \tag{4.57}$$

$$S^M = - \, [\, (\rho^* U^*)_{i+1/2,j} - (\rho^* U^*)_{i\text{-}1/2,j} + (\rho^* V^*)_{i,j+1/2} - (\rho^* V^*)_{i,j\text{-}1/2} \,] \tag{4.58}$$

$$S^{NO} = \left[\frac{\rho}{\overline{A_p - \Sigma A_{nb}}}\right]_{i+1/2,j} (\,a_{11}\,a_{21} + a_{12}\,a_{22}\,)_{i+1/2,j} \left(\frac{\partial P'}{\partial \eta}\right)_{i+1/2,j}$$

$$-\left[\frac{\rho}{A_p - \Sigma A_{nb}}\right]_{i-1/2,j}(a_{11}\,a_{21} + a_{12}\,a_{22})_{i-1/2,j}\left(\frac{\partial P'}{\partial \eta}\right)_{i-1/2,j}$$

$$+\left[\frac{\rho}{A_p - \Sigma A_{nb}}\right]_{i,j+1/2}(a_{21}\,a_{11} + a_{22}\,a_{12})_{i,j+1/2}\left(\frac{\partial P'}{\partial \xi}\right)_{i,j+1/2}$$

$$-\left[\frac{\rho}{A_p - \Sigma A_{nb}}\right]_{i,j-1/2}(a_{21}\,a_{11} + a_{22}\,a_{12})_{i,j-1/2}\left(\frac{\partial P'}{\partial \xi}\right)_{i,j-1/2} \qquad (4.59)$$

4.3. General Scalar Equation

After the momentum and continuity equations are solved, the solution to the scalar variables (k, ε, Y_{FU}, etc.) must be obtained. Since the scalar variables are stored at the cell centers along with the Cartesian velocity components, the discretized equation for u and v also serves as the discrete equation governing the distribution of any flow variable. Only the diffusive exchange coefficient and the source term will change for the solution to any particular flow variable. The exchange coefficients and source terms for the various scalar quantities used in the present numerical algorithm are given in Table 1.

In solving for the scalar variables, it was necessary to employ source term linearization (Patankar, 1980). All portions of the source terms which were positive were retained on the right hand side of the discrete equation. All negative quantities in the source term were taken to the left hand side of the discrete equation and incorporated into the central coefficient (A_p). This practice was found to be vitally important in ensuring that turbulent kinetic energy and turbulent dissipation rate not become negative.

4.4. Solution Procedure Summary

As mentioned previously, the solution procedure employed involves a sequential solution of various flow variables. Figure 4 presents the steps taken in obtaining a

54

converged solution to a given flow problem. The procedure involves solving for the Cartesian velocity components u and v. The pressure correction equation is then solved with a subsequent correction of the relevant flow variables (u, v, U, V, and P). The scalar variables are solved next. The order in which the scalars are solved is as follows:

* Swirl Velocity Component (w)

* Turbulent Kinetic Energy (k)

* Turbulent Dissipation Rate (ε)

* Mixture Fraction (f)

* Fuel Mass Fraction (Y_{fu})

* Concentration Fluctuation (g)

* Stagnation Enthalpy (h_o)

The final step in the iterative sequence involves an update of thermodynamic and transport properties.

The solution of any particular flow variable involves the solution of a set linear algebraic equations. An alternating direction implicit (ADI) method has been used for this purpose. The ADI uses a tridiagonal matrix algorithm (TDMA) to obtain a direct solution to all variables at a given ξ coordinate location (Anderson, et. al., 1984). After sweeps are performed in the ξ direction, a similar procedure is performed in the η direction. A certain number of sweeps through the ADI was performed for each flow variable. In general, 5 sweeps were used for the velocity components and scalars while 10-20 sweeps were used for the pressure correction.

In testing the present solution procedure, it was found beneficial to apply integral mass adjustments to the cell face fluxes for some flow problems. Two forms of implementation of the integral mass adjustment were tested. One procedure follows from the work of Patankar and Spalding, 1972 and involves adding a constant correction to all the contravariant velocities in a given plane so as to satisfy continuity. The pressure was also

55

corrected so as to reflect the change in the mass flux. The second procedure involved scaling the fluxes at a given downstream plane so that the total mass flow rate through the upstream and downstream planes was identical.

$$\left[\sum_{j=2}^{ny+1}(\rho U)_{i-1j}\right] + (\rho V)_{i,1} + (\rho V)_{i,ny+1} = \alpha\left[\sum_{j=2}^{ny+1}(\rho U)_{ij}\right] \qquad (4.\,60)$$

The factor α was calculated at a given plane based on the estimated mass flux through that plane. All fluxes were then multiplied or scaled by the factor α so as to satisfy integral mass conservation. A corresponding pressure correction was subsequently added to all the pressures on the downstream side of the given plane.

$$-\Delta P = \frac{\dot{m} - \sum_{j=2}^{ny+1}(\rho U)_{ij}}{\sum_{j=2}^{ny+1}\left[\dfrac{\rho\,(a_{11}^2 + a_{12}^2)}{A_p - \Sigma A_{nb}}\right]} \qquad (4.\,61)$$

By applying the integral mass adjustments to all the planes perpendicular to the main flow direction, overall mass conservation is satisfied.

Through tests of the computational procedure, it was found that the second method of integral mass adjustment worked better. This is presumably due to the fact that the addition of a correction to a given flux may cause it to change sign. Such an occurence would not be valid in a region of flow reversal. Further observations as regards integral mass adjustments and on the solution procedure as a whole are presented in the following chapter.

CHAPTER 5: EVALUATION OF NUMERICAL METHOD

It is essential to know the applicability and efficiency of any flowfield simulation. The applicability is assessed by the accuracy of predictions made with the simulation. The efficiency is gauged in part by the convergence rate and how it is affected by such factors as cell aspect ratio, grid density, grid distribution, and flow Reynolds number. The evaluation of the present simulation of turbulent reacting flow is made by comparing its predictions with experimental results found in the literature. Six flow configurations have been considered in evaluating the numerical simulation: developing turbulent flow in a straight pipe, turbulent flow in an axisymmetric sudden expansion, laminar diffusion flame, turbulent diffusion flame, turbulent premixed flame, and turbulent swirl flow in an axisymmetric sudden expansion. The flowfield predictions are compared with experimental results. Conclusions are made concerning the behavior of the numerical simulation so as to assess the efficiency and applicability of simulating turbulent reacting flows with the solution procedure.

5.1. Turbulent Pipe Flow

The developing turbulent flow in a pipe of circular cross section has been calculated using the numerical algorithm. The results of the computations have been compared with the experiments of Richman and Azad (Richman and Azad, 1973) and C. J. Lawn (Martinuzzi and Pollard, 1989). For the purpose of calculating the flowfield, the pipe was taken to be 40 units long with a radius of 0.5 units.

The calculation was made by assuming the existence of a uniform velocity profile at the pipe inlet. The inlet conditions for turbulent kinetic energy and dissipation rate were also given as uniform at values of $0.005 \, U^2$ and ($C_\mu k^{3/2} / 0.03R$) respectively (Martinuzzi and

Pollard, 1989). Since the flow was axisymmetric, the computational domain consisted of an axis of symmetry at the lower boundary and a wall at the upper boundary. A fully developed flow for all flow variables was prescribed at the outflow plane. The use of the hybrid differencing scheme however, does not allow the information at the outflow plane to propagate into the inner flow domain. The outflow boundary condition is thus one of parabolic flow (Patankar, 1980).

The comparison of experimental and numerically obtained mean velocity profiles for a Reynolds number of 300,000 is given in Figures 5 through 9. The mean streamwise velocity component (u) has been non-dimensionalized with the bulk velocity (U) and has been plotted as a function of the radius ratio (R is the pipe radius). The calculation has been performed using an 80 x 40 grid. The cell size in the axial direction up to x/D of 2 was given as 0.35 while the cell size thereafter was equal to 0.5. Therefore, only slight concentration of the mesh in the inlet region was utilized. It is observed that the calculation overpredicts experiment in the region close to the wall. The discrepancy is seemingly due to insufficient grid resolution in the axial direction. The calculated velocity profiles do progress toward the fully developed condition. The distance over which this development occurs (entrance length) is overpredicted with the use of an 80 x 40 grid. The comparison reveals that the discrepancy diminishes as the flow develops (Figure 9). The use of 80 cells in the axial direction is not entirely sufficient to capture the steeper gradients in mean flow velocity which occur in the inlet due to the merging boundary layers. A non-uniform grid with increased mesh concentration in the inlet region may prove more appropriate.

The streamwise velocity development at a given radius is seen in Figures 10 through 12. These results are consistent with the high Reynolds number k - ε model prediction given by Martinuzzi and Pollard, 1989. The prediction is observed to be better in the core than in the near wall region.

The dimensionless turbulent kinetic energy comparison given in Figure 13 is quite good (u* is the friction velocity). The experimental data are for fully developed turbulent pipe flow while the numerical results are for x/D equal to 40. The mild difference observed may be due to the fact that x/D equal to 40 may not be fully developed for a Reynolds number of 380,000 and hence the numerical results presented are not for fully developed flow. These results are comparable to those obtained by Martinuzzi and Pollard, 1989 for a high Reynolds number k-ε model.

These results reveal that the numerical algorithm presented can be used to predict not just the qualitative features of turbulent pipe flow but the quantitative features as well. The quantitative accuracy however, is dependent upon a sufficient resolution of the computational grid.

5.2. Turbulent Flow in an Axisymmetric Sudden Expansion

The experiments of Craig, et. al., 1984 are used for comparative purposes. The geometry considered is that of an axisymmetric sudden expansion of area ratio 3.57. The flow Reynolds number at the inlet was 86,293. Experimental data was obtained using a laser doppler velocimeter with consideration given to the velocity biasing which occurs (Craig, et. al., 1984). Further details of the experiment and the procedures followed are given by Craig, et. al., 1984.

The simulation of the flow in the sudden expansion was considered to be axisymmetric. This assumption is supported by the experimental findings (Craig, et. al., 1984). It was further assumed that the flow was time mean steady. The lower boundary of the computational grid (Figure 51) is thus specified as a symmetry boundary. The inlet velocity was specified as being uniformly distributed at 27 m/s. The inlet profiles of turbulent kinetic energy and turbulent dissipation rate were likewise prescribed as uniform.

The turbulent kinetic energy was given as 0.0009 U_{IN}^2 and the dissipation rate at 1.2(10^{-5}) in accordance with the simulation of Vanka, 1988. The outflow plane was placed at a distance of 16H (H is the step height) from the step. The flow at the outlet was considered to be fully developed as described in a previous chapter.

The comparison of experimental and calculated profiles for the mean velocity and turbulent kinetic energy reveal a good qualitative agreement (Figures 14 to 21). The most notable disparities in experimental and calculated profiles occur in two regions, in the recirculation region behind the expansion and near the exit of the combustor.

The mean velocity profile at x/H equal to 13.5 is overpredicted for the use of 40 x 20 and 50 x 30 grids (Figure 17). The calculation on a 60 x 40 grid resulted in a similar result even with further grid refinement in the vicinity of the combustor exit.

Quantitative disagreement is also observed in the flow recirculation region behind the step. In fact, the qualitative agreement is erroneous. The experiment shows an increase in reverse flow velocity behind the step (Figure 14). The reverse flow velocity subsequently decreases as the edge of the shear layer is reached. The calculation on all three grids reveals a monotonic decrease in the magnitude of the reverse flow velocity. This observation was also made by Obi, et. al., 1991 when a k-ε turbulence model was used. They did not observe this disagreement for use of a second moment closure.

The profiles of turbulent kinetic energy all reveal that the simulation underpredicts this quantity (Figure 18 to 21). The predicted profiles of turbulent kinetic energy reveal that radial diffusion of k does not occur soon enough along the axis of the duct. Even at x/H equal to 7.8 (Figure 20), the centerline turbulent kinetic energy is still approximately zero. The experimental results are seen to exhibit more diffusive effects than the calculation.

Figure 22 gives the convergence histories corresponding to the three grids used in the simulation. The solutions were assumed to be converged when the mass residual was reduced by 5 orders of magnitude. As expected, finer meshes result in more iterations to

60

reach convergence. These calculations were made without considering the non-orthogonal terms in the pressure correction equation. Inclusion of these terms may result in a slightly better convergence. Also, the harmonic mean determination for cell face values of exchange coefficient was not used. In the context of a non-orthogonal grid, it led to convergence difficulties and in some instances divergence.

The convergence rates given are for varying relaxation factors. The solution on finer grids required more relaxation in general. The relaxation factors for velocity, pressure, and turbulence quantities were 0.7, 1.0, and 0.8 for use of a 40 x 20 grid, 0.7, 0.9, and 0.7 for the 50 x 30 grid, and 0.6, 0.5, 0.6 for the calculation on the 60 x 40 grid.

5.3. Laminar Diffusion Flame

The usefulness of the one step infinite rate chemistry assumption for modelling laminar diffusion flames was assessed by simulating the experiment of Mitchell, et. al., 1980. The flow configuration involved a confined laminar methane diffusion flame. The overall equivalence ratio was approximately 0.3. Radial profiles of temperature, velocity, and specie mole fraction were obtained at various axial locations. Comparison with these results gives an indication of the accuracy of the present numerical simulation.

The geometry for the given problem is a simple pipe. The flow was assumed to be axisymmetric. Inlet velocity profiles for both the fuel and the air were taken to be uniform. The fuel velocity was specified at 4.5 cm/s and the air at 9.88 cm/s. The outflow plane was specified at 13 tube diameters (13D) from the inlet. The flow was assumed to be fully developed at this location.

The simulation used an 80 x 46 grid. The grid was refined near the inlet so as to better resolve the physics of the flame. Also, the simulation utilized the harmonic mean for

61

interpolating the laminar viscosity. A laminar Schmidt number of unity was used in the simulation.

Figures 23 through 25 reveal a qualitatively good agreement with experiment. The calculated temperatures are greater that experiment due to radiation and finite rate effects. The fuel mole fraction profiles (Figure 29 and 30) show that the flame width is captured well. Consideration of fuel pyrolysis in the numerical simulation would improve the prediction of fuel mole fraction. The fast chemistry model tacitly assumes that all unreacted carbon is bound up in the fuel. In reality, this not the case (Mitchell, et. al., 1980). Figures 31a and b give color contours of temperature and velocity. The flame shape as well as the predicted outer flow recirculation are readily apparent.

The predicted velocity profiles all agree well with experiment (Figures 26 to 28). The outer flow recirculation was also captured by the simulation (Figure 31b). The presence of the recirculation region was the reason for use of such a long calculation domain. Placement of the outflow boundary in the region of the recirculation region would be an ill-prescribed boundary condition and would most likely lead to divergence of the numerical procedure.

5.4. Turbulent Diffusion Flame

The turbulent diffusion flame studied by Lewis and Smoot, 1981 was analyzed using the present solution procedure. The experiment which was simulated involved the issuing of coaxial jets of fuel and air into an axisymmetric sudden expansion. The fuel used in the experiment was a mixture of methane and ethane. The momentum ratio of air to fuel was 1.18 and the air-fuel ratio was 12.78. The overall equivalence ratio was approximately 1.12. The air and fuel were injected into the combustor at different temperatures. The inlet temperature of the fuel was 300 K while that of the air was at 589 K. A comprehensive

description of the experimental rig and an analysis of experimental results can be found in Lewis and Smoot, 1981.

The numerical simulation of the turbulent diffusion flame utilized two different grids, a 40 x 20 grid and a 60 x 30 grid. A representative 40 x 10 grid is given is Figure 32. The grid was concentrated in the region between the fuel and air streams so as to obtain some measure of resolution of the shear layer between these two flowing streams. Such a resolution resulted in rather large cell aspect ratios in the downstream portion of the combustor ($\Delta x/\Delta y = 100$). The large aspect ratio did not however pose a problem in obtaining reasonable convergence for this flow.

The inlet air and fuel streams were assumed to have uniform velocity, turbulent kinetic energy, and turbulent dissipation rate profiles. A turbulent intensity of six percent was assumed for both streams. The turbulent length scale for the fuel was given as five percent of the jet diameter. The turbulent length scale for the air stream was assumed to be ten percent of the annular separation distance (i.e. $0.1(r_o - r_i)$). The numerical solution of the flow was assumed converged when the mass residual was reduced 4 orders of magnitude.

The comparisons of experimental and calculated temperature profiles at various axial locations (given by x/D where D is the diameter of the combustor) are given in Figures 33 to 35. The predicted temperatures are consistently larger than those given by experiment. The 60 x 30 grid is seen to yield better results. For x/D of 0.47, the temperature profiles are discontinuous. Sharp temperature gradients are possible for laminar flames but are not observed in the mean flowfield of a turbulent flow. Turbulent fluctuations act to diffuse such features for turbulent flows. This rather curious behavior is the result of the double delta function pdf. Jones and Whitelaw, 1982 found that a double delta function pdf can yield discontinuities in the weighted temperature field. Similar observations have been made by other researchers studying boundary layer diffusion flames (Chen, et. al., 1991). The calculated temperature profiles indicate that the temperature increases nearer the walls

and with distance along the combustion chamber. The experimental observations indicate a similar behavior except at x/D of 2.34. The temperature data at this location were not corrected for conduction and radiation losses. It is not clear how influential this is in making comparisons of experiment and calculation.

The calculated profiles of mean mixture fraction given in Figures 36 through 39 give reasonable agreement with experiment. The mixture fraction decreases with increase in radius and with distance along the duct. This is consistent with the increase in temperature in these regions. The form of the pdf does not lead to discontinuities in the mean mixture fraction. This was also observed by Chen, et. al., 1991 for a turbulent boundary layer diffusion flame.

The convergence rates corresponding to the calculations performed in this simulation are given in Figure 40. The 60 x 30 grid calculation exhibits some initial oscillations but is still convergent. The oscillations may be the result of high under relaxation (0.7 for all variables except pressure which was not relaxed). The calculations presented did not use a harmonic mean for interpolating the exchange coefficient. Use of a harmonic mean was detrimental to convergence rate (1200 iterations to converge the 60 x 30 grid) and was not observed to improve the calculation in this case.

5.5. Turbulent Premixed Flame

The model of turbulent premixed flames was assessed by comparisons with data obtained from the flow in a sudden expansion dump combustor of area ratio equal to 2.25. A propane/air mixture of equivalence ratio 0.65 was fed into an axisymmetric sudden expansion. The inlet Reynolds number was approximately 128,000 and the flow Mach number was quite low at 0.05. The inlet flow to the combustion chamber was experimentally observed to be axisymmetric.

64

The flow was simulated on two different grids, a 50 x 20 and a 60 x 30 grid. The grid structure was refined in the near wall regions so as to better resolve the large flow gradients. The inlet velocity and kinetic energy were specified according to the experimental data. Since the azimuthal fluctuations could not be obtained, it was assumed that the turbulence at the inlet was isotropic. Therefore,

$$\overline{w'w'} = 1/2 \, (\, \overline{u'u'} + \overline{v'v'} \,) \tag{5.1}$$

The turbulent kinetic energy at the inlet was thus determined as follows:

$$k = 3/4 \, (\, \overline{u'u'} + \overline{v'v'} \,) \tag{5.2}$$

The turbulence dissipation rate, ε at the inlet was determined from the following relation:

$$\varepsilon = \frac{C_\mu \, k^{3/2}}{L_T} \tag{5.3}$$

The distribution of the turbulent length scale was obtained from Schlichting, 1979 for a fully developed pipe flow:

$$L_T = R \, [\, 0.14 - 0.08 \, (\, 1 - \frac{y}{R})^2 - 0.06 \, (\, 1 - \frac{y}{R})^4 \,] \tag{5.4}$$

The turbulent length scale was so specified so as to minimize arbitrariness in the specification of the boundary conditions for the turbulence quantities. All calculations of the turbulent premixed flame were presumed to be converged when the mass residual was reduced by five orders of magnitude.

The results for the mean velocity profiles imply that the core region is predicted to be essentially inviscid (Figures 41 to 44, where H is the step height). The uniform velocity

distribution corresponds to a predicted uniform distribution of the turbulent kinetic energy (Figures 46 to 49). Apparently, the production of turbulence kinetic energy from the shear layer has not been given sufficient opportunity to diffuse radially for the axial locations near the inlet (i.e., x/H = 2, x/H = 8). With distance along the combustor axis, the mean velocity is underpredicted (Figures 43 and 44). The velocity distribution at x/H equal to 18 seems to imply that the combustion is occurring primarily at the wall. This is clearly seen in the temperature contours given in Figure 45. The higher temperatures at the wall lower the fluid density and thus the velocity increases to satisfy the continuity constraint. The experimental results clearly indicate a greater velocity at the wall than at the centerline (Figure 44).

The profiles of the turbulent kinetic energy (Figures 46 through 49) reveal the region of high turbulence production caused by the shear layer between the core flow and recirculating flow. The turbulent kinetic energy as given in Figure 46 clearly reveals the region of maximum turbulence intensity as obtained from prediction. The turbulence kinetic energy is predicted to dissipate with length along the combustor whereas the experiment reveals a substantial increase in turbulence kinetic energy. This increase is seen to be extremely large at x/H equal to 18 (Figure 49). The region in which k increases the most is near the combustor wall. It is also within this region where most of the combustion seems to be occurring. The underprediction in the turbulent kinetic energy may therefore stem from the assumption of constant density flow which was invoked in the development of the turbulence model.

The convergence histories given in Figure 50 show that the calculation of turbulent reacting flow is convergent. The calculation on a 50 x 20 grid used a relaxation of 0.7 on all variables except pressure. Pressure was not relaxed for this case. The calculation on a 60 x 30 grid also used a relaxation of 0.7 on all variables except the pressure. For the 60 x 30 grid calculation, the pressure relaxation factor was 0.8. When compared to the

convergence histories for the isothermal turbulent sudden expansion flow (Figure 22), it is obvious that a variable density flow requires much more computational effort.

5.6. Turbulent Swirl Flow in an Axisymmetric Sudden Expansion

The results of a turbulent swirl flow prediction are very sensitive to the prescribed inlet conditions (Nallasamy and Chen, 1985). Without proper knowledge of all variables at the inlet, predictions may differ substantially from the experimental results (Abujelala and Lilley, 1983). The present calculation has been made in order to demonstrate that the solution procedure is convergent for calculations made for turbulent swirling flows. The accuracy of the prediction is a function of the turbulence model, accuracy of the discretization, and the correctness of the prescribed inlet conditions.

The experimental results of Nejad, et. al., 1989 were used for comparative purposes. The inlet flow Reynolds number was 125,000 and the swirl number was 0.3. In the experimental setup, the swirler was positioned upstream of the dump plane at a distance equivalent to the inlet pipe radius. The flow field was probed for velocities and turbulent fluctuations using a two-component four-beam laser doppler velocimeter. Further details regarding the experimental setup and the results obtained from the experiment are to be found in Nejad, et. al., 1989.

The flowfield simulation of the turbulent swirling flow was made using two different grids: a 50 x 20 and a 60 x 40 grid. The 50 x 20 grid is given in Figure 51. Note that the grid structure is non-orthogonal. It was desired to know what effect the non-orthogonality would have on the convergence rate for a swirling flow calculation.

The inlet boundary plane was selected to be just downstream of the swirler. It was assumed that the flow from the swirler was essentially a solid body rotation (Abujelala and Lilley, 1983). The radial component of velocity was assumed to be zero. The inlet axial

67

velocity was specified as uniform as were the distributions of turbulent kinetic energy and dissipation rate. The inlet turbulence intensity was assumed to be six percent and the turbulent length scale was specified as equal to ten percent of the inlet radius.

Figures 52 to 56 show the axial velocity profiles at various axial locations (H is the step height). The comparison is fairly good in the inlet region (x/H = 4). The flow development however is not well predicted. The experimental results reveal that the flow at x/H equal to 18 is essentially a solid body rotation (see Figure 56 and 61). The experimentally obtained axial velocity profile is seen to be essentially uniform (Figure 56) while the swirl velocity varies linearly with radius (Figure 61). The predictions of turbulent kinetic energy are qualitatively correct near the inlet (Figure 62), but do not develop in the same manner as the experimentally obtained values. Near the combustor exit, the experiment reveals an essentially constant turbulent kinetic energy whereas the prediction varies substantially with radius (Figure 66).

The convergence histories for the calculations made on 50 x 20 and 60 x 40 grids are given in Figure 67. The relaxation factors used for the 50 x 20 calculation were: 0.7 for u and v, 1.0 for pressure, 0.5 for the swirl velocity, and 0.8 for turbulence variables k, ε, and μ_T. The relaxation factors used for the 60 x 40 calculation were: 0.5 for u and v, 0.6 for pressure, 0.3 for the swirl velocity, and 0.7 for turbulence variables k, ε, and μ_T. The solution was seen to be convergent for both calculations. As in other calculations using non-orthogonal grids, use of a harmonic mean for interpolation led to convergence difficulties. In some cases, an otherwise convergent solution would diverge if the harmonic mean was used.

CHAPTER 6: SUMMARY AND RECOMMENDATIONS

A numerical algorithm for simulating turbulent reacting flows has been developed. The method is based on the solution of the Favre averaged equations which govern a turbulent reacting flow. To obtain closure of the governing equations, the algorithm employs the standard k-ε model with wall functions (Launder and Spalding, 1974). Combustion models appropriate for diffusion and premixed flames have been incorporated into the algorithm. The model for diffusion flames assumes mixing limited combustion and uses a double-delta function pdf for the determination of the mass fraction, temperature, and density distributions. The model for premixed flames also assumes a mixing limited combustion process. An eddy break up model of the form proposed by Magnussen and Hjertager, 1976 is used to relate the average reaction rate to the mean flow variables.

The governing equations are solved numerically by using a finite volume method based on a non-staggered grid for velocities and pressure (Rodi, et. al., 1987). The use of a non-staggered grid eliminates the use of grid sensitive curvature terms. The governing equations are written in terms of non-orthogonal curvilinear coordinates (i.e. body fitted coordinates) and are discretized using the hybrid differencing scheme. A decoupled or segregated solution procedure has been adopted for the solution of the set of equations which govern a turbulent reacting flow.

Tests of the flowfield simulation technique reveal that the major shortcomings are in the mathematical models which are used to close the governing equations. Observations concerning the k-ε turbulence model are consistent with the findings of other researchers (Martinuzzi and Pollard, 1989). Fully developed pipe flow and to some extent sudden expansion flows are adequately predicted with a k-ε model. Turbulent swirl flows are not well described by the standard k-ε turbulence model.

Simulation of a turbulent diffusion flame reveals the inadequacy of a double delta function pdf. Discontinuities in the temperature profiles are clearly unphysical for this flow. The calculation of a turbulent premixed flame in an axisymmetric sudden expansion resulted in reasonable qualitative comparisons with the experimental mean velocity profiles. Turbulent kinetic energy was not successfully predicted. Possibly this is due to simplifications made in the equations for k and ε.

The solution procedure itself was found to be convergent for all tests considered. Proper source terms linearization was found to be an imperative for obtaining convergence. The use of a harmonic mean for interpolating the exchange coefficient was adopted for some tests but was found to be detrimental to the convergence rate.

The pressure correction equation implemented in the present algorithm is appropriate for coordinate systems which are non-orthogonal. Retention of the non-orthogonal terms in the pressure correction equation was found to improve the convergence behavior of the algorithm for grids exhibiting significant grid skewness (Peric, 1990). Although use of highly non-orthogonal grids is not advisable due to loss of accuracy (Fletcher, 1988b), it is unavoidable for some cases. In such instances, the use of the full pressure correction equation will remain convergent.

Based on the results obtained from tests of the numerical algorithm, it is recommended that only low Mach number flows be simulated with the present procedure. Issues and questions relevant to finite rate effects in combustion systems cannot be addressed with the present numerical algorithm. Further improvements of the present procedure will involve increasing the accuracy of the discretization procedure and implementing a multi-grid based algorithm. In the tests of the present method, clear evaluations of the models used could not be made without considering grid dependencies. By incorporating a high order accurate scheme and using a multi-grid method for fine grid calculations, it is hoped that the grid dependency issue can be resolved. In this way, an efficient and accurate numerical

method will be available for testing the strengths and weaknesses of various physical models and for simulating the flow and combustion processes in modern combustion chambers.

REFERENCES

Abujelala, M. T. and Lilley, D. G. (1983). " Confined Swirling Flow Predictions ". AIAA-83-0316. January 1983.

Acharya, S. and Moukalled, F. H. (1989). " Improvements to Incompressible Flow Calculation on a Nonstaggered Curvilinear Grid ". Numerical Heat Transfer. Vol. 15. pp. 131-152.

Ahmed, S. A. and Nejad, A. S. (1990). " Premixed, Turbulent Combustion of Axisymmetric Sudden Expansion Flows ". International Journal of Heat and Fluid Flow. to appear.

Anderson, Dale A., Tannehill, John C., and Pletcher, Richard H. (1984). Computational Fluid Mechanics and Heat Transfer. Hemisphere Publishing Company.

Bilger, R. W. (1975). " A Note on Favre Averaging in Variable Density Flows ". Combustion Science and Technology. Vol. 11. pp. 215-217.

Bilger, R. W. (1980). " Turbulent Flows with Nonpremixed Reactants ". in Turbulent Reacting Flows. eds. P. A. Libby and F. A. Williams. pp. 65-113. Springer-Verlag. Berlin.

Bilger, R. W. (1989). " Turbulent Diffusion Flames ". Annual Review of Fluid Mechanics. Vol. 21. pp. 101-135.

Bray, K. N. C. (1980). " Turbulent Flows with Premixed Reactants ". in Turbulent Reacting Flows. eds. P. A. Libby and F. A. Williams. pp. 115-183. Springer-Verlag. Berlin.

Burmeister, Louis C. (1983). Convective Heat Transfer. John Wiley and Sons, Inc. New York.

Chen, C. H., Lan, C. Y., and Shan, D. Y. (1991). " Turbulent Boundary Layer Diffusion Flame: Effects of Probability Density Function ". AIAA Journal. Vol. 29. No. 3. pp. 371-379.

Correa, S. M. and Shyy, W. (1987). " Computational Models and Methods for Continuous Gaseous Turbulent Combustion ". Progress in Energy and Combustion Science. Vol. 13. pp. 249-292.

Craig, R. R., Nejad, A. S., and Schwartzkopf, K. G. (1984). " A General Approach for Obtaining Unbiased LDV Data in Highly Turbulent Non-Reacting and Reacting Flows ". AIAA-84-0366. January, 1984.

Demirdzic, I., Issa, R. I., and Lilek, Z. (1990). " Solution Method for Viscous Flows at All Speeds in Complex Domains ". Proceedings of the 8th GAMM conference on Numerical Methods in Fluid Mechanics. pp. 89-98.

Edelman, R. B., and Harsha, P. T. (1978). " Laminar and Turbulent Gas Dynamics in Combustors - Current Status ". Progress in Energy and Combustion Science. Vol. 4. pp. 1-62.

Fletcher, C. A. J. (1988a). Computational Techniques for Fluid Dynamics. Vol. 1. Springer-Verlag. Berlin.

Fletcher, C. A. J. (1988b). Computational Techniques for Fluid Dynamics. Vol. 2. Springer-Verlag. Berlin.

Galpin, P. F., VanDoormaal, J. P., and Raithby, G. D. (1985). " Solution of the Incompressible Mass and Momentum Equations by Application of a Coupled Equation Line Solver ". International Journal for Numerical Methods in Fluids. Vol. 5. pp. 615-625.

Gordon, Sanford and McBride, Bonnie J. (1976). " Computer Program for Calculation of Complex Chemical Equilibrium Compositions, Rocket Performance, Incident and Reflected Shocks, and Chapman-Jouguet Detonations ". NASA-SP-273. March 1976.

Hogg, Robert V. and Ledolter, Johannes. (1987). Engineering Statistics. MacMillan Publishing Company. New York.

Hwang, Y. H. and Liou, T. M. (1991). " Expressions for k and ε Near Walls ". AIAA Journal. Vol. 29. No. 3. pp. 477-479.

Issa, R. I., and Lockwood, F. C. (1977). " On the Prediction of Two Dimensional Supersonic Viscous Interactions Near Walls ". AIAA Journal. Vol. 15. No. 2. pp. 182-188.

Jachimowski, Casimir J. (1984). " Chemical Kinetic Reaction Mechanism for the Combustion of Propane ". Combustion and Flame. Vol. 55. pp. 213-224.

Jones, W. P. and Whitelaw, J. H. (1982). " Calculation Methods for Reacting Turbulent Flows: A Review ". Combustion and Flame. Vol. 48. pp. 1-26.

Joshi, D. S. and Vanka, S. P. (1990). " A Multigrid Calculation Procedure for Internal Flows in Complex Geometries ". AIAA-90-0442. January 1990.

Jou, W. H., and Riley, James J. (1989). " Progress in Direct Numerical Simulations of Turbulent Reacting Flows ". AIAA Journal. Vol. 27. No.11. pp. 1543-1556.

Karki, K. C. and Patankar, S. V. (1988). " A Pressure Based Calculation Procedure for Viscous Flows at All Speeds in Arbitrary Configurations ". AIAA-88-0058. January 1988.

Kobayashi, M. H. and Pereira, J. C. F. (1991). " Calculation of Incompressible Laminar Flows on a Nonstaggered, Nonorthogonal Grid ". Numerical Heat Transfer. Vol. 19. pp. 243-262.

Kuo, Kenneth K. (1986). Principles of Combustion. John Wiley and Sons, Inc. New York.

Launder, B. E. and Spalding, D. B. (1974). " The Numerical Computation of Turbulent Flows ". Computer Methods in Applied Mechanics and Engineering. Vol. 3. pp. 269-289.

Leonard, B. P. (1979). " A Stable and Accurate Convective Modelling Procedure Based on Quadratic Upstream Interpolation ". <u>Computer Methods in Applied Mechanics and Engineering</u>. Vol. 19. pp. 59-98.

Lentini, D. (1990). " Numerical Prediction of Nonpremixed Turbulent Flames ". AIAA-90-0730. January 1990.

Lewis, M. H. and Smoot, L. D. (1981). " Turbulent Gaseous Combustion. Part I: Local Species Concentration Measurements ". <u>Combustion and Flame</u>. Vol. 42. pp. 183-196.

Libby, P. A., and Williams, F. A. (1980). " Fundamental Aspects ". in <u>Turbulent Reacting Flows</u>. eds. P. A. Libby and F. A. Williams. pp. 1-43. Springer-Verlag. Berlin.

Lockwood, F. C. (1977). " The Modelling of Turbulent Premixed and Diffusion Combustion in the Computation of Engineering Flows ". <u>Combustion and Flame</u>. Vol. 29. No. 2. pp. 111-122.

Lockwood, F. C. and Naguib, A. S. (1975). " The Prediction of the Fluctuations in the Properties of Free, Round-Jet, Turbulent, Diffusion Flames ". <u>Combustion and Flame</u>. Vol. 24. pp. 109-124.

Magnussen, B. F. and Hjertager, B. H. (1976). " On Mathematical Modelling of Turbulent Combustion with Special Emphasis on Soot Formation and Combustion ". Sixteenth Symposium (International) on Combustion. pp. 719-729.

76

Majumdar, S. (1988). " Role of Underrelaxation in Momentum Interpolation for Calculation of Flow with Nonstaggered Grids ". Numerical Heat Transfer. Vol. 13. pp. 125-132.

Maliska, C. R. and Raithby, G. D. (1984). " A Method for Computing Three-Dimensional Flows using Non-Orthogonal Boundary Fitted Coordinates ". International Journal for Numerical Methods in Fluids. Vol. 4. pp. 519-537.

Martinuzzi, R. and Pollard, A. (1989). " Comparative Study of Turbulence Models in Predicting Turbulent Pipe Flow. Part I: Algebraic Stress and k-ε Models ". AIAA Journal. Vol. 27. No. 1. pp. 29-36.

Menon, Suresh, and Jou, Wen-Huei (1991). " Large-Eddy Simulations of Combustion Instability in an Axisymmetric Ramjet Combustor ". Combustion Science and Technology. Vol. 75. pp. 53-72.

Miller, T. F. and Schmidt, F. W. (1988). " Use of a Pressure Weighted Interpolation Method for the Solution of the Incompressible Navier-Stokes Equations on a Nonstaggered Grid System ". Numerical Heat Transfer. Vol. 14. pp. 213-233.

Mitchell, R. E., Sarofim, A. F., and Clomburg, L. A. (1980). " Experimental and Numerical Investigation of Confined Lmainar Diffusion Flames ". Combustion and Flame. Vol. 37. pp. 227-244.

Moin, P., and Kim, J. (1982). " Numerical Investigation of Turbulent Channel Flow ". Journal of Fluid Mechanics. Vol. 118. pp. 341-377.

Nallasamy, M. and Chen, C. P. (1985). " Studies of Effects of Boundary Conditions in Confined Turbulent Flow Predictions ". NASA-CR-3929. September 1985.

Nallasamy, M. (1987). " Turbulence Models and Their Applications to the Prediction of Internal Flows: A Review ". Computers and Fluids. Vol. 15. No. 2. pp. 151-194.

Nejad, A. S., Vanka, S. P., Favaloro, S. C., Samimy, M. , and Langenfeld, C. A. (1989). " Application of Laser Velocimetry for Characterization of Confined Swirling Flow ". Journal of Engineering for Gas Turbines and Power. Vol. 111. pp. 36-45.

Obi, S., Peric, M., and Scheuerer, G. (1991). " Second Moment Calculation Procedure for Turbulent Flows with Collocated Variable Arrangement ". AIAA Journal. Vol. 29. No. 4. pp. 585-590.

Patankar, S. V. (1980). Numerical Heat Transfer and Fluid Flow. Hemisphere Publishing Company.

Patankar, S. V. and Spalding, D. B. (1972). " A Calculation Procedure for Heat, Mass and Momentum Transfer in Three-Dimensional Parabolic Flows ". International Journal of Heat and Mass Transfer. Vol. 15. pp. 1787-1806.

Patel, Virenda C., Rodi, Wolfgang, and Scheuerer, Georg (1985). " Turbulence Models for Near Wall and Low Reynolds Number Flows: A Review ". AIAA Journal. Vol. 23. No. 9. pp.1308-1319.

Peric, M., Kessler, R., and Scheuerer, G. (1988). " Comparison of Finite Volume Numerical Methods with Staggered and Colocated Grids ". Computers and Fluids. Vol. 16. No. 4. pp. 389-403.

Peric, M. (1990). " Analysis of Pressure-Velocity Coupling on Nonorthogonal Grids ". Numerical Heat Transfer. Vol. 17. pp. 63-82.

Pollard, A. and Siu, A. L. W. (1982). " The Calculation of Some Laminar Flows Using Various Discretization Schemes ". Computer Methods in Applied Mechanics and Engineering. Vol. 35. pp. 293-313.

Pope, S. B. (1990). " Computations of Turbulent Combustion: Progress and Challenges". Twenty-Third Symposium (International) on Combustion. pp. 1-41.

Raithby, G. D. (1976). " Skew Upstream Differencing for Problems Involving Fluid Flow ". Computer Methods in Applied Mechanics and Engineering. Vol. 9. pp. 153-164.

Rhie, C. M. and Chow, W. L. (1983). " Numerical Study of the Turbulent Flow Past an Airfoil with Trailing Edge Separation ". AIAA Journal. Vol. 21. No. 11. pp. 1525-1532.

Rhie, Chae M. and Stowers, Steven T. (1988). " Navier Stokes Analysis for High Speed Flows using a Pressure Correction Algorithm ". Journal of Propulsion and Power. Vol. 4. No. 6. pp. 564-570.

Rhie, Chae M. and Stowers, Steven T. (1989). " Numerical Analysis of Reacting Flows using Finite Rate Chemistry Models ". AIAA-89-0459. January 1989.

Rhie, Chae M. and Syed, Saadat A. (1990). " Critical Evaluation of Three Dimensional Supersonic Combustor Calculations ". AIAA-90-0207. January 1990.

Rhode, D. L., Lilley, D. G., and McLaughlin, D. K. (1982). " On the Prediction of Swirling Flowfields Found in Axisymmetric Combustor Geometries ". Journal of Fluids Engineering. Vol. 104. pp. 378-384.

Richman, J. W. and Azad, R. S. (1973). " Developing Turbulent Flow in Smooth Pipes ". Applied Scientific Research. Vol. 28. pp. 419-440.

Rodi, W., Majumdar, S., and Schonung, B. (1987). " Finite Volume Methods for Two Dimensional Incompressible Flows with Complex Boundaries ". Paper presented at the 8th International Conference on Computing Methods in Applied Sciences and Engineering. Versailles, France. December 14-17, 1987.

Schlichting, Hermann. (1979). Boundary Layer Theory. 7th edition. McGraw-Hill Publishing Company.

Shyy, W. and Braaten, Mark E. (1988). " Adaptive Grid Computation for Inviscid Compressible Flows Using a Pressure Correction Method ". 1st National Fluid Dynamics Congress, Cincinnati, Ohio. July 25-29, 1988. Paper No. 88-3566.

Shyy, W. and Correa, S. M. (1985). " A Systematic Comparison of Several Numerical Schemes for Complex Flow Calculations ". AIAA-85-0440. January 1985.

Shyy, W., Tong, S. S., and Correa, S. M. (1985). " Numerical Recirculating Flow Calculation using a Body-Fitted Coordinate System ". Numerical Heat Transfer. Vol. 8. pp. 99-113.

Spalding, D. B. (1971). " Concentration Fluctuations in a Round Turbulent Free Jet ". Chemical Engineering Science. Vol. 26. pp. 95-107.

Spalding, D. B. (1976). " Mathematical Models of Turbulent Flames: A Review ". Combustion Science and Technology. Vol. 13. pp. 3-25.

Speziale, C. G. (1991). " Analytical Methods for the Development of Reynolds Stress Closures in Turbulence ". Annual Review of Fluid Mechanics. Vol. 23. pp. 107-157.

Sturgess, G. J. and McManus, K. R. (1984). " Calculations of Turbulent Mass Transport in a Bluff Body Diffusion Flame Combustor ". AIAA-84-0372. January 1984.

Tafti, D. K., and Vanka, S. P. (1990). " Large Eddy Simulation of Channel Flow using Finite Difference Techniques ". Department of Mechanical and Industrial Engineering. University of Illinois. Urbana-Champaign, Illinois. Report No. CFD 90-01.

Thiart, G. D. (1990). " Finite Difference Scheme for the Numerical Solution of Fluid Flow and Heat Transfer Problems on Nonstaggered Grids ". Numerical Heat Transfer. Vol. 17. pp. 43-62.

Thompson, Joe F., Thames, Frank C., and Mastin, C. Wayne (1974). " Automatic Numerical Generation of Body-Fitted Curvilinear Coordinate System for Field Containing Any Number of Arbitrary Two-Dimensional Bodies ". Journal of Computational Physics. Vol. 15. pp. 299-319.

Van Doormaal, J. P. and Raithby, G. D. (1984). " Enhancements of the SIMPLE Method for Predicting Incompressible Fluid Flows ". Numerical Heat Transfer. Vol. 7. pp. 147-163.

Vanka, S. P. (1986). " Block Implicit Multigrid Solution of Navier Stokes Equations in Primitive Variables ". Journal of Computational Physics. Vol. 65. pp. 138-158.

Vanka, S. P. (1988). " Analytical Studies of Three-Dimensional Combustion Processes ". AFWAL-TR-88-2140. May 1989.

Vanka, S. P., Krazinski, J. L., and Nejad, A. S. (1989). " Efficient Computational Tool for Ramjet Combustor Research ". Journal of Propulsion and Power. Vol. 5. No. 4. pp. 431-437.

Westbrook, Charles K. and Dryer, Frederick L. (1981). " Simplified Reaction Mechanisms for the Oxidation of Hydrocarbon Fuels in Flames ". <u>Combustion Science and Technology</u>. Vol. 27. pp. 31-43.

White, Frank M. (1974). <u>Viscous Fluid Flow</u>. McGraw-Hill Publishing Company.

Zhou, Lixing. (1989). " A Series of Lectures on the Numerical Modelling of Gas-Particle (Droplet) Flows and Combustion ". Presented at the University of Illinois at Urbana-Champaign. September 13 - October 25, 1989.

Table 1: Values of diffusive exchange coefficient and source term for variables used in simulation of turbulent reacting flow.

ϕ	Γ_{eff}	S^ϕ
1	0	0
$\tilde{u}$	$\mu + \mu_T$	$S_{TR}^u - \left(a_{11}\dfrac{\partial P}{\partial \xi} + a_{21}\dfrac{\partial P}{\partial \eta} \right)$
$\tilde{v}$	$\mu + \mu_T$	$S_{TR}^v - \left(a_{12}\dfrac{\partial P}{\partial \xi} + a_{22}\dfrac{\partial P}{\partial \eta} \right) + |J|\left(-2\Gamma_{eff}\dfrac{\tilde{v}}{r^2} + \dfrac{\bar{\rho}\tilde{w}^2}{r} \right)$
$\tilde{w}$	$\mu + \mu_T$	$S_{TR}^w - \left[\dfrac{\rho\tilde{v}\tilde{w}}{r} - \Gamma_{eff}\dfrac{\tilde{w}}{r^2} - \dfrac{\tilde{w}}{r}\dfrac{\partial \Gamma_{eff}}{\partial r} \right]|J|$
k	$\mu + \dfrac{\mu_T}{Pr_k}$	$(P_k - \rho\varepsilon)|J| + S_{TR}^k$
ε	$\mu + \dfrac{\mu_T}{Pr_\varepsilon}$	$\dfrac{\varepsilon}{k}(C_1 P_k - C_2\rho\varepsilon)|J| + S_{TR}^\varepsilon$
$\tilde{f}$	$\mu + \dfrac{\mu_T}{Pr_f}$	S_{TR}^f
$\tilde{g}$	$\mu + \dfrac{\mu_T}{Pr_g}$	$C_{g1}\mu_T\left\{ \left[\dfrac{\partial f}{\partial z}\right]^2 + \left[\dfrac{\partial f}{\partial r}\right]^2 \right\}|J| - \dfrac{C_{g2}\rho g\varepsilon}{k}|J| + S_{TR}^g$
$\tilde{Y}_{FU}$	$\mu + \dfrac{\mu_T}{Pr_Y}$	$\overline{\dot{\omega}}\,|J| + S_{TR}^Y$
$\tilde{h}_o$	$\mu + \dfrac{\mu_T}{Pr_{ho}}$	$S_{TR}^{ho} - |J|\displaystyle\sum_{i=1}^{N}\overline{\dot{\omega}}_i\, h_i^o$
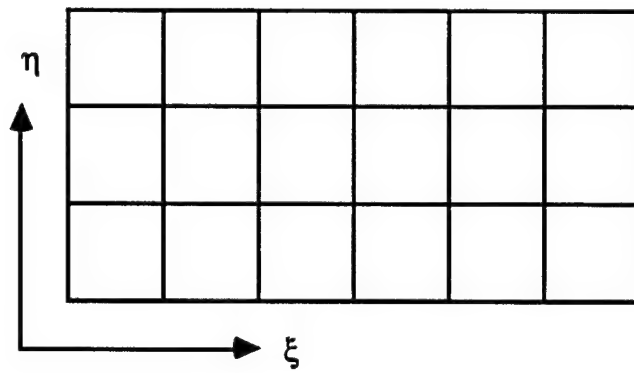
(a) Transformed Plane
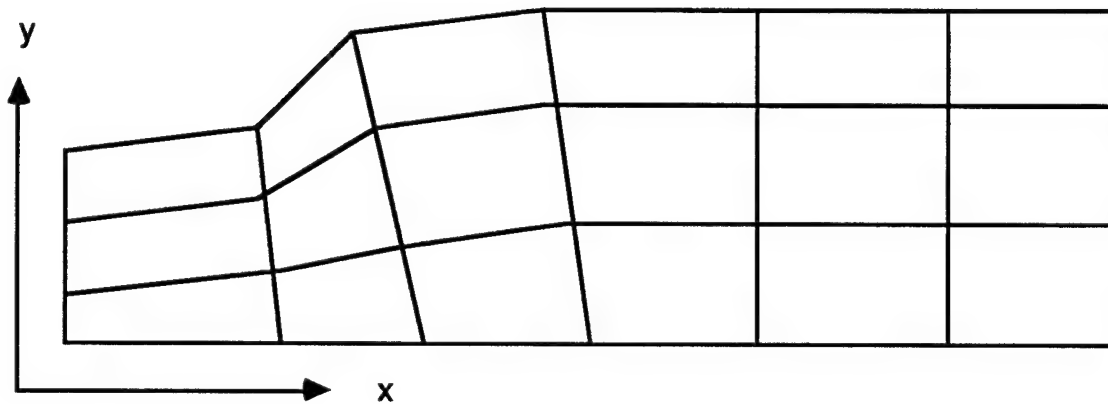
(b) Physical Plane

Figure 1: The grid in the transformed plane (a) appears as non-orthogonal in the physical plane (b).
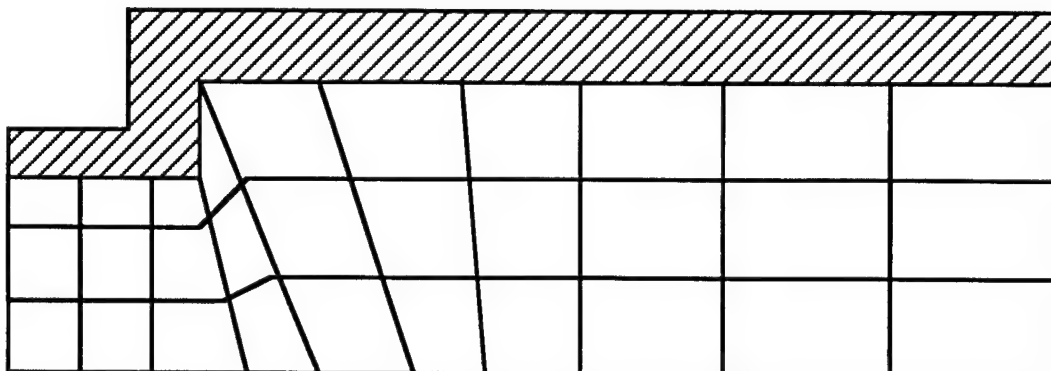
Figure 2: The discretization of the governing flow equations is accomplished by dividing the domain into finite control volumes. A sudden expansion geometry with a 10 x 3 grid is given as an example.
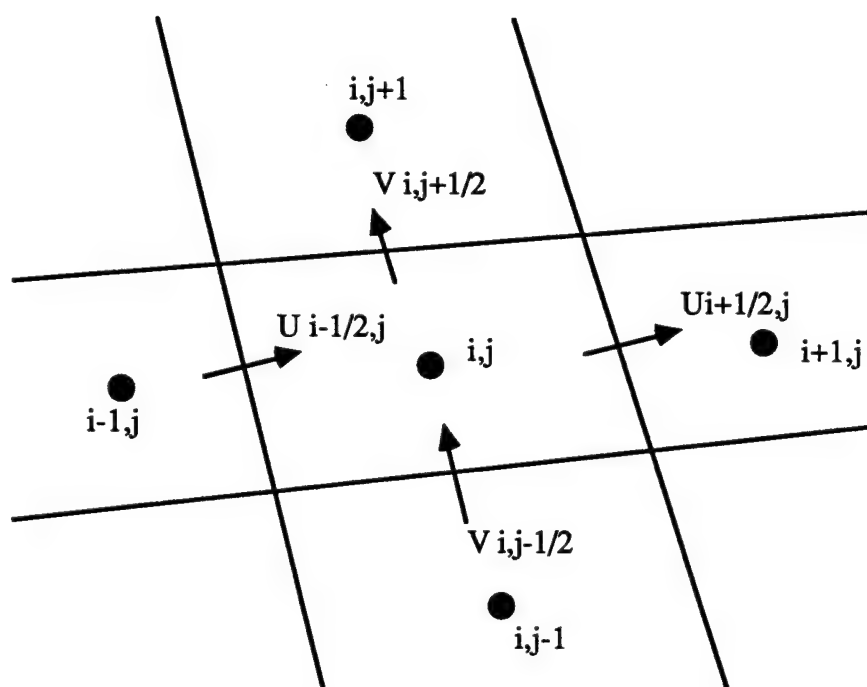
Figure 3: A finite control volume with its nearest neighbors is shown. Integration of the governing equations over this finite control volume results in a set of non-linear algebraic equations.

```
┌────────────────────────────────────────────────────────┐◄──────┐
│  Calculate cell face values of exchange coefficient    │       │
└────────────────────────────────────────────────────────┘       │
                                                                  │
            Calculate coefficients ( Ae, Aw, etc. )               │
                                                                  │
         Solve for the u component of velocity:                   │
            1) Determine source term for u.                       │
            2) Submit to adi routine for solution.                │
                                                                  │
                                                                  │
         Solve for the v component of velocity:                   │
            1) Determine source term for v.                       │
            2) Submit to adi routine for solution.                │
                                                                  │
                                                                  │
                  Calculate cell face fluxes.                     │
                                                                  │
┌──────────────────┐   YES   ┌───────────────────────┐           │
│  Output solution │◄────────│  Converged solution ?  │           │
└──────────────────┘         └───────────────────────┘           │
                                        │                         │
                                        │ NO                      │
                                        ▼                         │
         Solve for the pressure correction:                       │
            1) Calculate coefficients.                            │
            2) Calculate source terms for P'.                     │
            3) Submit to adi routine for solution.                │
                                                                  │
                                                                  │
               Correct u, v, U, V, and P                          │
                                                                  │
                                                                  │
          Apply integral mass adjustment if desired               │
                                                                  │
                                                                  │
      Solve for scalar variables:                                 │
         1) Calculate cell face values of exchange coefficient    │
         2) Calculate coefficients of discretized equation        │
         3) Calculate source term                                 │
         4) Submit to adi routine for solution                    │
                                                                  │
┌────────────────────────────────────────────────────────┐       │
│  Update thermodynamic and transport properties          │───────┘
└────────────────────────────────────────────────────────┘
```

Figure 4: Order of events in obtaining a solution to the discretized equations
             governing the flow.
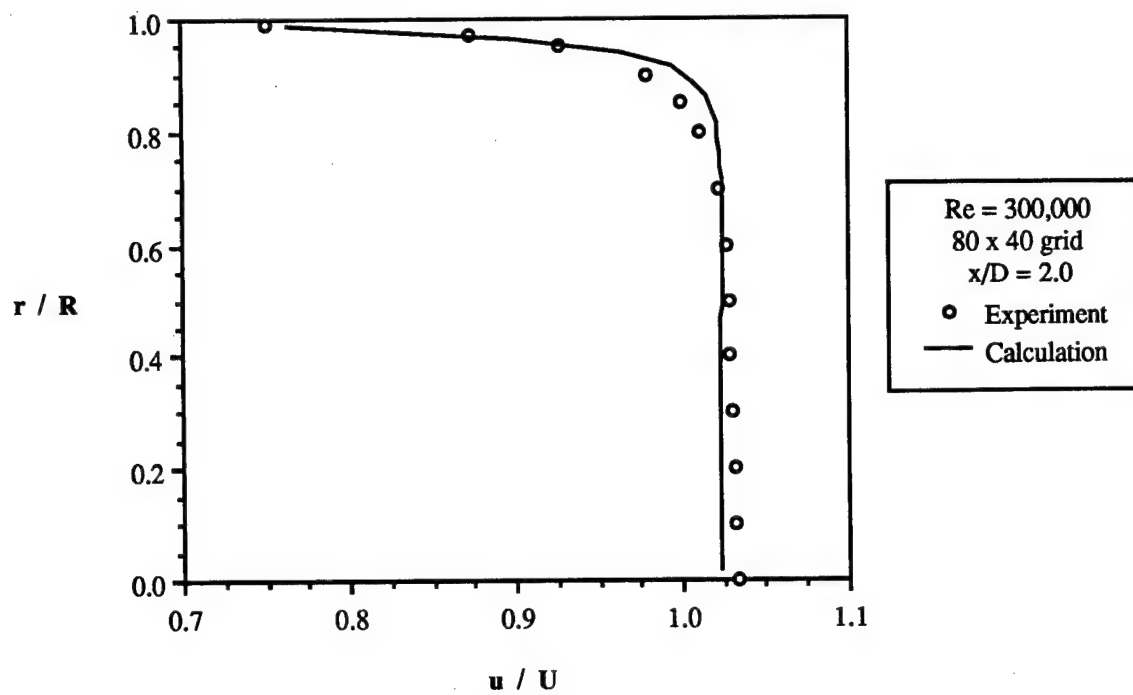
Figure 5: Comparison of experimentally and numerically obtained profiles of mean velocity at x/D equal to 2 in a developing turbulent pipe flow. Experimental results are those obtained by Richman and Azad, 1973.
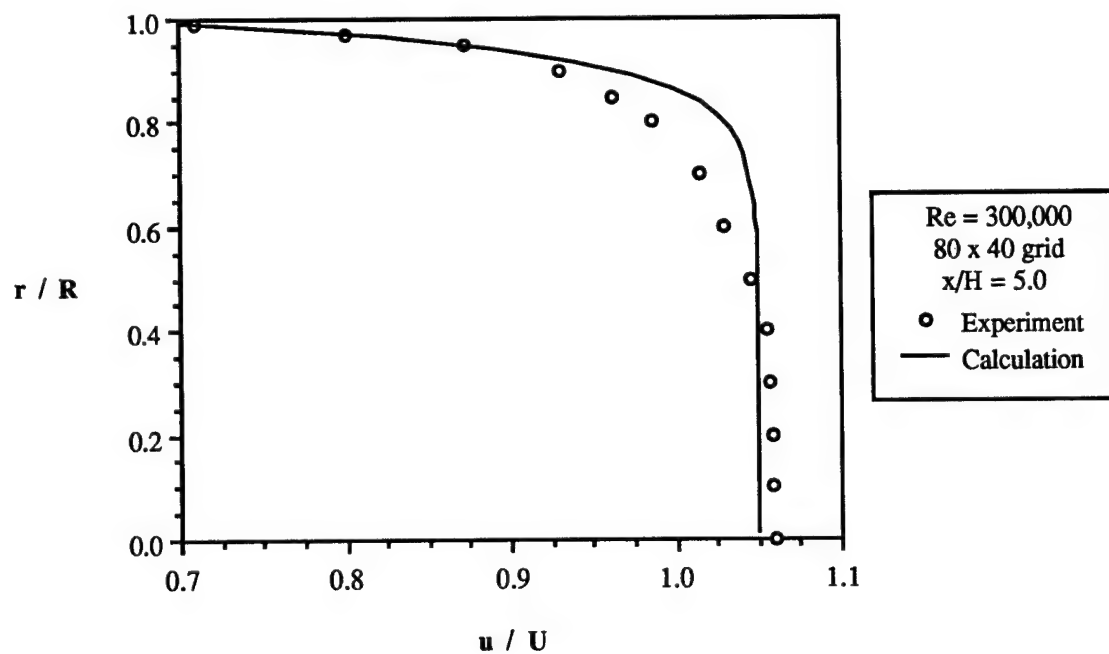
Figure 6: Comparison of experimentally and numerically obtained profiles of mean velocity at x/D equal to 5 in a developing turbulent pipe flow. Experimental results are those by Richman and Azad, 1973.
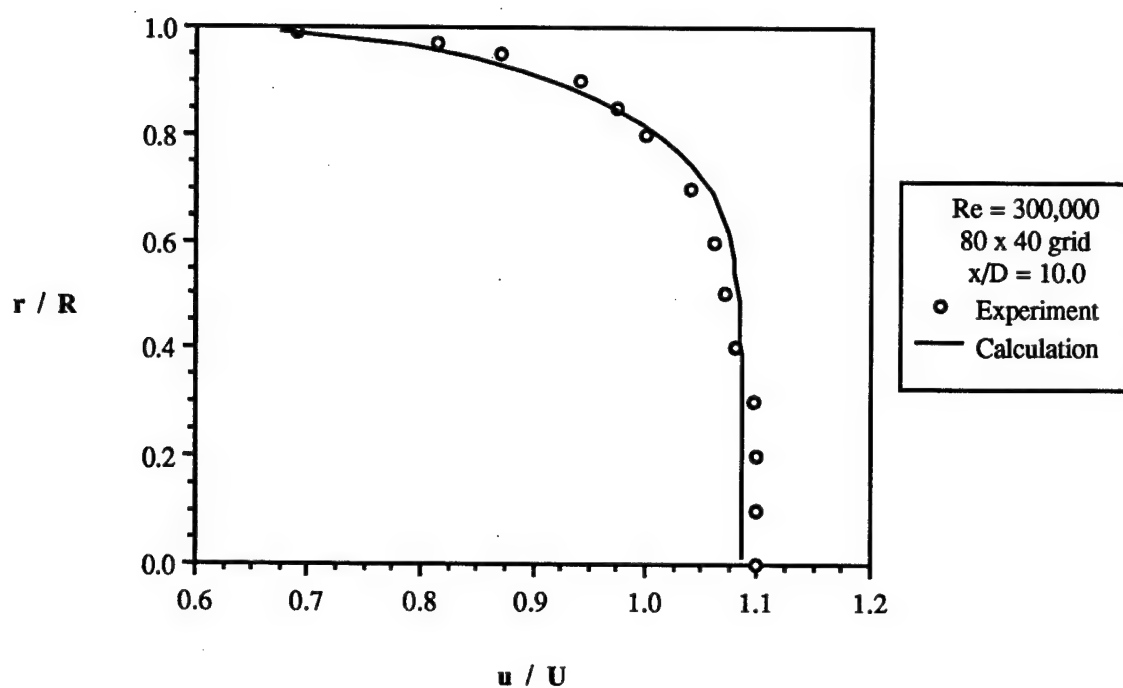
Figure 7: Comparison of experimentally and numerically obtained profiles of mean velocity at x/D equal to 10 in a developing turbulent pipe flow. Experimental results are those obtained by Richman and Azad, 1973.
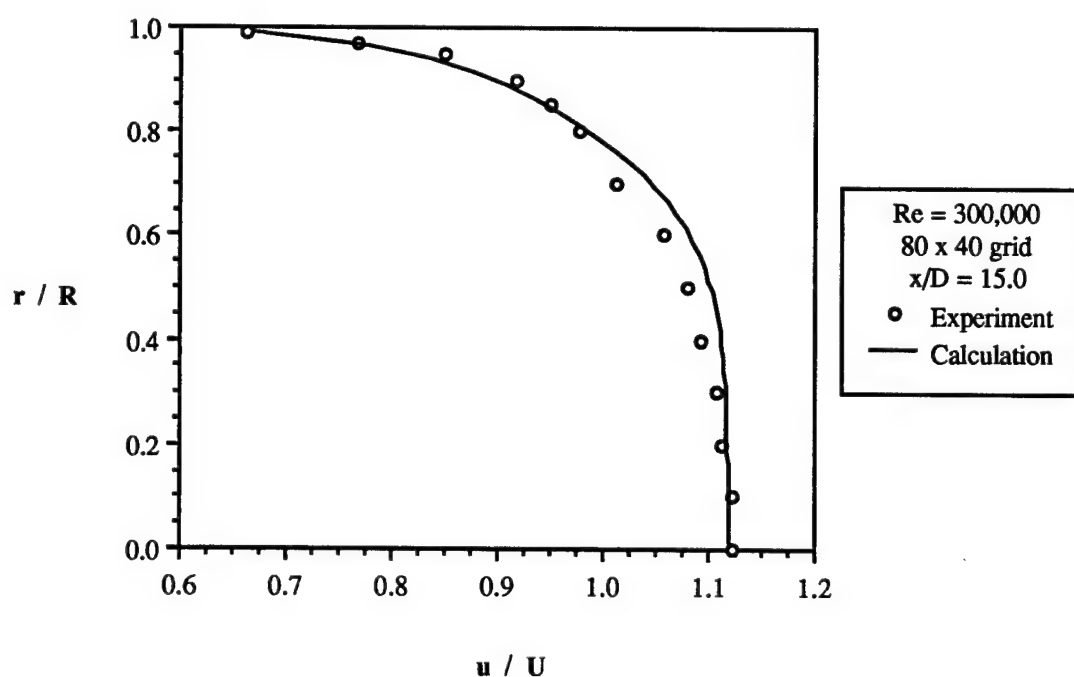
Figure 8: Comparison of experimentally and numerically obtained profiles of mean velocity at x/D equal to 15 in a developing turbulent pipe flow. Experimental results are those obtained by Richman and Azad, 1973.
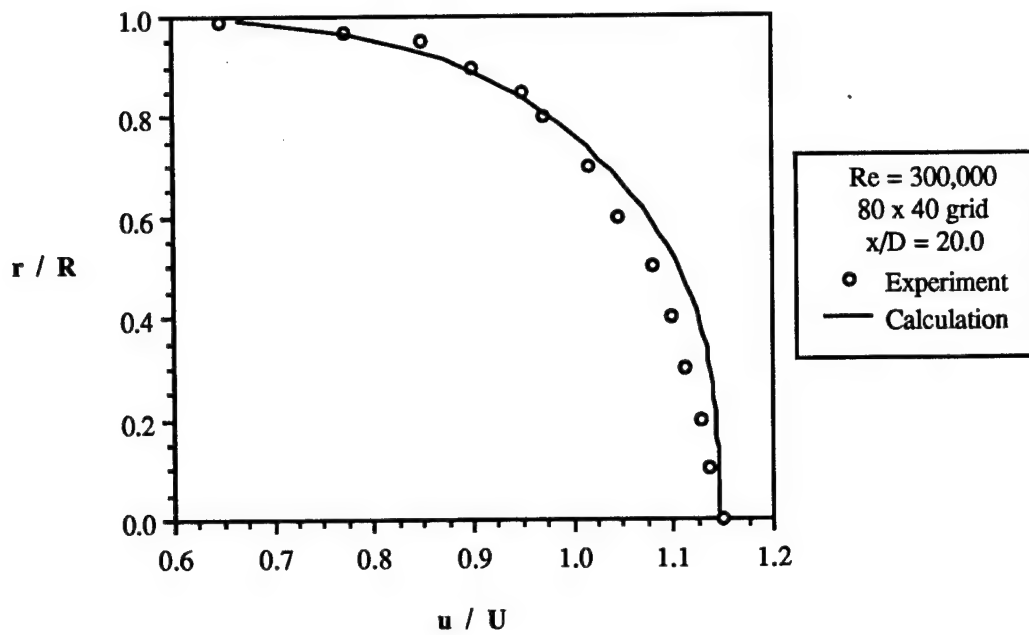
Figure 9: Comparison of experimentally numerically obtained profiles of mean velocity at x/D equal to 20 in a developing turbulent pipe flow. Experimental results are those obtained by Richman and Azad, 1973.
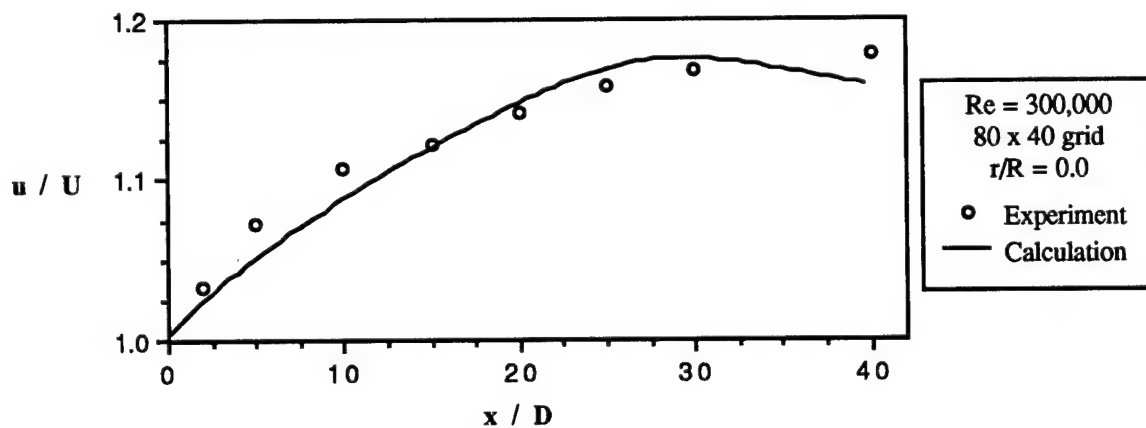
Figure 10: Comparison of experimentally and numerically obtained values of the mean streamwise velocity component along the pipe centerline. Experimental results are those obtained by Richman and Azad, 1973.
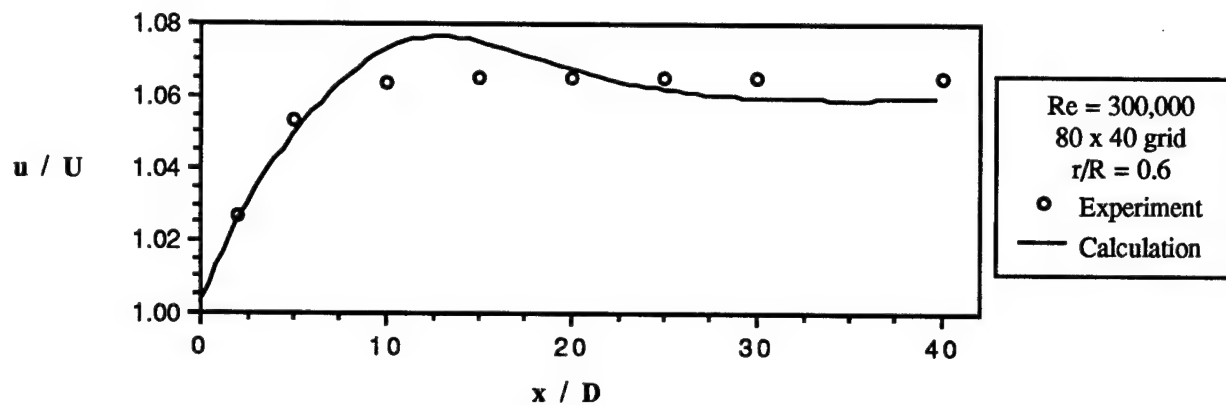
Figure 11: Comparison of experimentally and numerically obtained values of the mean streamwise velocity component at a radius ratio of 0.6. Experimental results are those obtained by Richman and Azad, 1973.
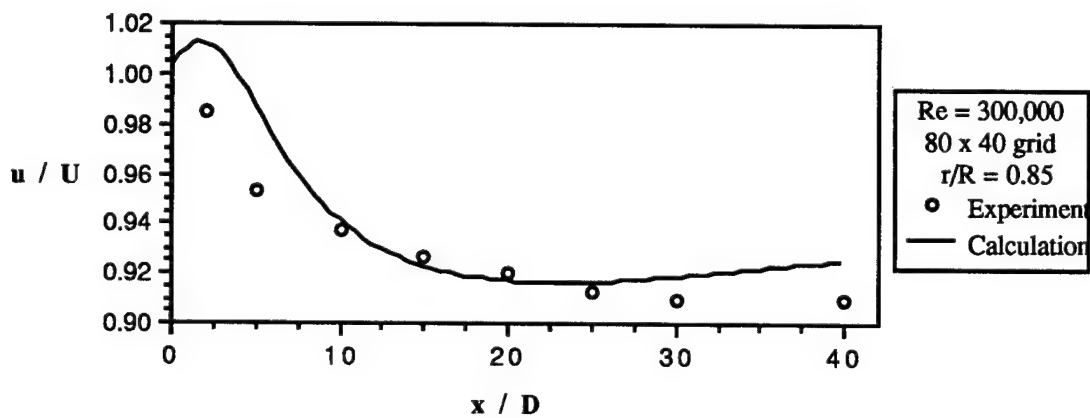
Figure 12: Comparison of experimentally and numerically obtained values of the mean streamwise velocity component at a radius ratio of 0.85. Experimental results are those obtained by Richman and Azad, 1973.
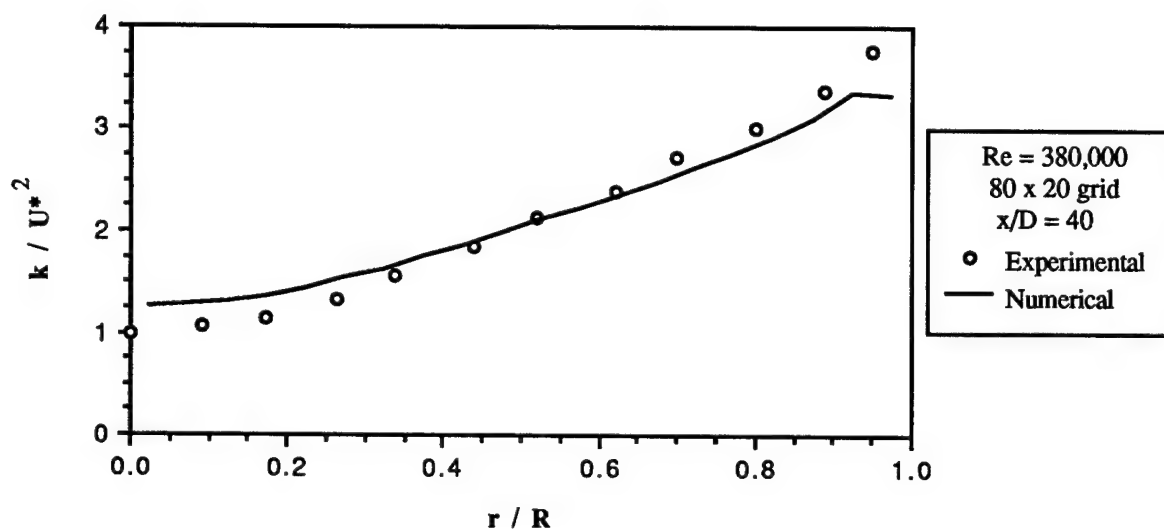
Figure 13: Comparison of experimental and numerically obtained profiles of dimensionless turbulent kinetic energy for fully developed turbulent pipe flow.
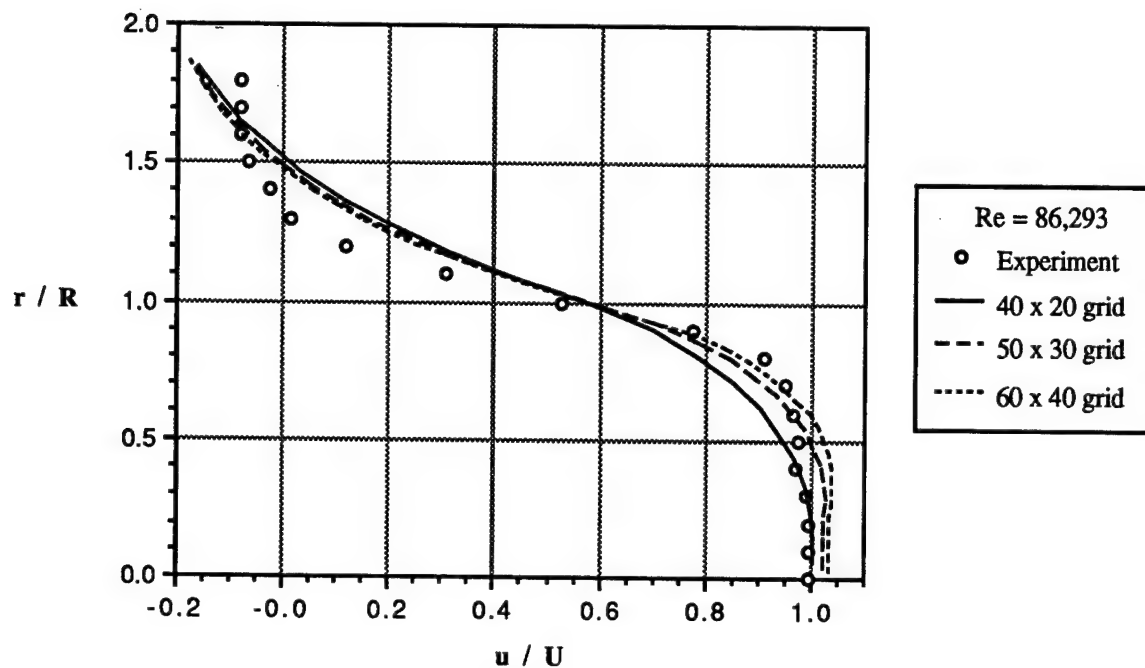
Figure 14: Comparison of experimentally and numerically obtained velocity profiles at x/H of 2.25 for turbulent flow in an axisymmetric sudden expansion. Experimental results from Craig (Craig, et. al., 1984).
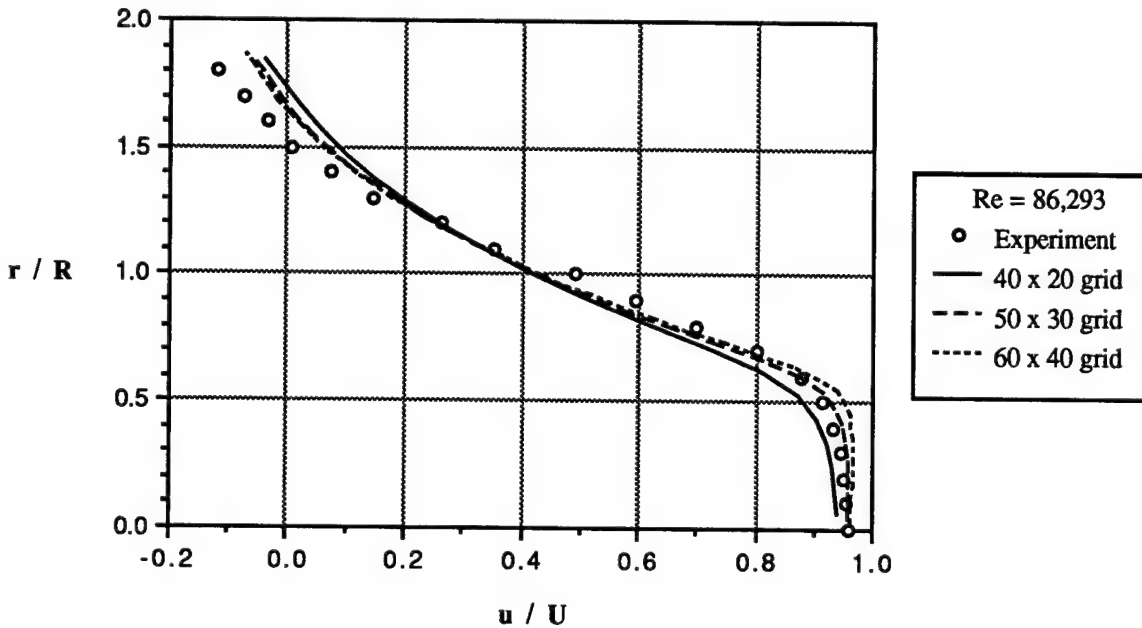
Figure 15: Comparison of experimentally and numerically obtained velocity profiles at x/H of 5.6 for turbulent flow in and axisymmetric sudden expansion. Experimental results from Craig (Craig, et. al., 1984).
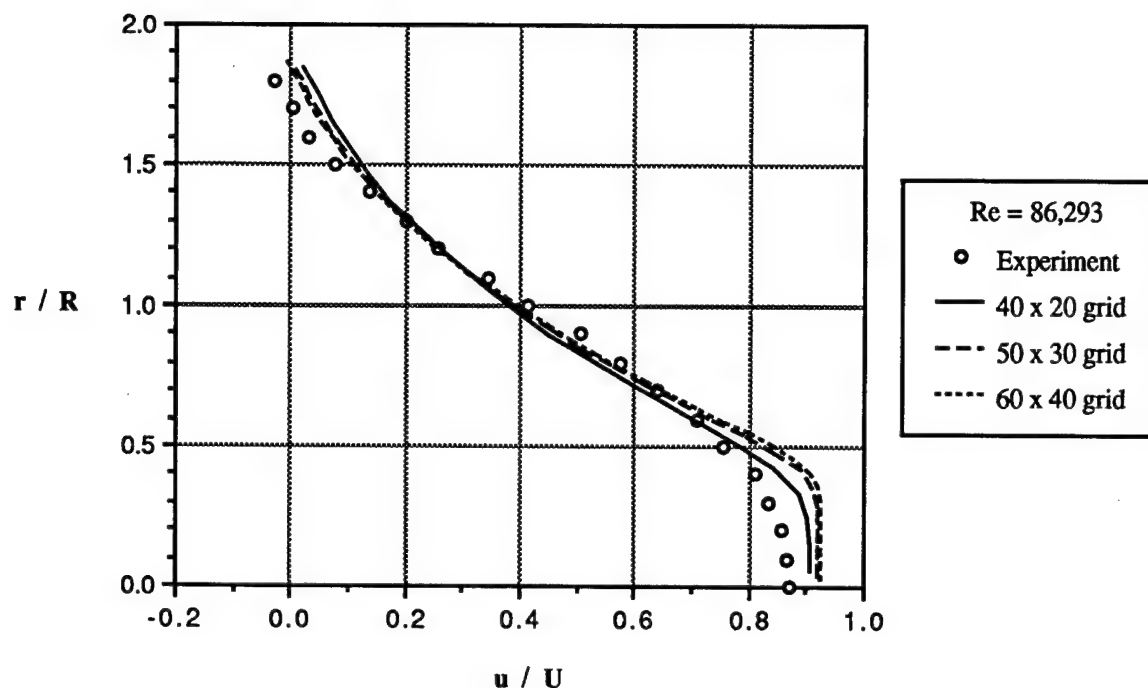
Figure 16: Comparison of experimentally and numerically obtained velocity profiles at x/H of 7.8 for turbulent flow in an axisymmetric sudden expansion. Experimental results from Craig (Craig, et. al., 1984).
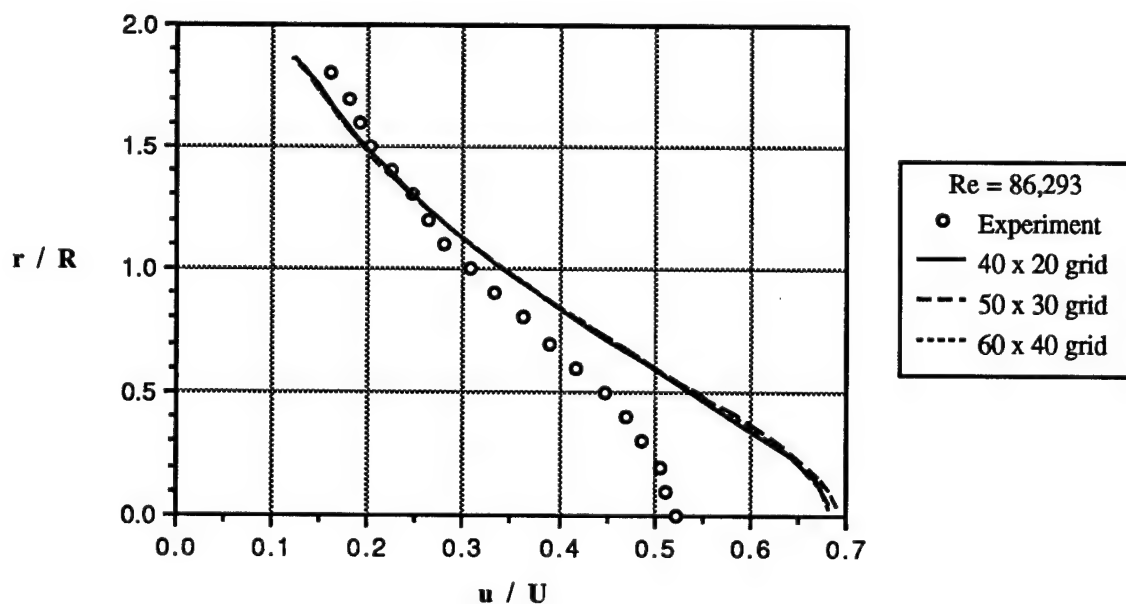
Figure 17: Comparison of experimentally and numerically obtained velocity profiles at x/H of 13.5 for turbulent flow in an axisymmetric sudden expansion. Experimental results from Craig (Craig, et. al., 1984).
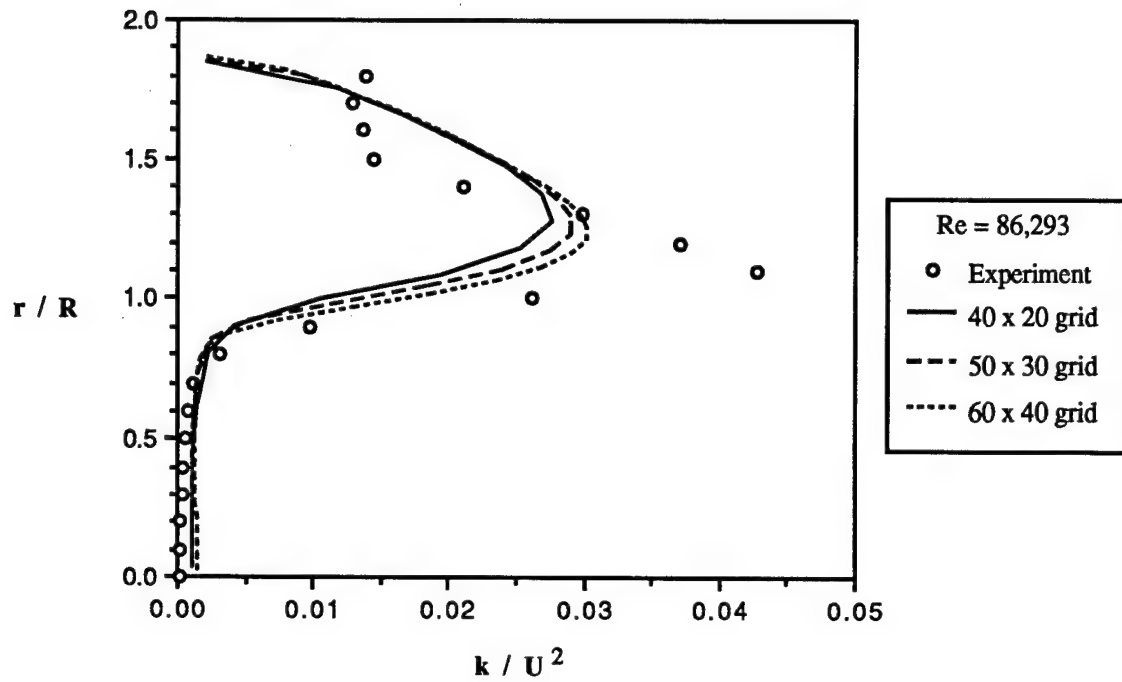
Figure 18: Comparison of experimentally and numerically obtained profiles of turbulent kinetic energy ratio at x/H of 2.25 for flow in an axisymmetric sudden expansion. Experimental results from Craig (Craig, et. al., 1984).
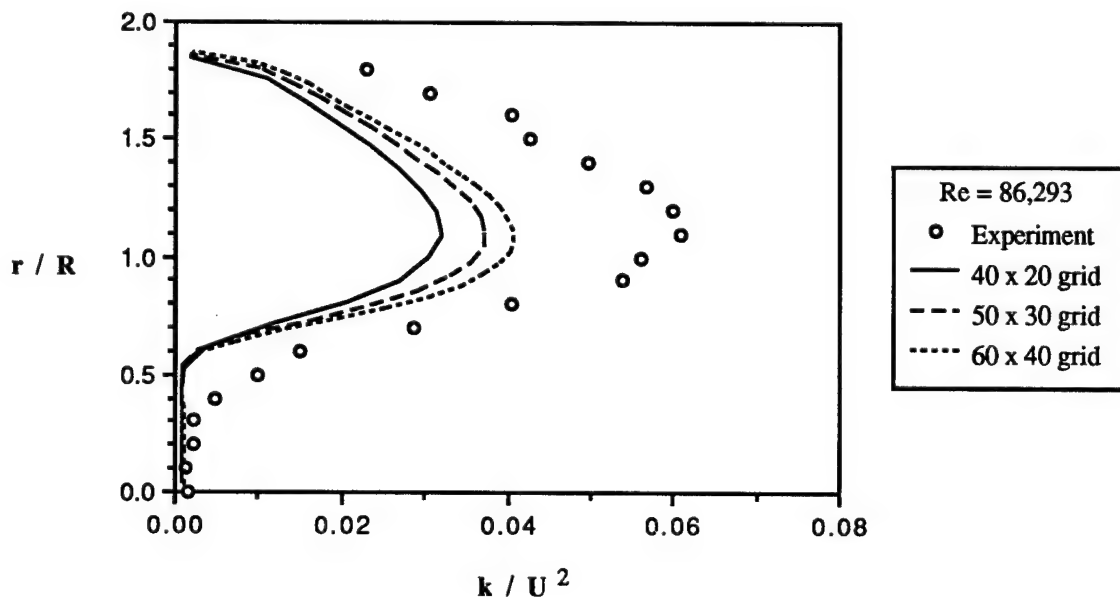
Figure 19: Comparison of experimentally and numerically obtained profiles of turbulent kinetic energy at x/H of 5.6 for flow in an axisymmetric sudden expansion. Experimental results from Craig (Craig, et. al., 1984).
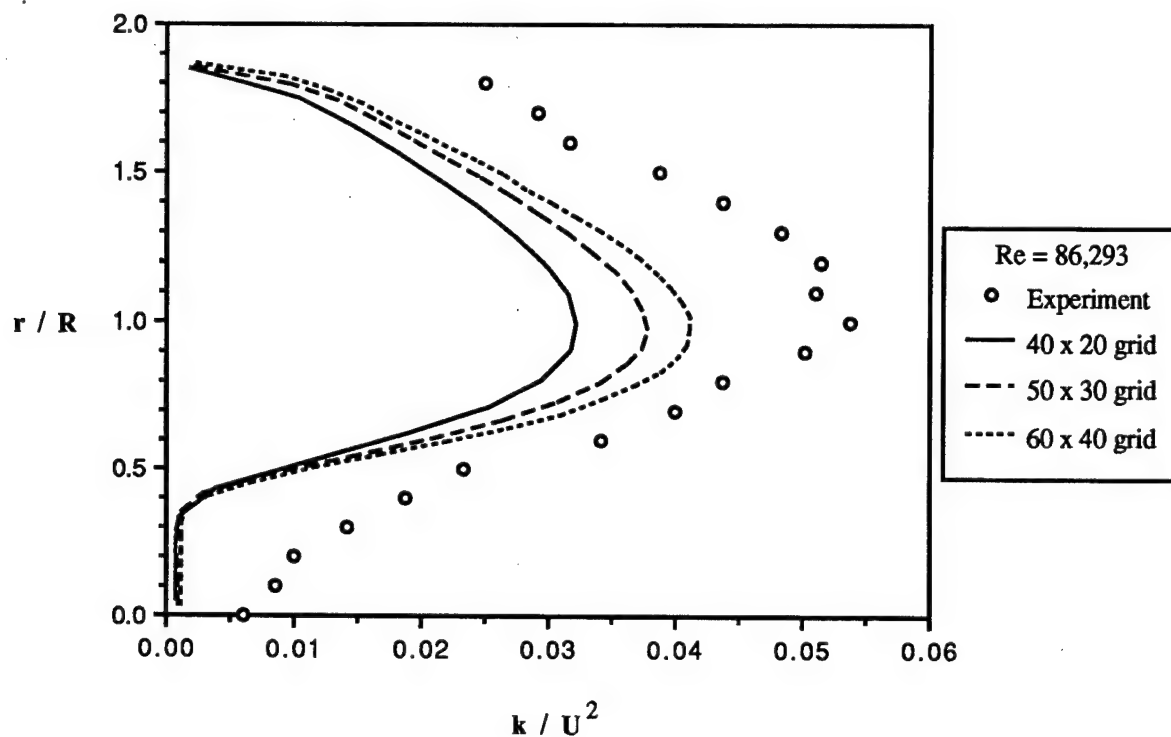
Figure 20: Comparison of experimentally and numerically obtained profiles of turbulent kinetic energy at x/H of 7.8 for flow in an axisymmetric sudden expansion. Experimental results from Craig (Craig, et. al., 1984).
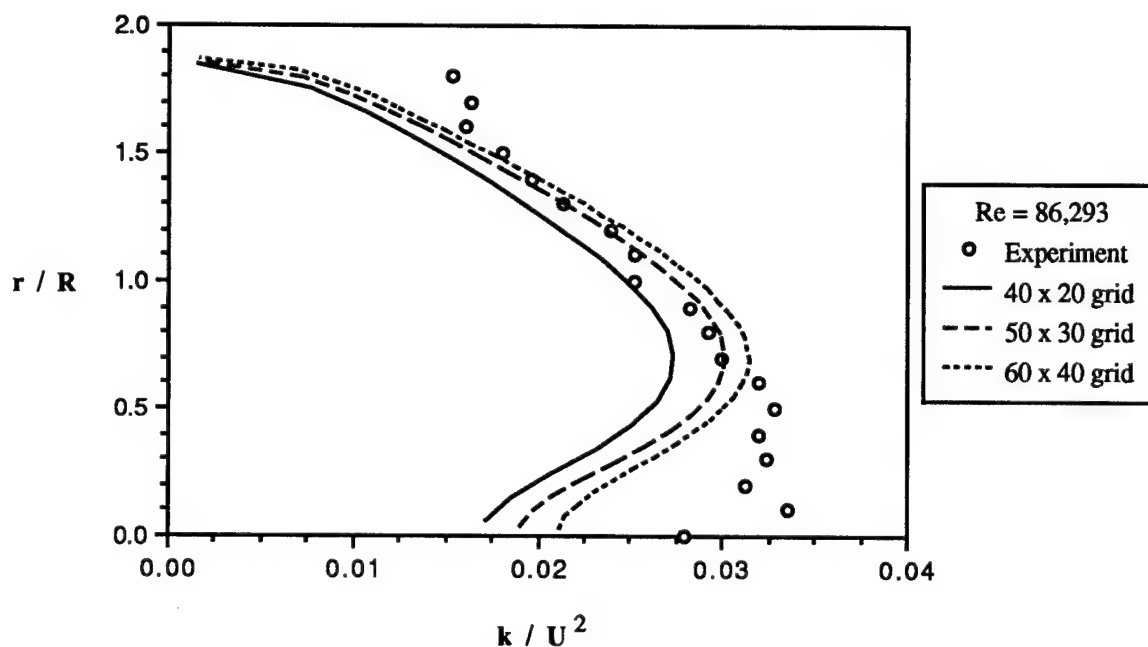
Figure 21: Comparison of experimentally and numerically obtained profiles of turbulent kinetic energy at x/H of 13.5 for flow in an axisymmetric sudden expansion. Experimental results from Craig (Craig, et. al., 1984).

96
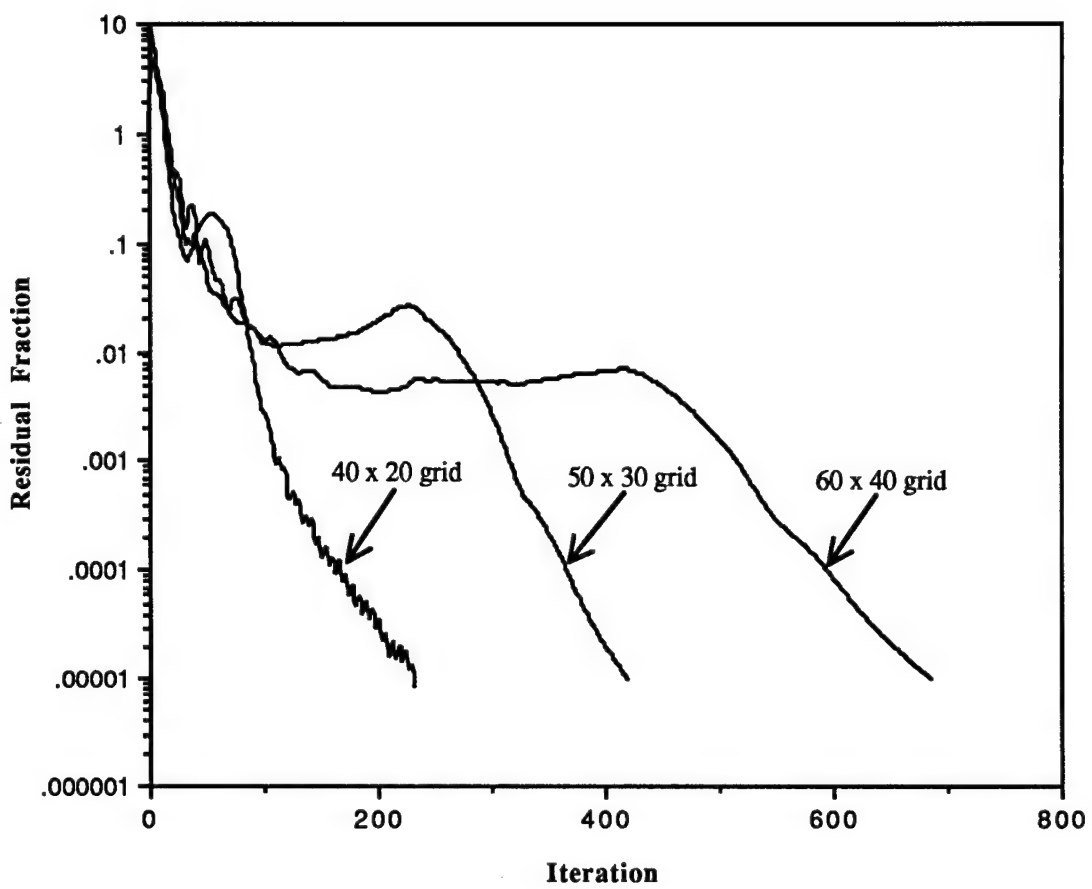
Figure 22: Convergence histories corresponding to calculations of turbulent flow in an axisymmetric sudden expansion.
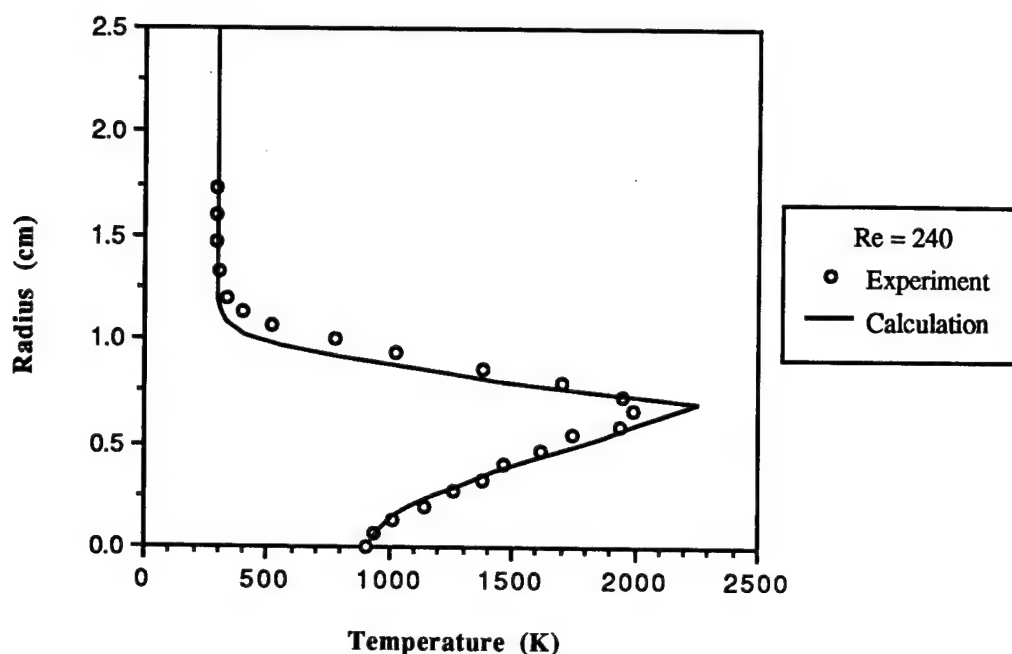
Figure 23: Comparison of experimental and calculated temperature profiles for the laminar diffusion flame of Mitchell, et. al., 1980. The results correspond to an axial location of x/D equal to 0.24.
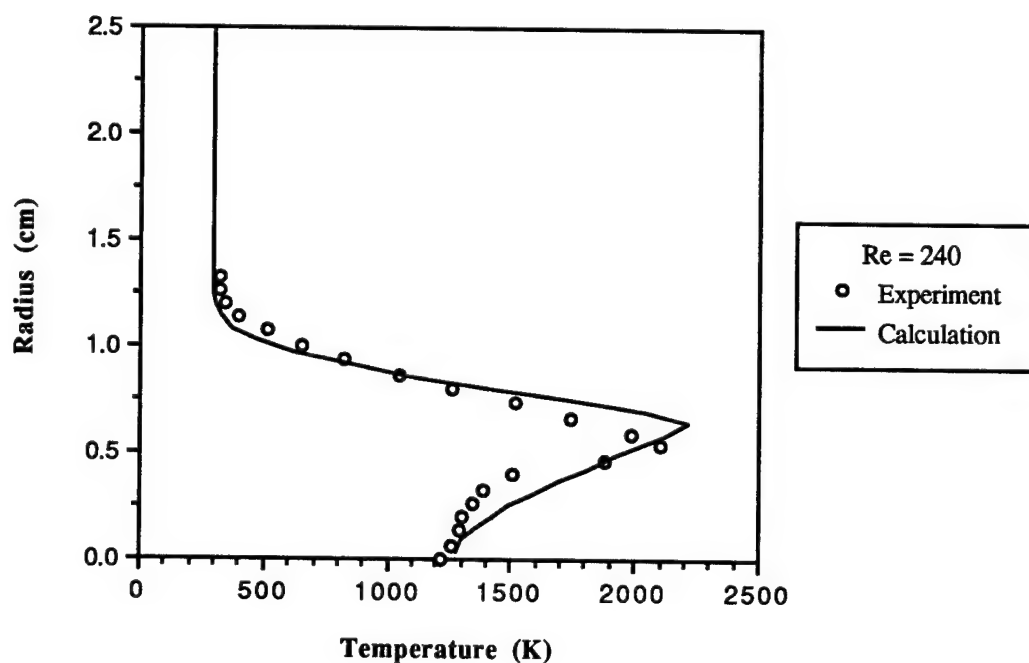
Figure 24: Comparison of experimental and calculated temperature profiles for the laminar diffusion flame of Mitchell, et. al., 1980. The results correspond to an axial location of x/D equal to 0.47.
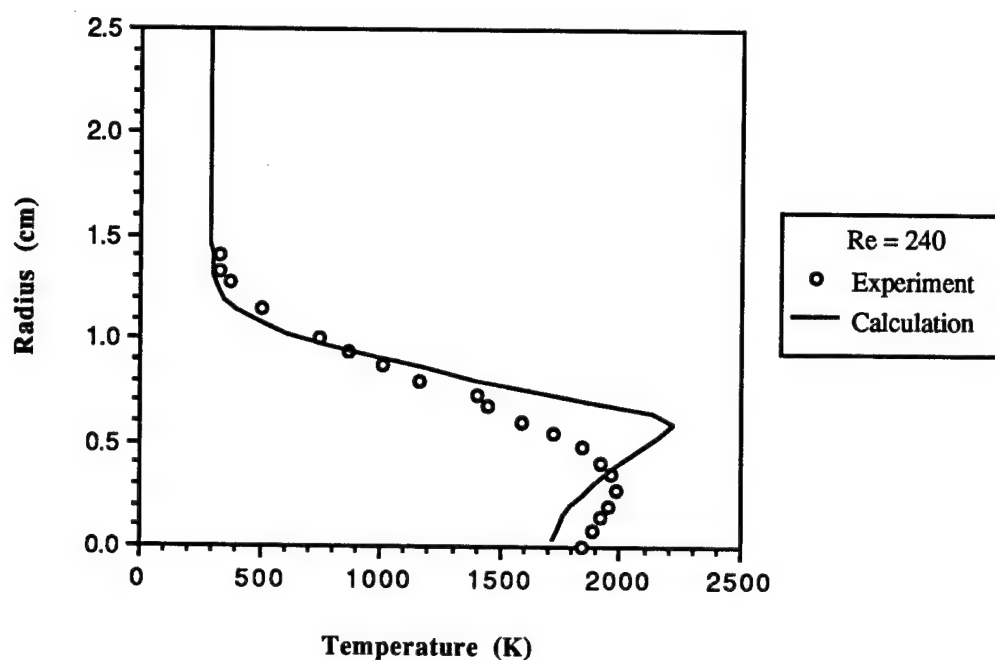
Figure 25: Comparison of experimental and calculated temperature profiles for the laminar diffusion flame of Mitchell, et. al., 1980. The results correspond to an axial location of x/D equal to 0.98.
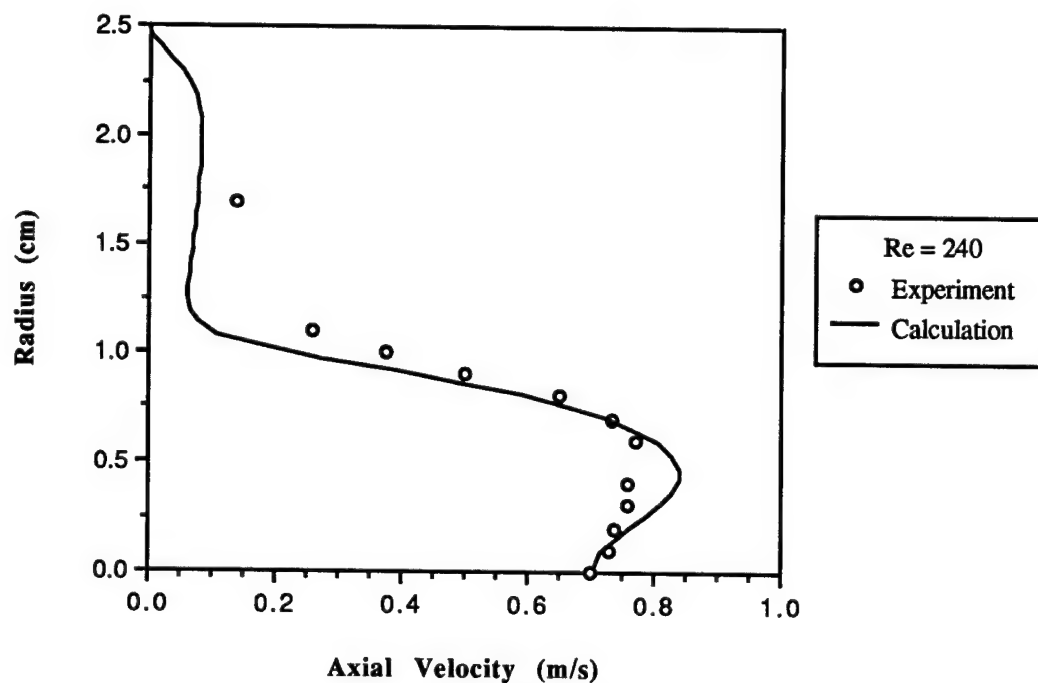
Figure 26: Comparison of experimental and calculated velocity profiles for the laminar diffusion flame of Mitchell, et. al., 1980. The results correspond to an axial location of x/D equal to 0.24.

Figure 27: Comparison of experimental and calculated velocity profiles for the laminar diffusion flame of Mitchell, et. al., 1980. The results correspond to an axial location of x/D equal to 0.47.

Figure 28: Comparison of experimental and calculated velocity profiles for the laminar diffusion flame of Mitchell, et. al., 1980. The results correspond to an axial location of x/D equal to 0.98.

100
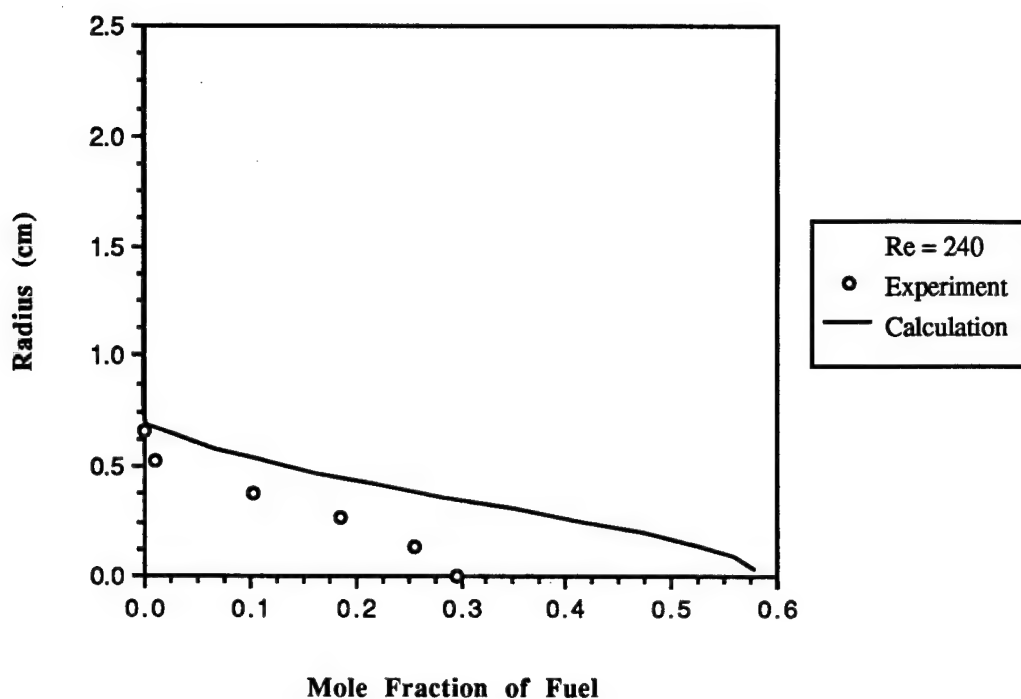
Figure 29: Comparison of experimental and calculated fuel fraction profiles for the laminar diffusion flame of Mitchell, et. al., 1980. The results correspond to an axial location of x/D equal to 0.24.
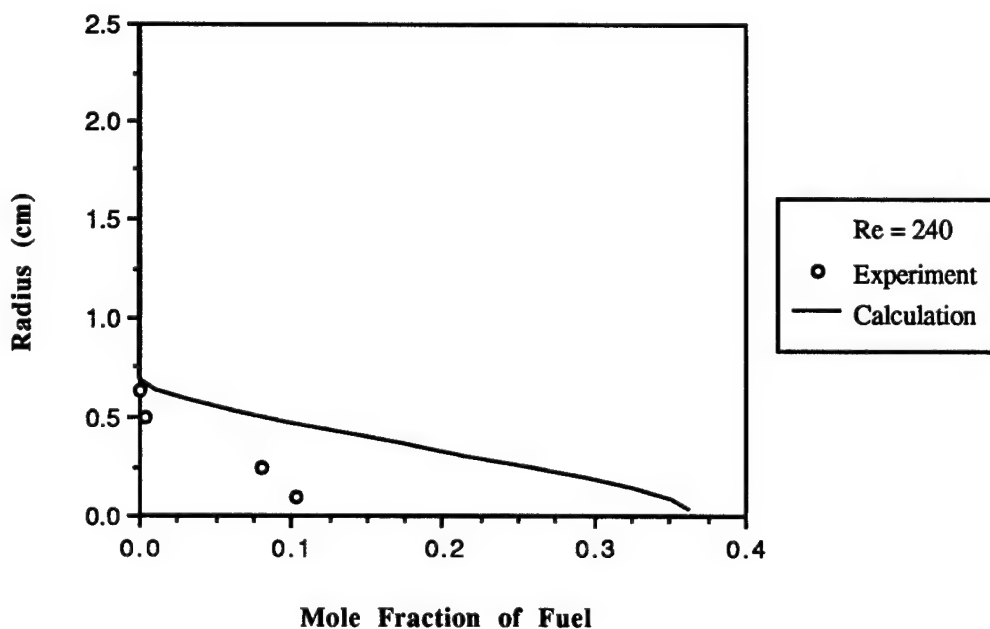
Figure 30: Comparison of experimental and calculated fuel fraction profiles for the laminar diffusion flame of Mitchell, et. al., 1980. The results correspond to an axial location of x/D equal to 0.47.
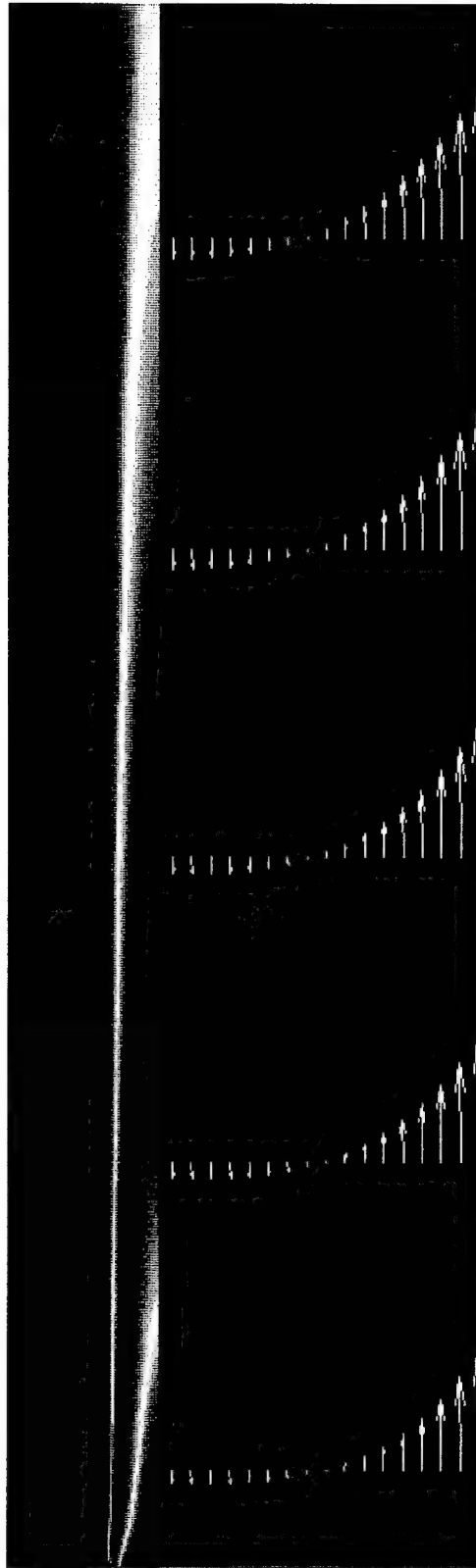
Figure 31: Results of the simulation of the laminar diffusion flame of Mitchell, et. al., 1980. (a) Above is the distribution of temperature in the flame (Blue = 300K, Yellow = 1500K, and Red = 2300K). (b) Below is a magnification of the velocity in the region near the flame tip.
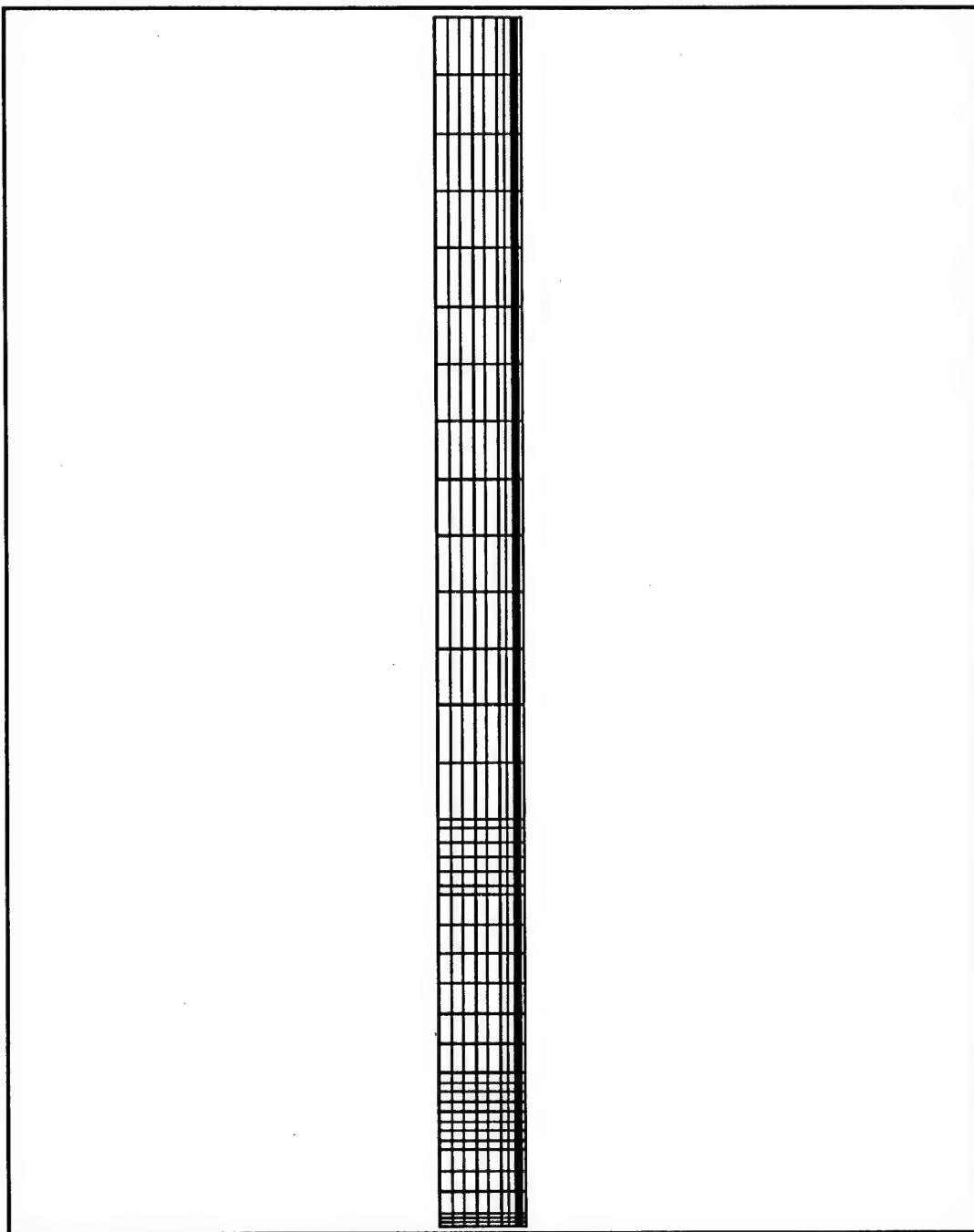
Figure 32: A representative grid used for the calculation of the turbulent diffusion flame of Lewis and Smoot, 1981. The left boundary is the fuel/air inlet. The 40 x 10 grid is refined in the separation region between fuel and air thus leading to high aspect ratios near the combustor exit.
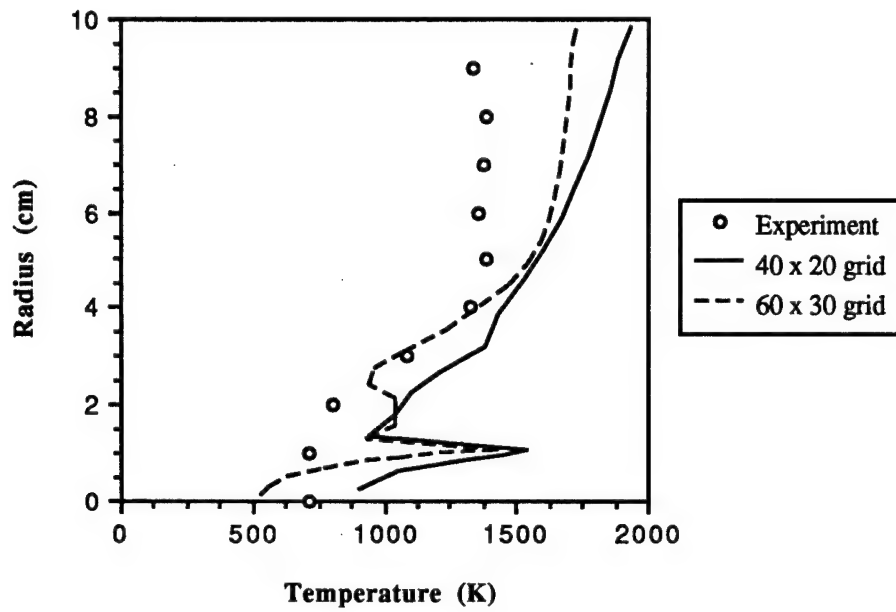
Figure 33: Comparison of experimental and calculated temperature profiles for the turbulent diffusion flame of Lewis and Smoot, 1981. The profiles correspond to an axial location of x/D equal to 0.47.
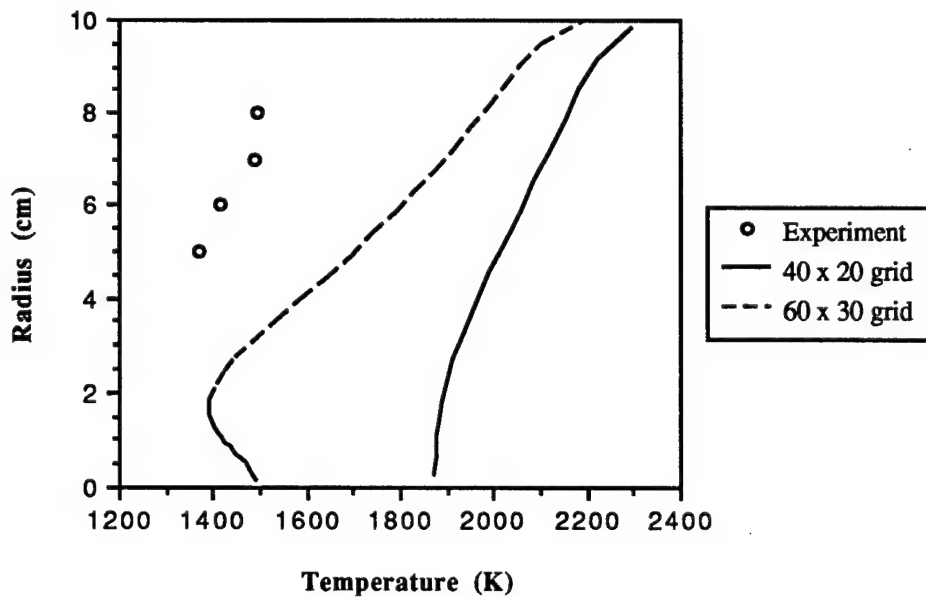
Figure 34: Comparison of experimental and calculated temperature profiles for the turbulent diffusion flame of Lewis and Smoot, 1981. The profiles correspond to an axial location of x/D equal to 1.96.
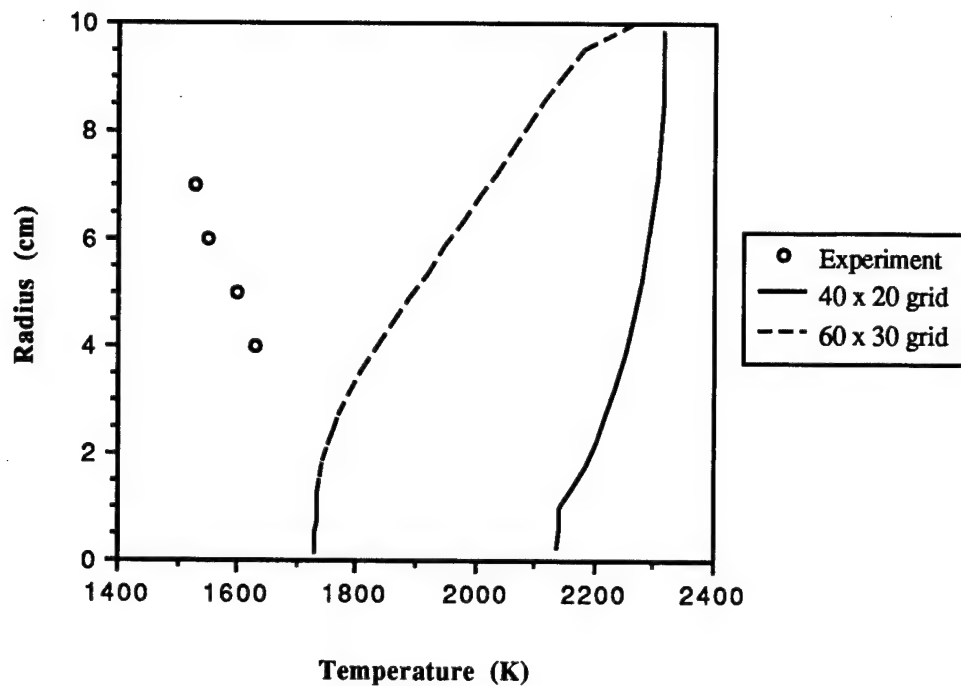
Figure 35: Comparison of experimental and calculated temperature profiles for the turbulent diffusion flame of Lewis and Smoot, 1981. The profiles correspond to an axial location of x/D equal to 2.34.
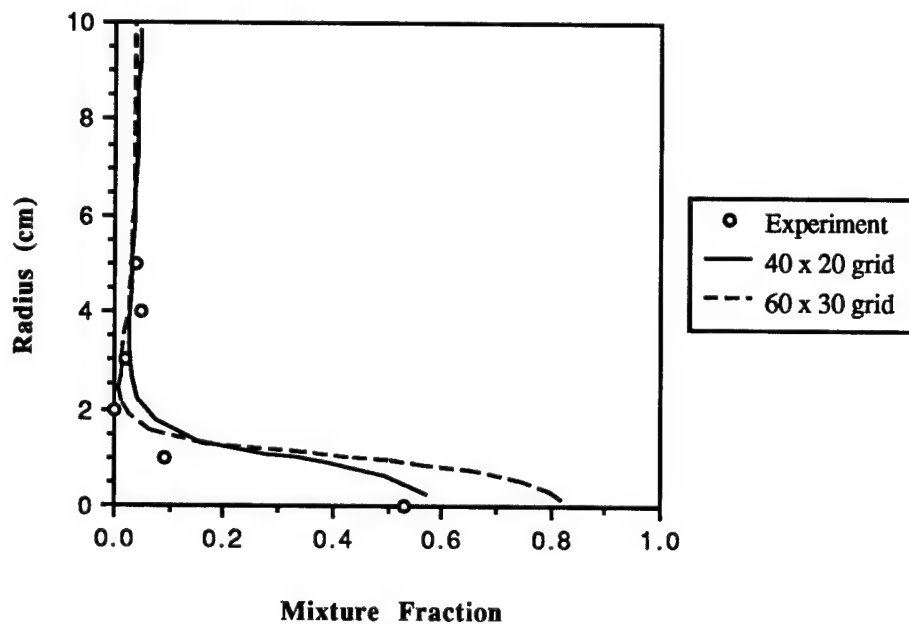
Figure 36: Comparison of experimental and calculated mixture fraction profiles for the turbulent diffusion flame of Lewis and Smoot, 1981. The profiles correspond to an axial location of x/D equal to 0.47.

105
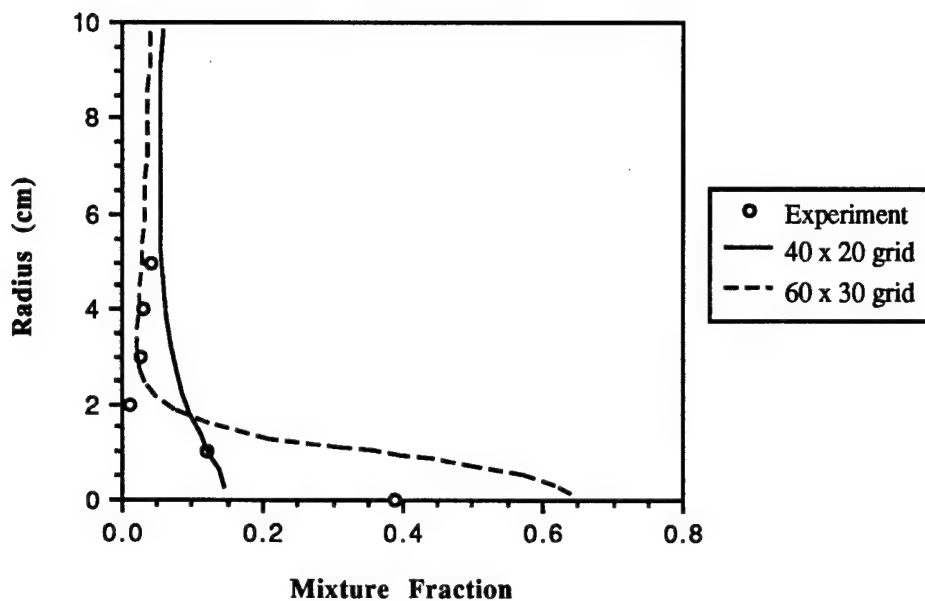
Figure 37: Comparison of experimental and calculated mixture fraction profiles for the turbulent diffusion flame of Lewis and Smoot, 1981. The profiles correspond to an axial location of x/D equal to 0.86.
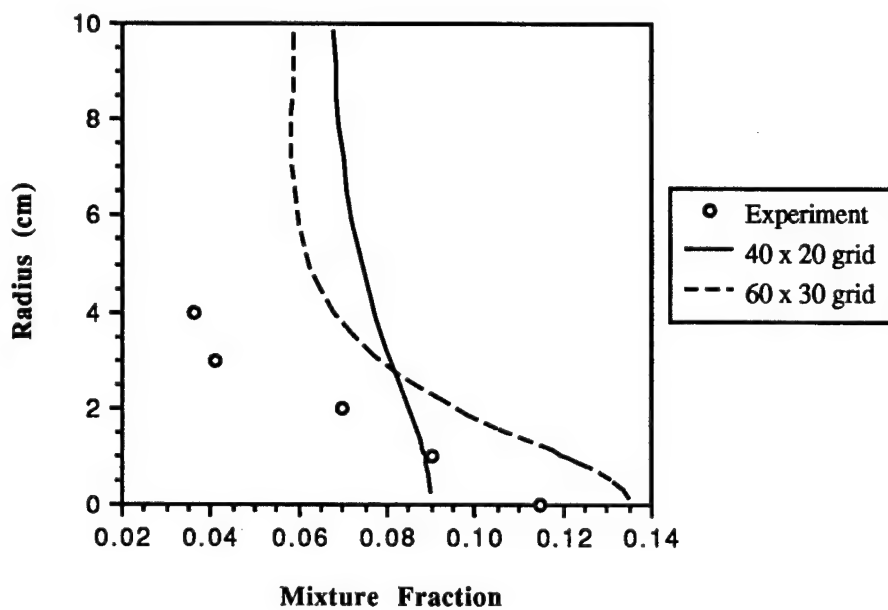
Figure 38: Comparison of experimental and calculated profiles of mixture fraction for the turbulent diffusion flame of Lewis and Smoot, 1981. The profiles correspond to an axial location of x/D equal to 1.96.

106
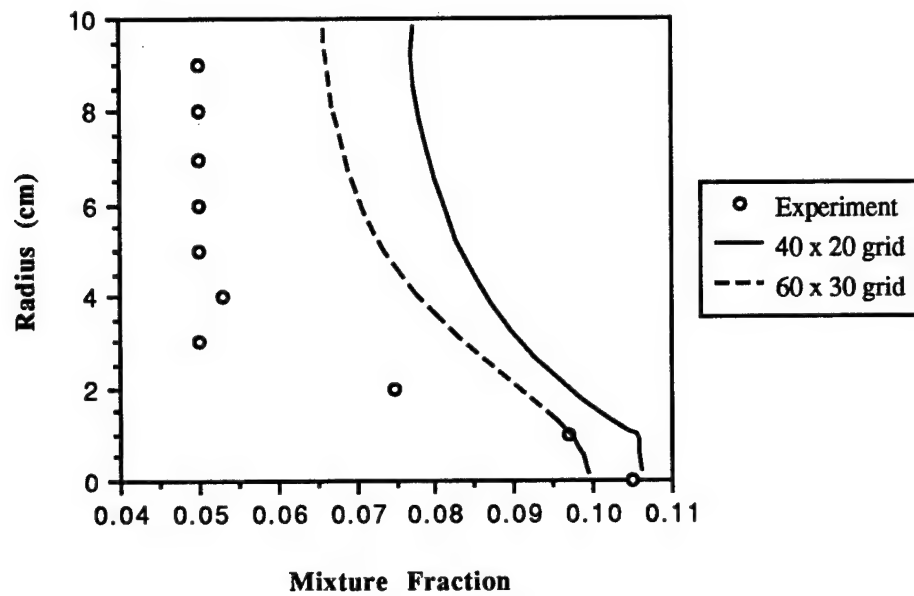
Figure 39: Comparison of experimental and calculated mixture fraction profiles for the turbulent diffusion flame of Lewis and Smoot, 1981. The profiles correspond to an axial location of x/D equal to 2.34.
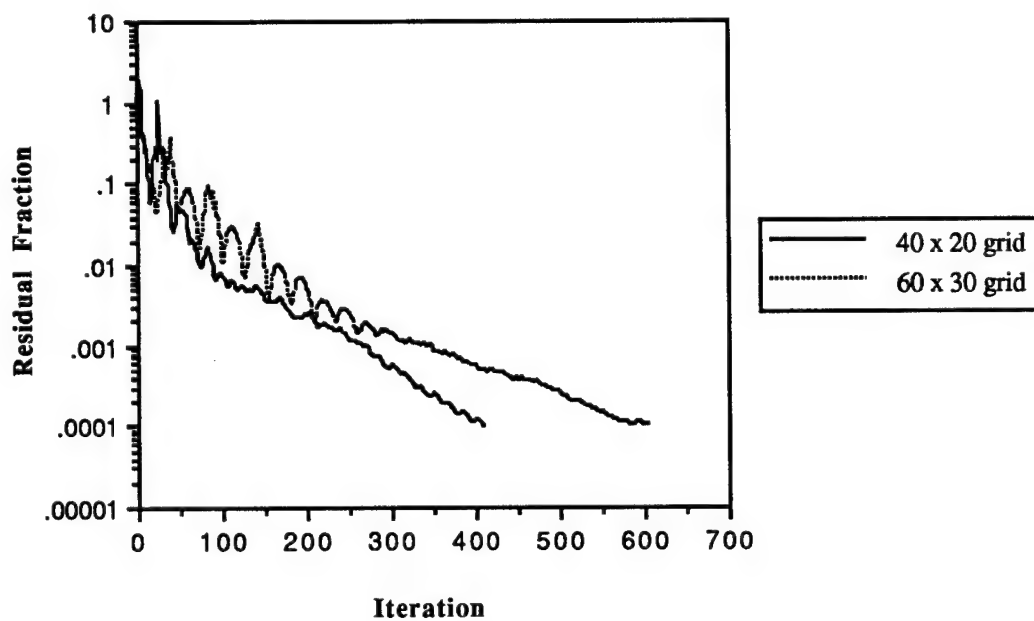
Figure 40: The convergence histories for the two calculations made of the turbulent diffusion flame of Lewis and Smoot, 1981.
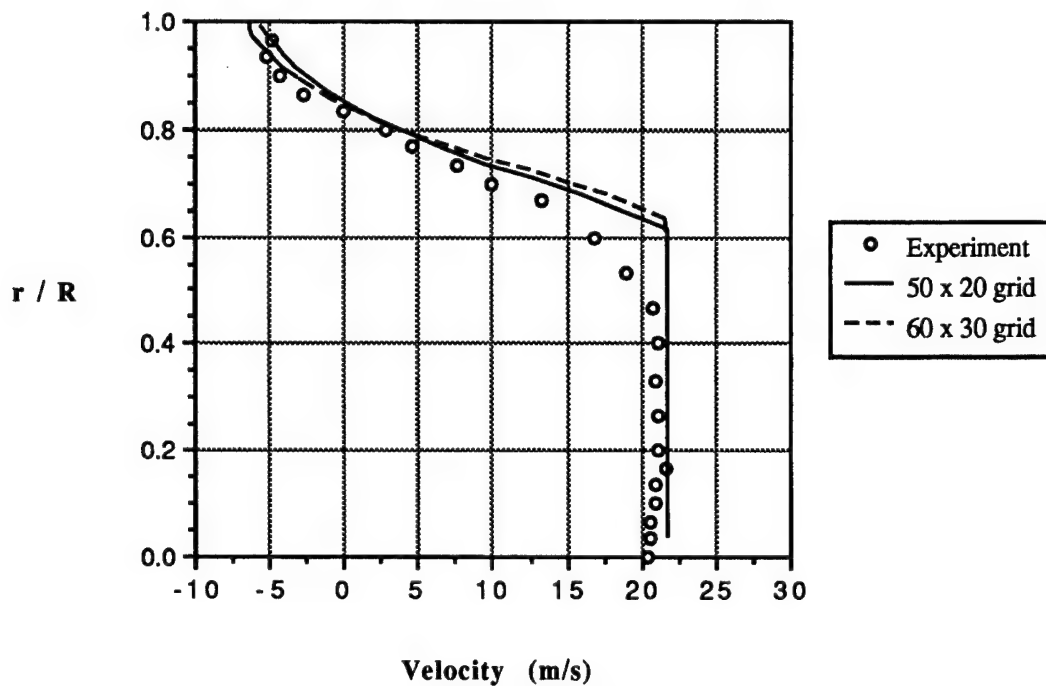
Figure 41: Comparison of experimentally and numerically obtained axial velocity profiles at x/H equal to 2 for a turbulent premixed flame. Experimental results from Ahmed and Nejad, 1990.
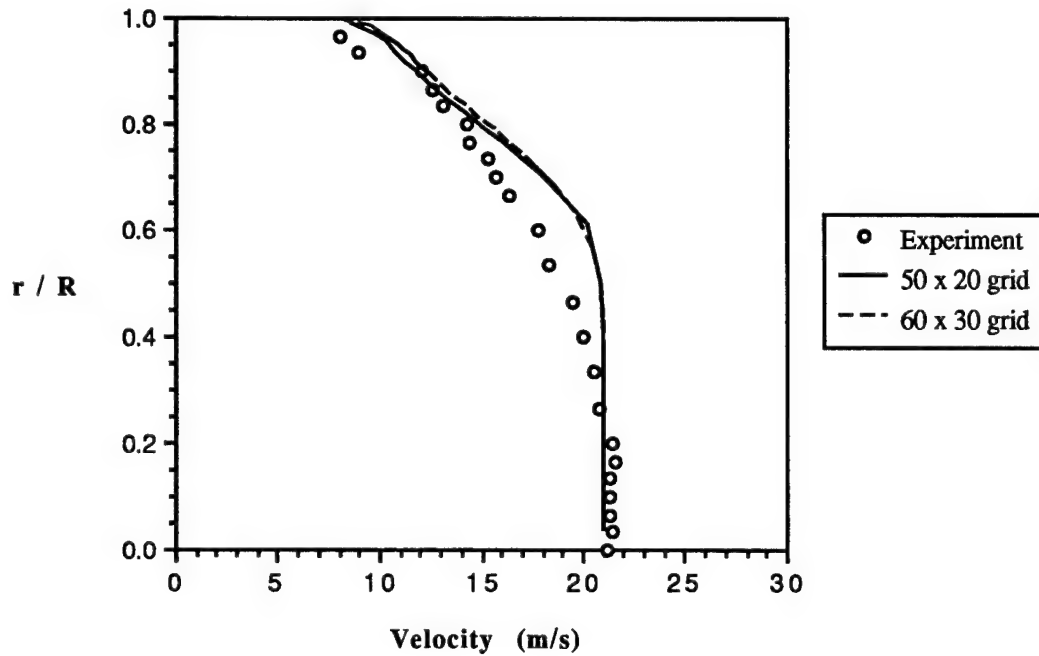
Figure 42: Comparison of experimentally and numerically obtained axial velocity profiles at x/H equal to 8 for a turbulent premixed flame. Experimental results from Ahmed and Nejad, 1990.

108
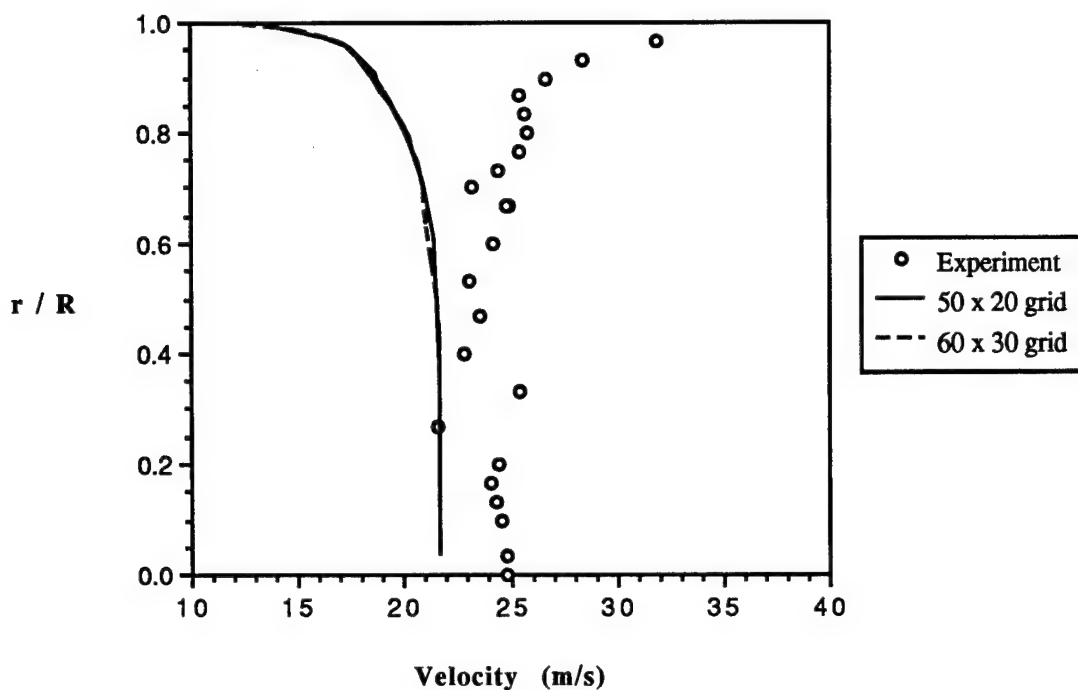
Figure 43: Comparison of experimentally and numerically obtained axial velocity profiles at x/H equal to 12 for a turbulent premixed flame. Experimental results from Ahmed and Nejad, 1990.
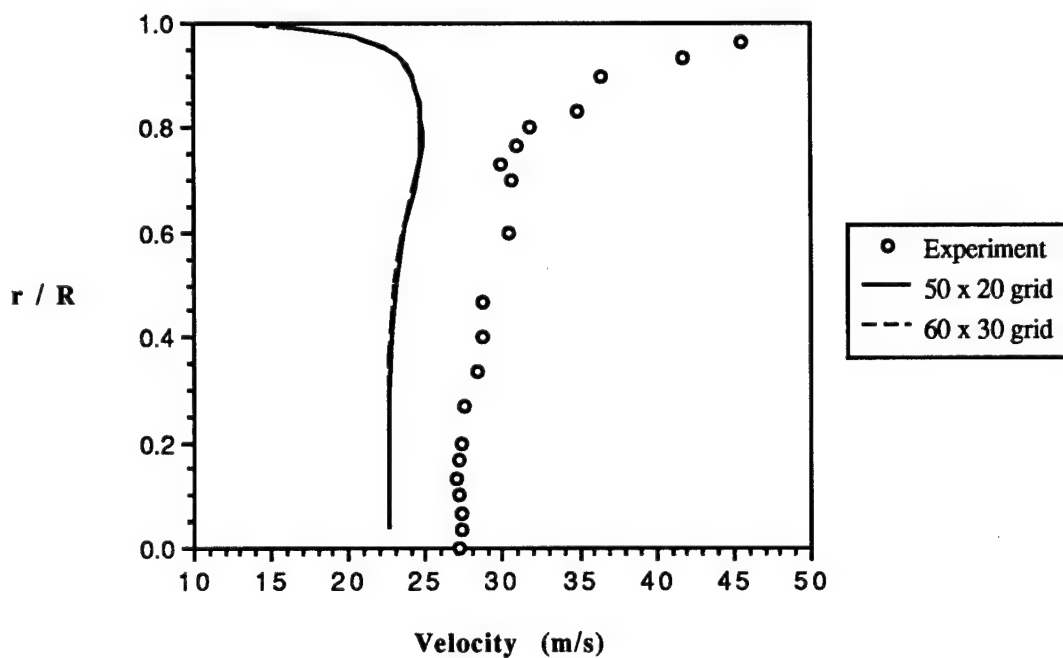
Figure 44: Comparison of experimentally and numerically obtained axial velocity profiles at x/H equal to 18 for a turbulent premixed flame. Experimental results from Ahmed and Nejad, 1990.
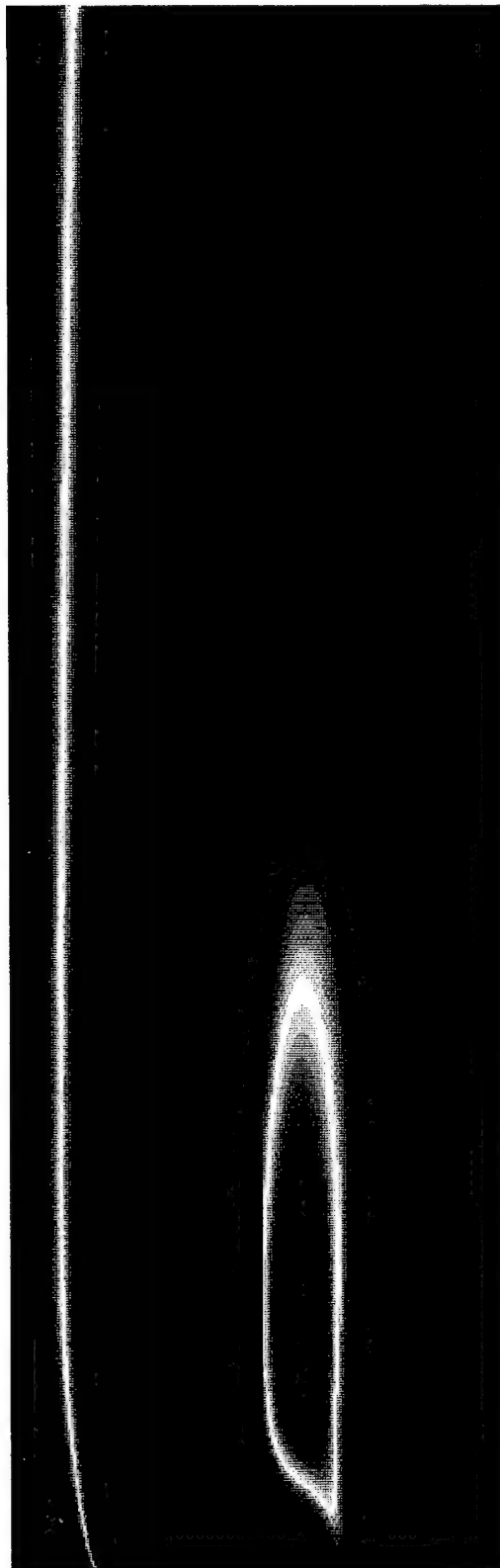
Figure 45: Results of the simulation of the turbulent premixed flame of Ahmed and Nejad, 1990. (a) Above is the temperature distribution in the combustor (Blue = 300K, Yellow = 1300K, Red = 2000K). (b) Below is the distribution of turbulent kinetic energy in the combustor (Blue = 1m^2/s^2, Green= 15 m^2/s^2, and Red = 32 m^2/s^2).
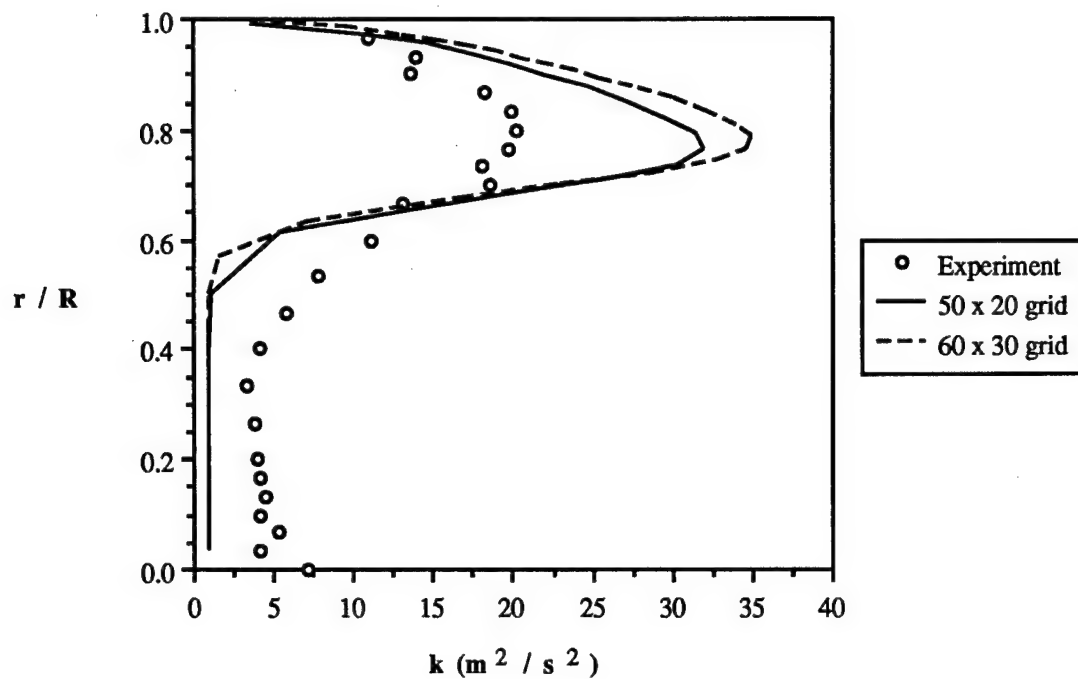
Figure 46: Comparison of experimentally and numerically obtained turbulent kinetic energy profiles at x/H equal to 2. Experimental results from Ahmed and Nejad, 1990.
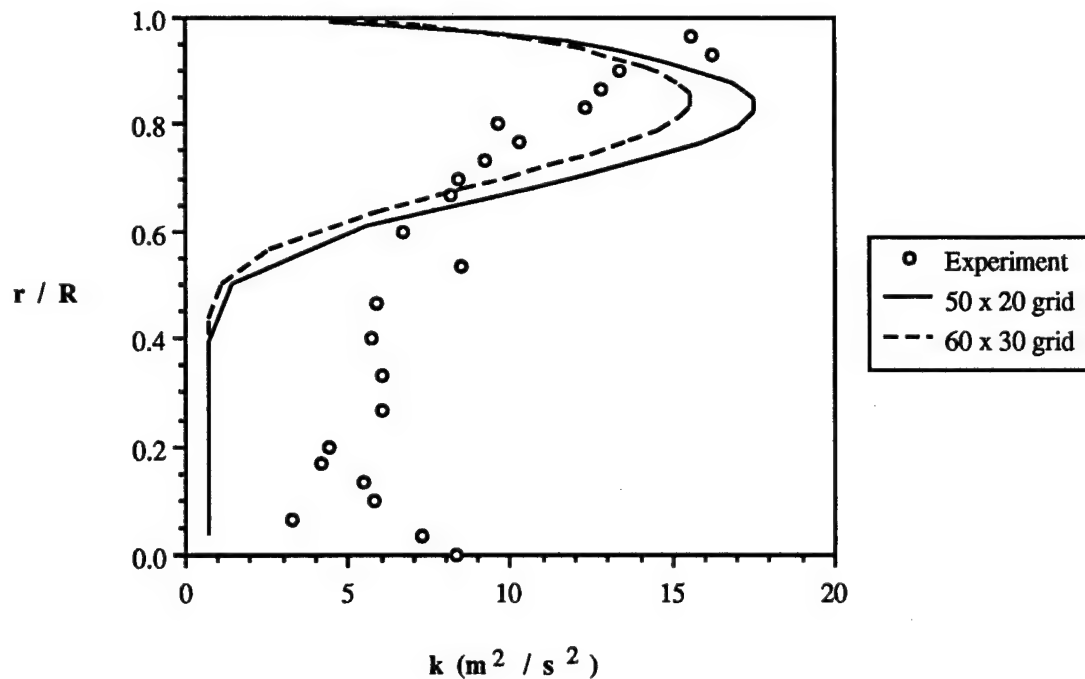
Figure 47: Comparison of experimentally and numerically obtained turbulent kinetic energy profiles at x/H equal to 8. Experimental results from Ahmed and Nejad, 1990.

111
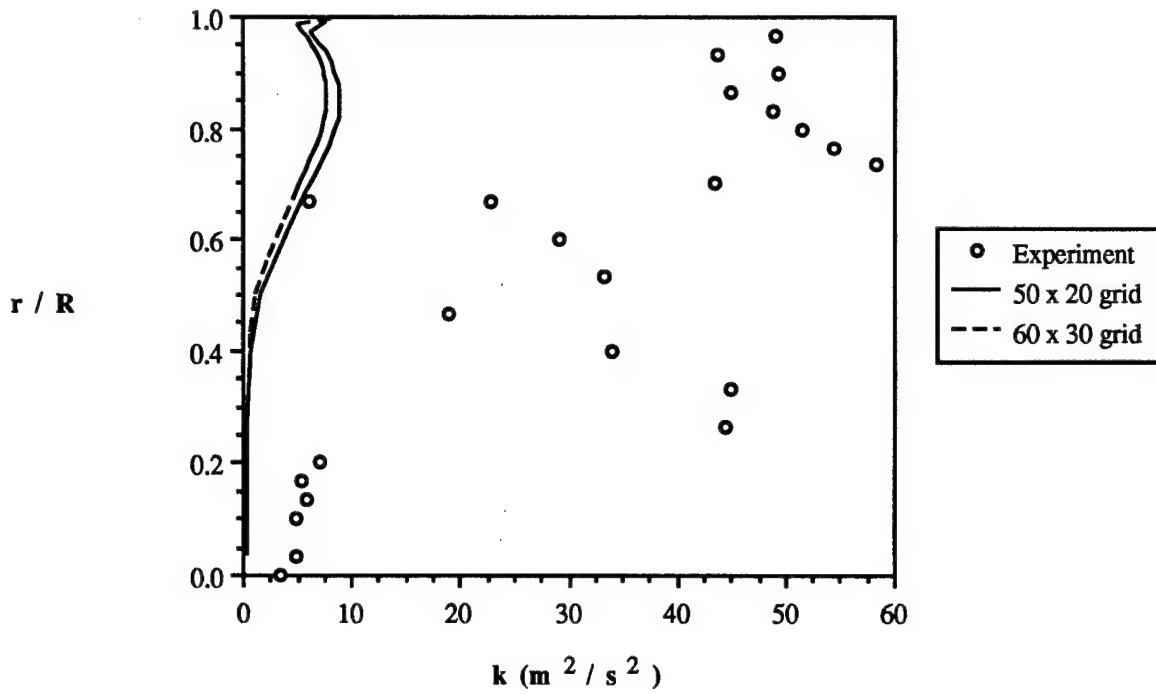
Figure 48: Comparison of experimentally and numerically obtained turbulent kinetic energy profiles at x/H equal to 12. Experimental results from Ahmed and Nejad, 1990.
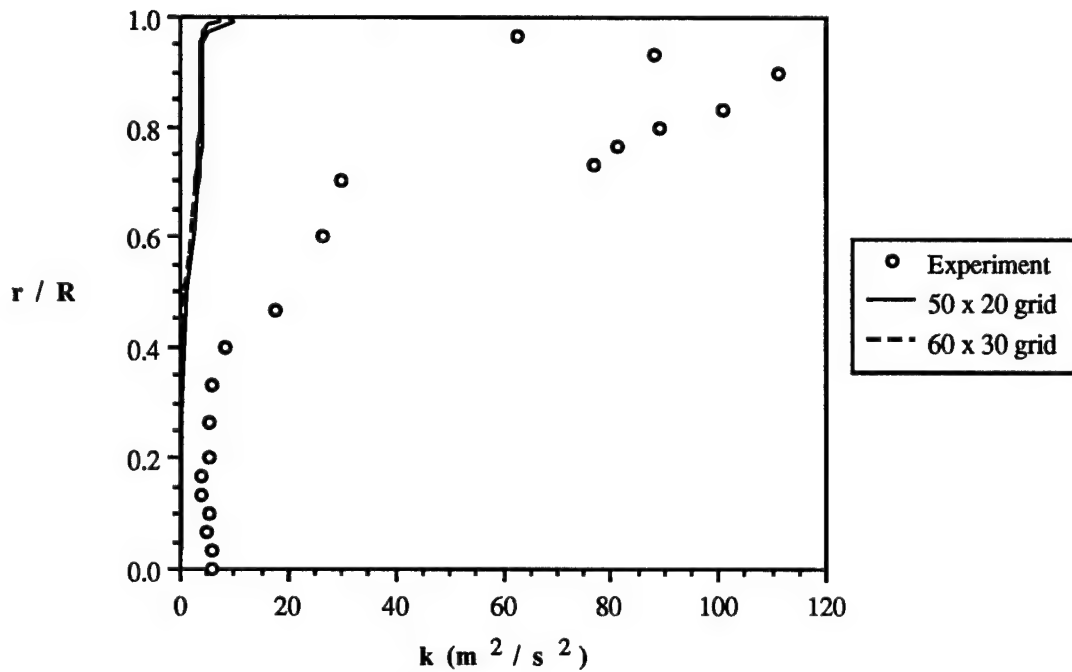
Figure 49: Comparison of experimentally and numerically obtained turbulent kinetic energy profiles at x/H equal to 18. Experimental results from Ahmed and Nejad, 1990.
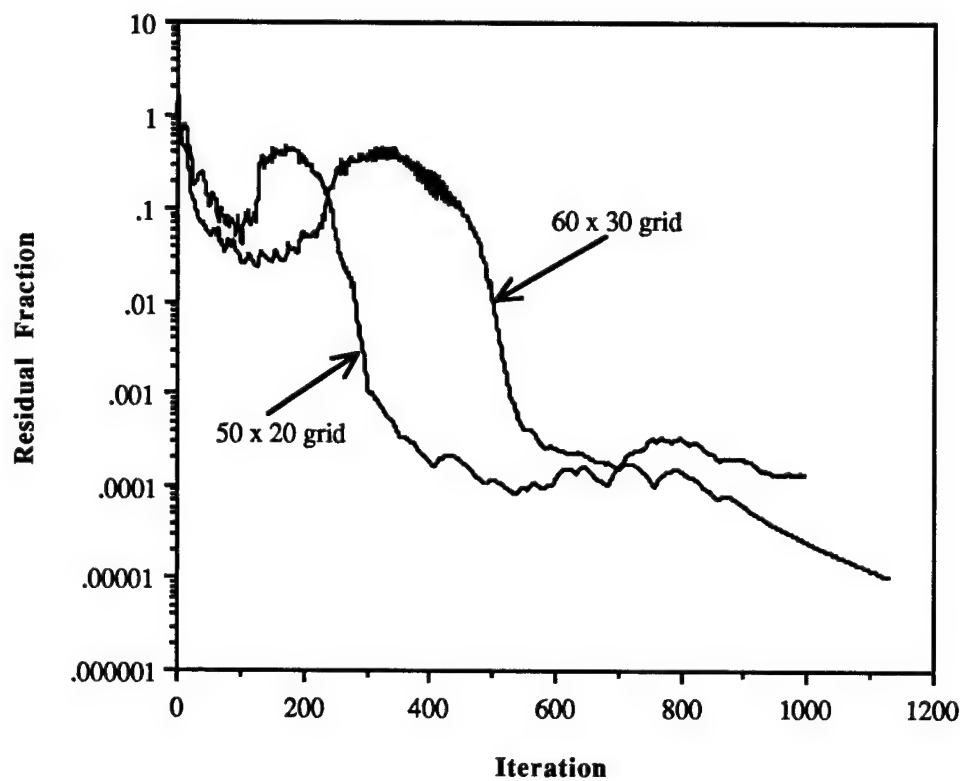
Figure 50: Convergence histories for the calculations made of the turbulent premixed flame of Ahmed and Nejad, 1990.

113
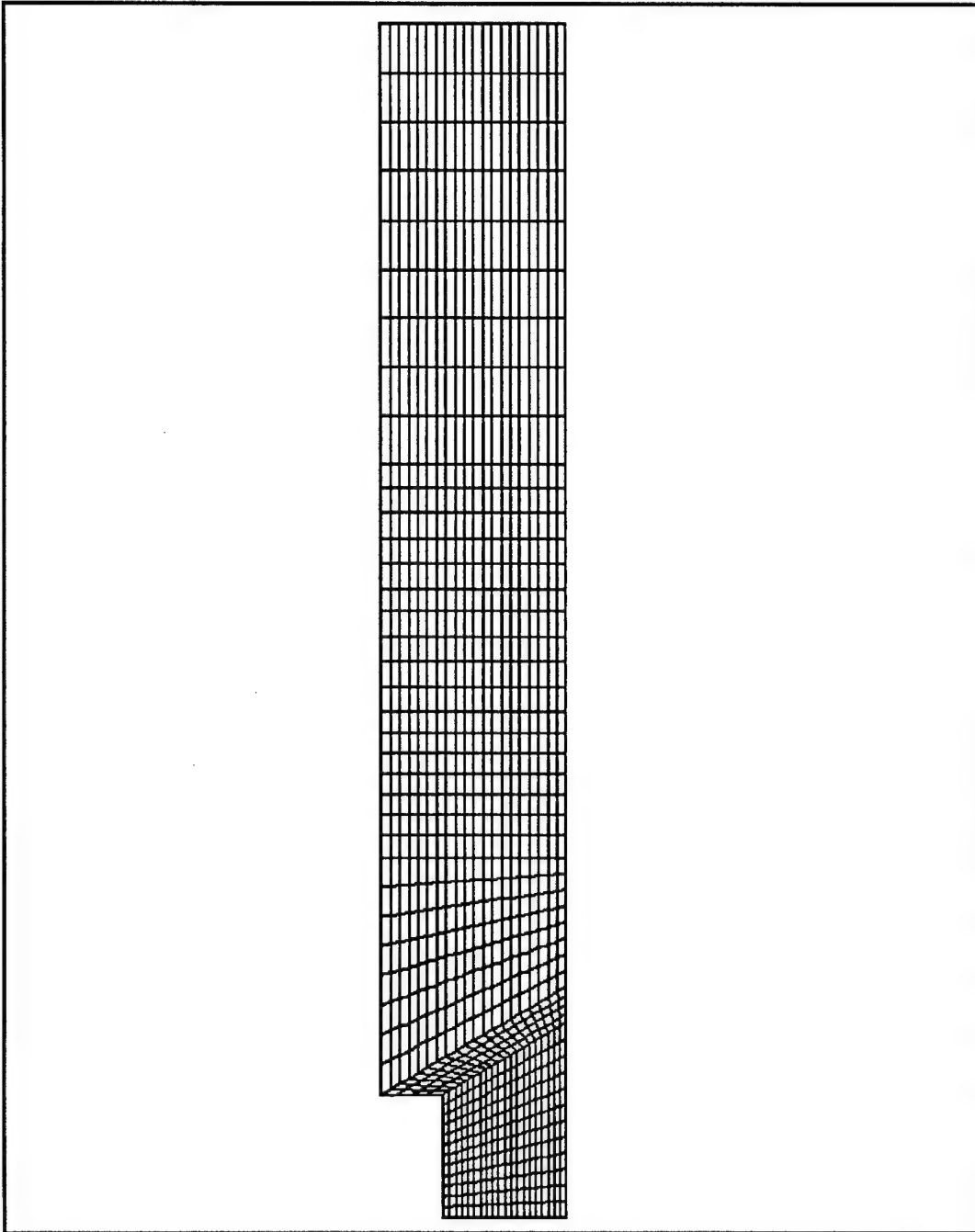
Figure 51: Grid distribution used in calculating turbulent flow in an axisymmetric sudden expansion with and without swirl.
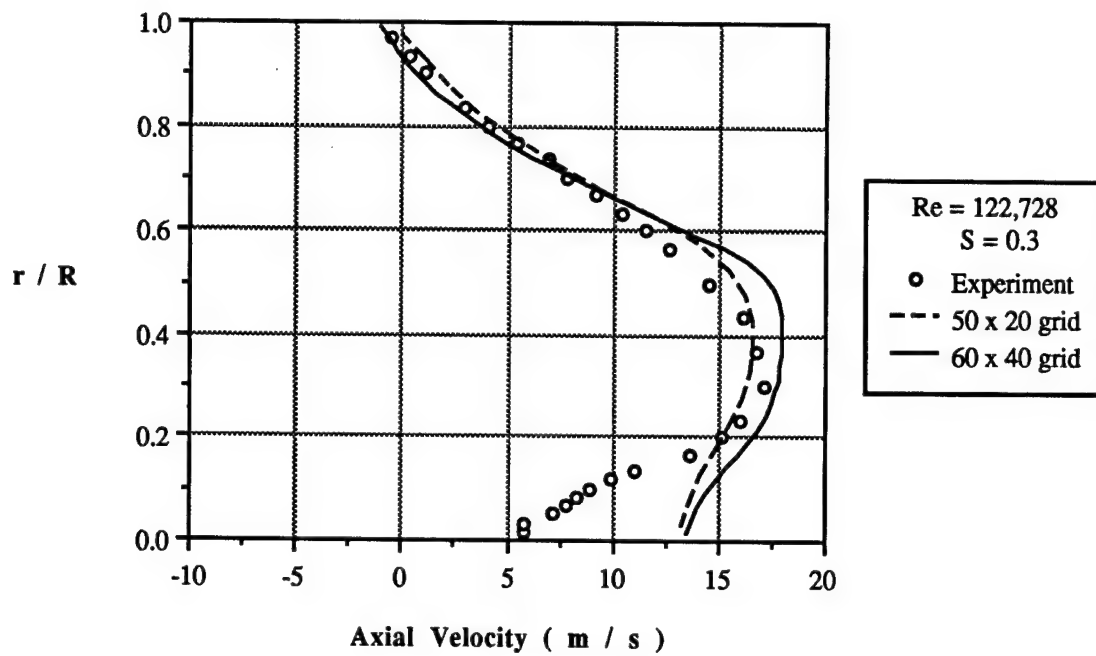
Figure 52: Comparison of the calculated and experimental axial velocity
profiles for a turbulent swirling flow. The results are presented
for x/H equal to 4. Experimental results from Nejad, et. al., 1989.
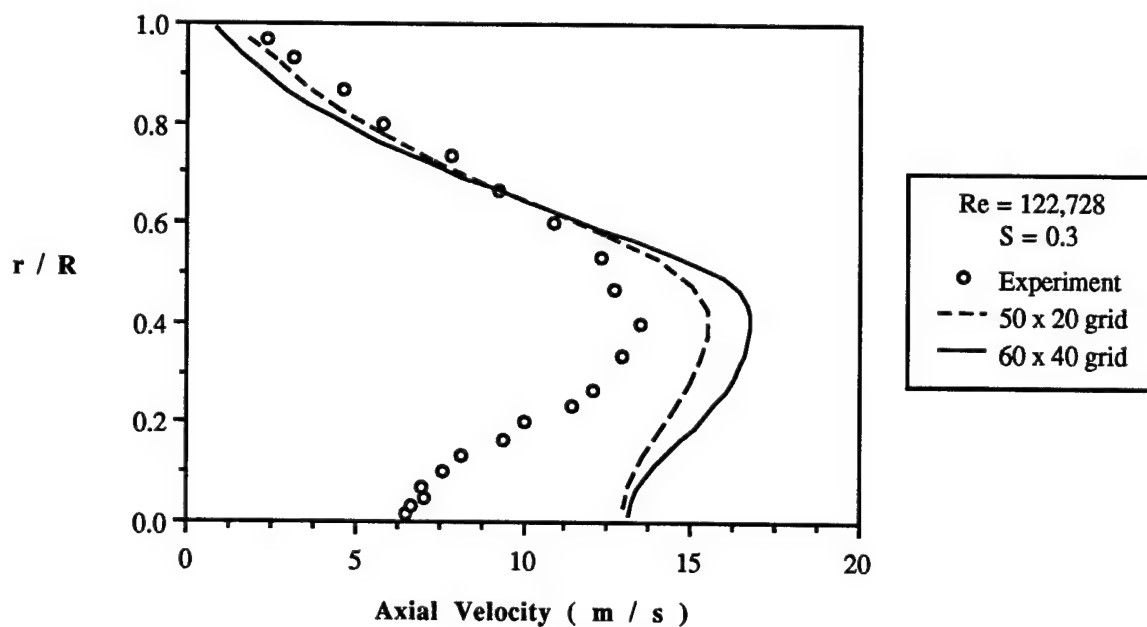
Figure 53: Comparison of experimentally and numerically obtained axial
velocity profiles for a turbulent swirling flow. The profiles correspond
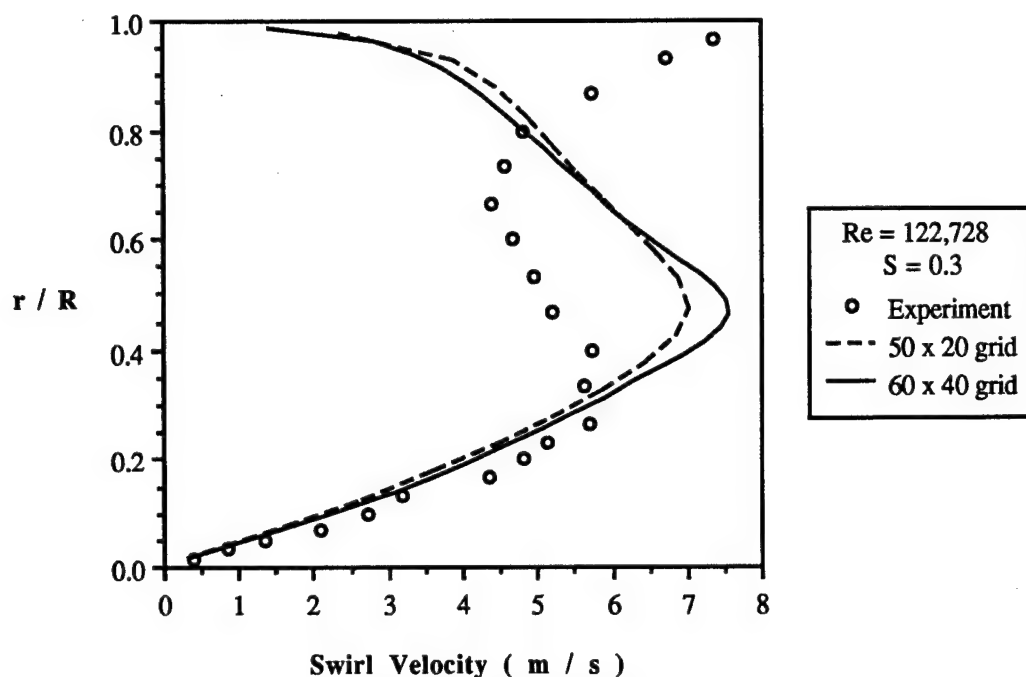to x/H equal to 6. Experimental results from Nejad, et. al., 1989.
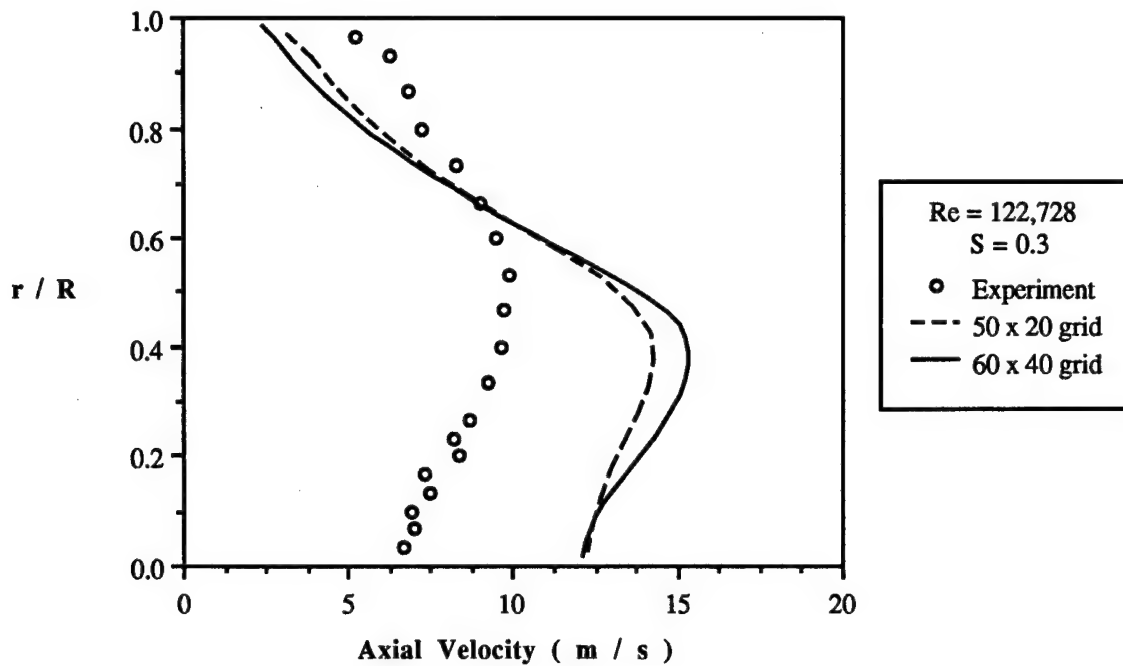
Figure 54: Comparison of experimentally and numerically obtained axial velocity profiles for a turbulent swirling flow. The profiles correspond to an axial location of x/H equal to 8. Experimental results from Nejad, et. al., 1989.
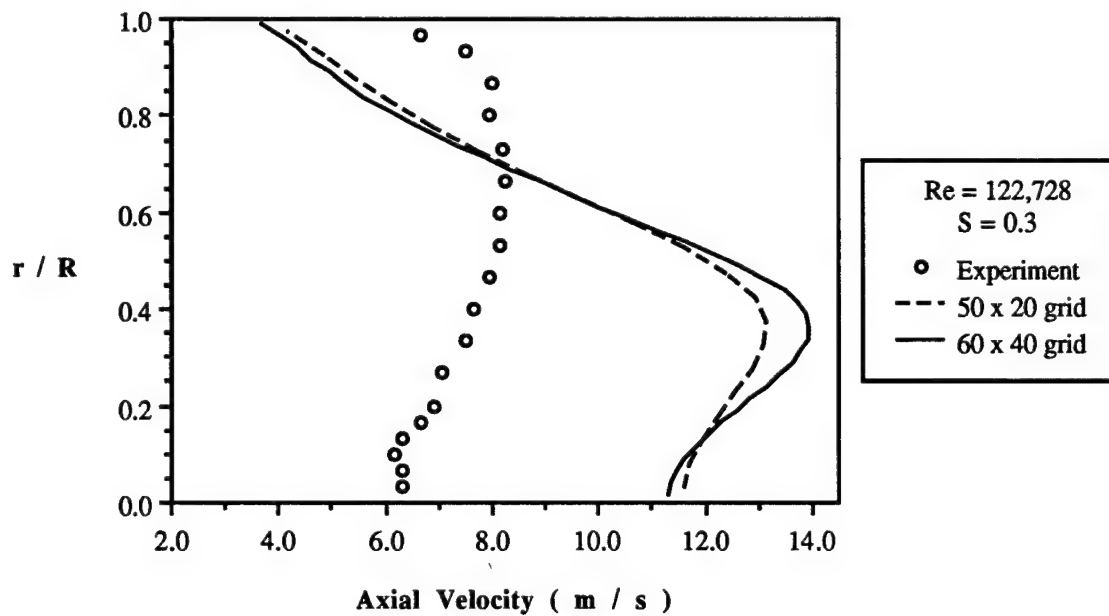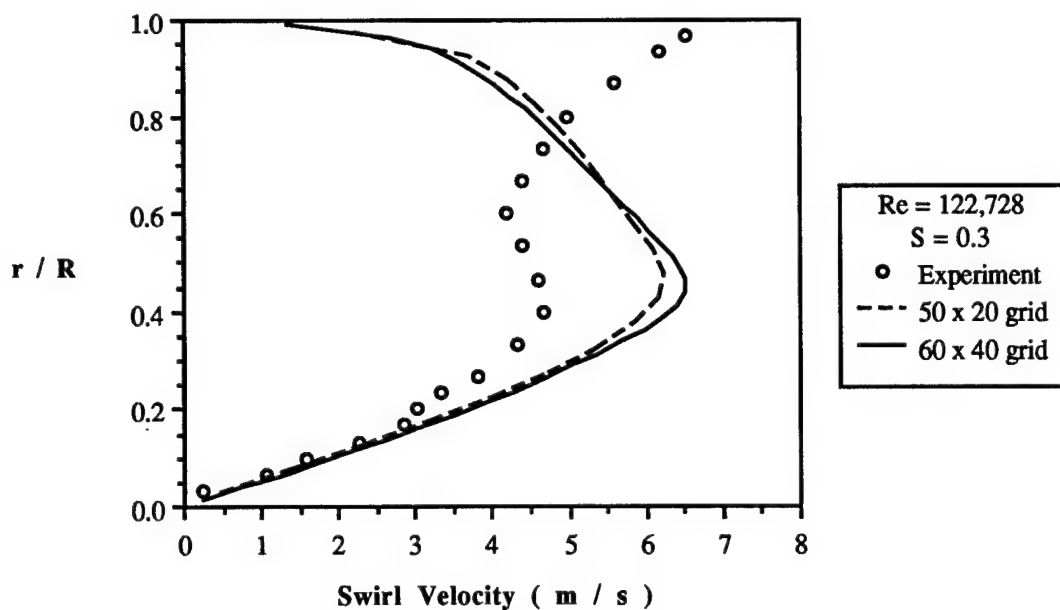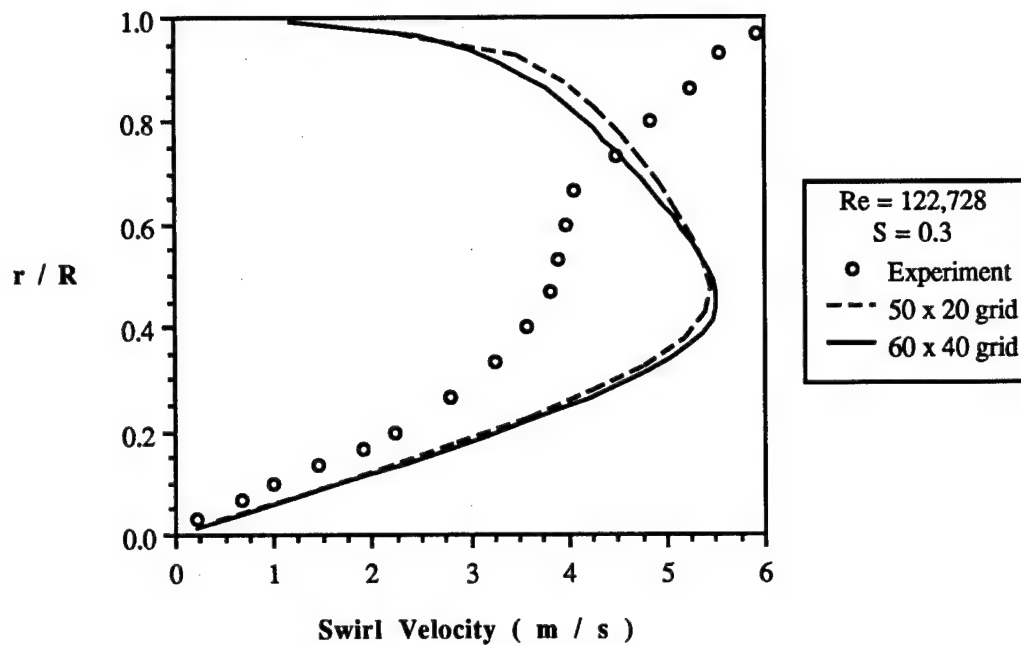

Figure 55: Comparison of experimentally and numerically obtained axial velocity profiles for a turbulent swirling flow. The profiles correspond to an axial location of x/H equal to 10. Experimental results from Nejad, et. al., 1989.

116
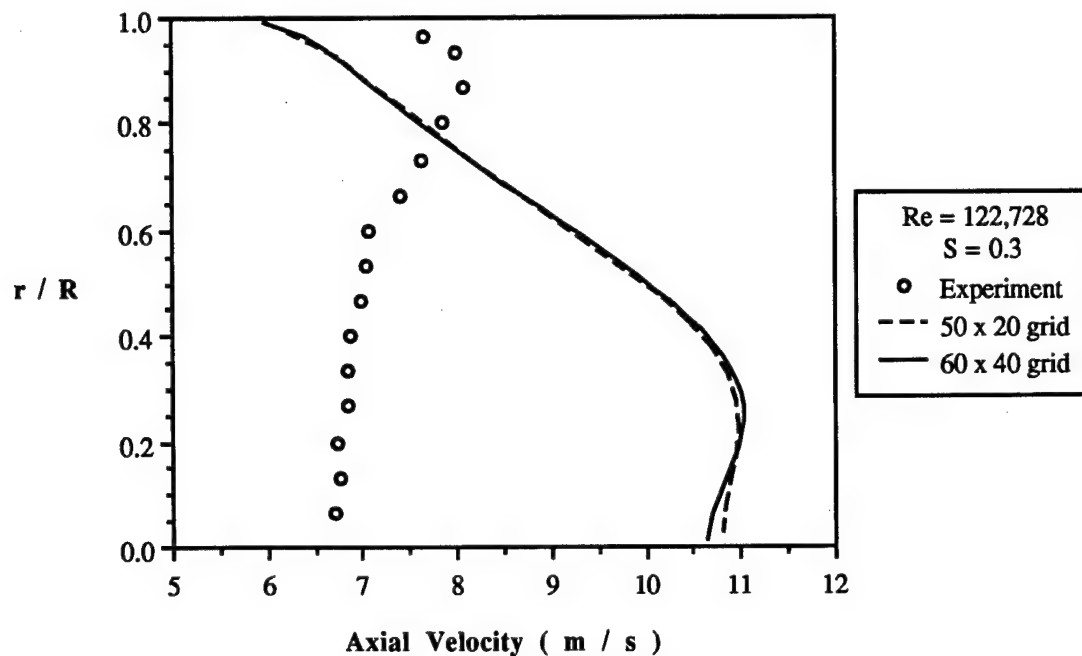
Figure 56: Comparison of experimentally and numerically obtained axial velocity profiles for a turbulent swirling flow. The profiles correspond to an axial location of x/H equal to 18. Experimental results from Nejad, et. al., 1989.
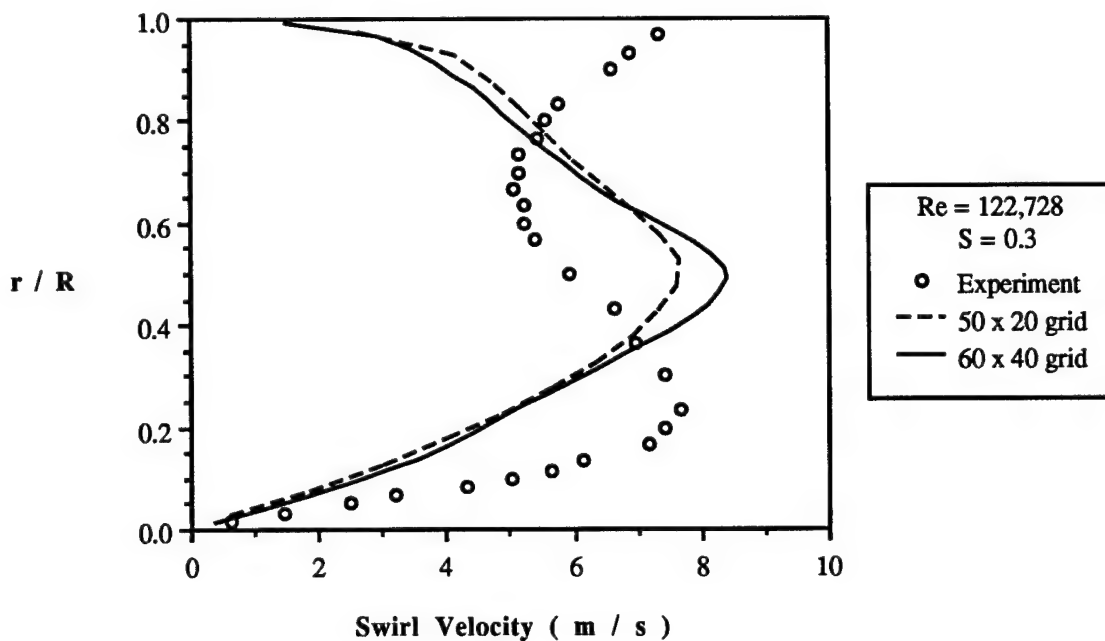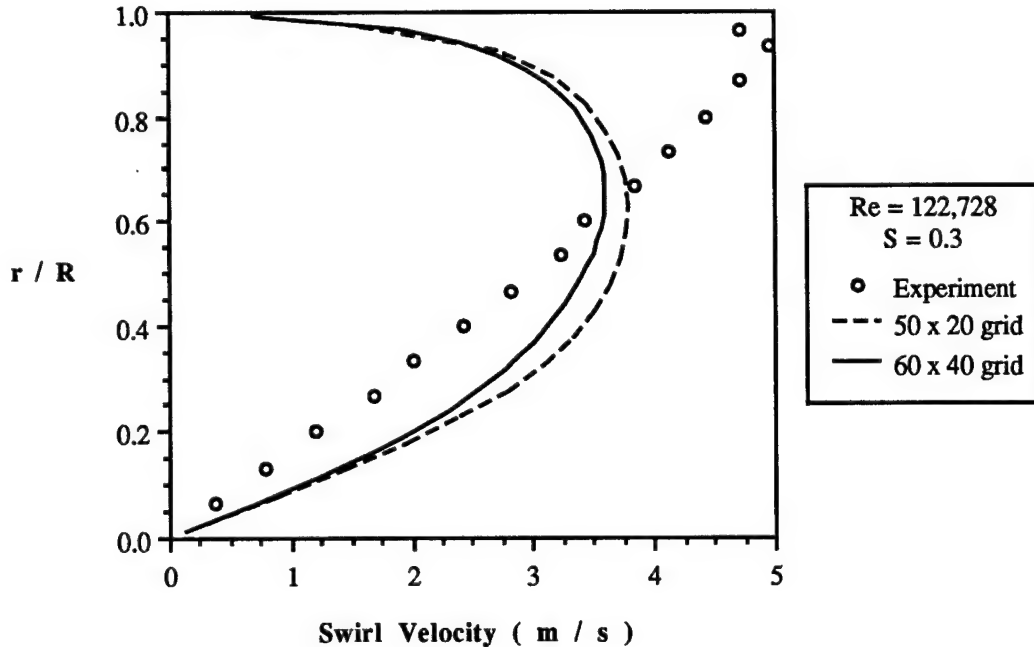

Figure 57: Comparison of experimentally and numerically obtained swirl velocity profiles for a turbulent swirling flow. The profiles correspond to an axial location of x/H equal to 4. Experimental results from Nejad, et. al., 1989.

Figure 58: Comparison of experimentally and numerically obtained profiles of swirl velocity for a turbulent swirling flow. The profiles correspond to an axial location of x/H equal to 6. Experimental results from Nejad, et. al., 1989.
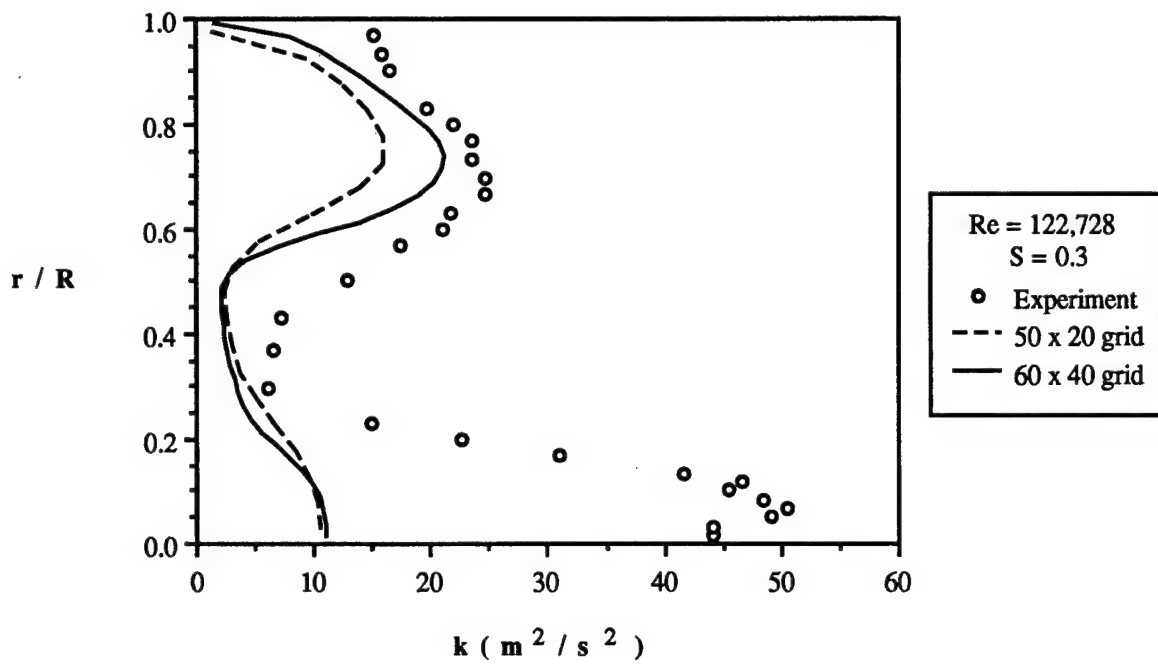

Figure 59: Comparison of experimentally and numerically obtained swirl velocity profiles in a turbulent swirling flow. The profiles correspond to a location of x/H equal to 8. Experimental results from Nejad, et. al., 1989.

Figure 60: Comparison of experimentally and numerically obtained swirl velocity profiles for a turbulent swirling flow. The profiles correspond to an axial location of x/H equal to 10. Experimental results from Nejad, et. al., 1989.

Figure 61: Comparison of experimentally and numerically obtained swirl velocity profiles for a turbulent swirling flow. The profiles correspond to an axial location of x/H equal to 18. Experimental results from Nejad, et. al., 1989.
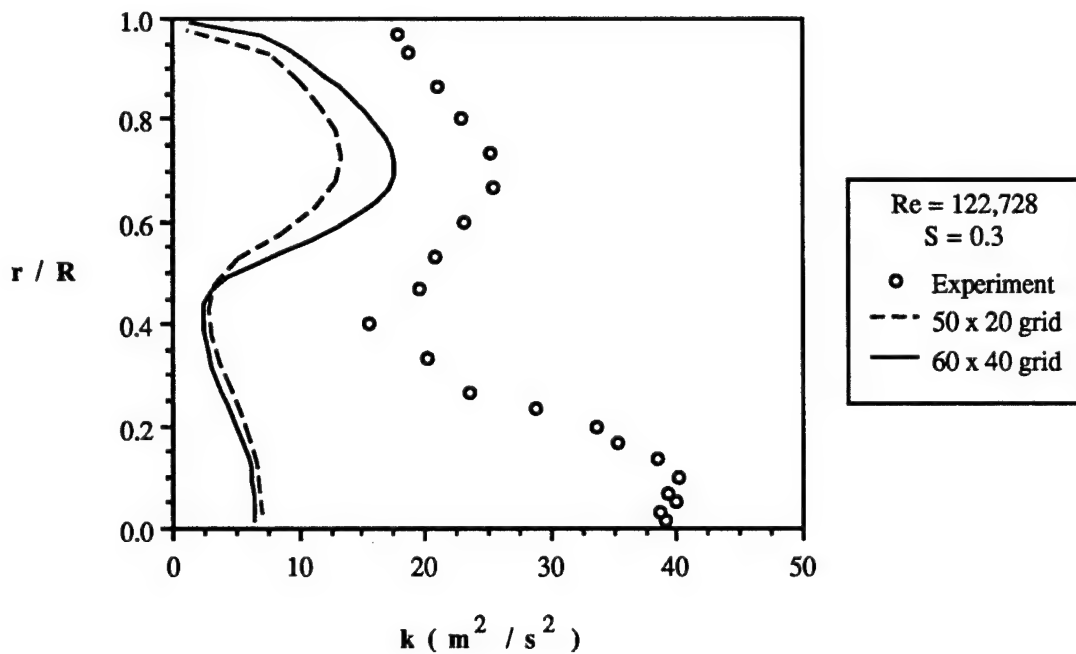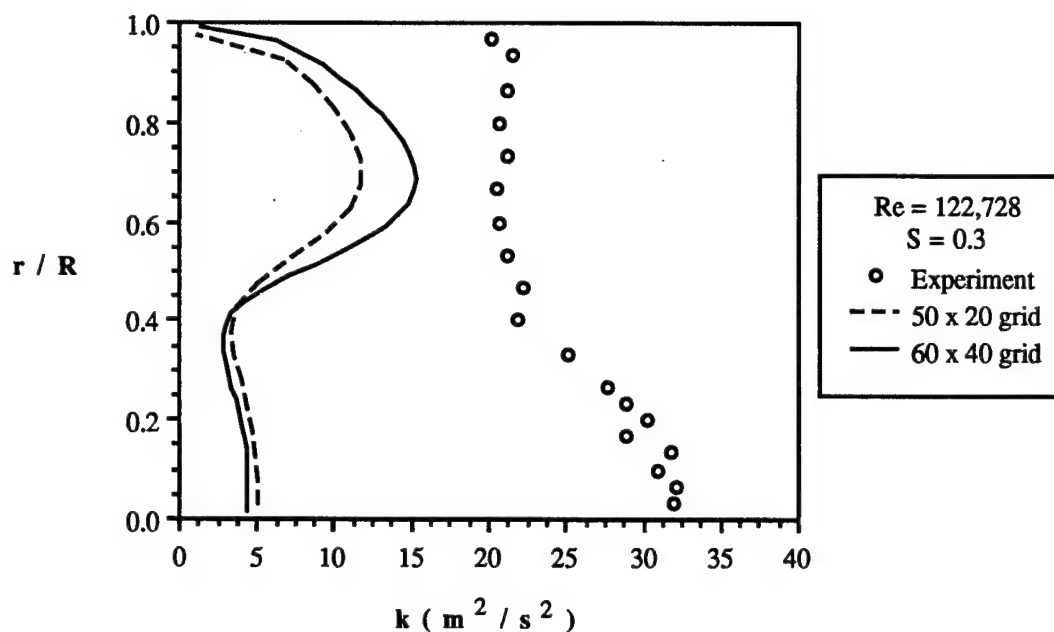
119

Figure 62: Comparison of experimentally and numerically obtained turbulent kinetic energy profiles for a turbulent swirling flow. The profiles correspond to x/H equal to 4. Experimental results from Nejad, et. al., 1989.
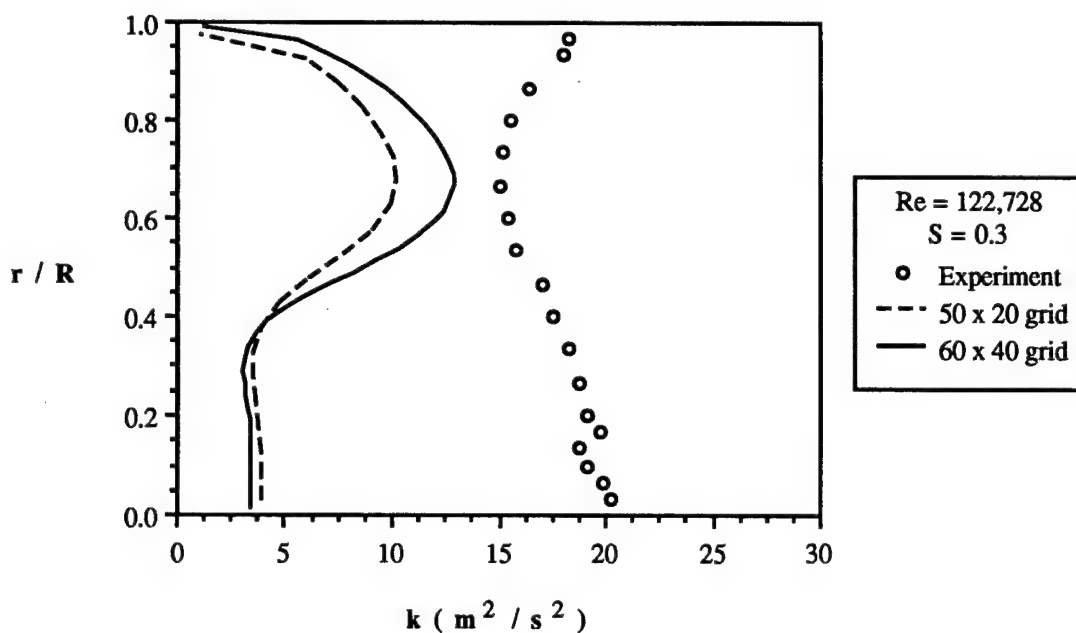

Figure 63: Comparison of experimentally and numerically obtained turbulent kinetic energy profiles for a turbulent swirling flow. The profiles correspond to x/H equal to 6. Experimental results from Nejad, et. al., 1989.

Figure 64: Comparison of experimentally and numerically obtained
turbulent kinetic energy profiles for a turbulent swirling flow. The
profiles correspond to an axial location of x/H equal to 8. Experimental
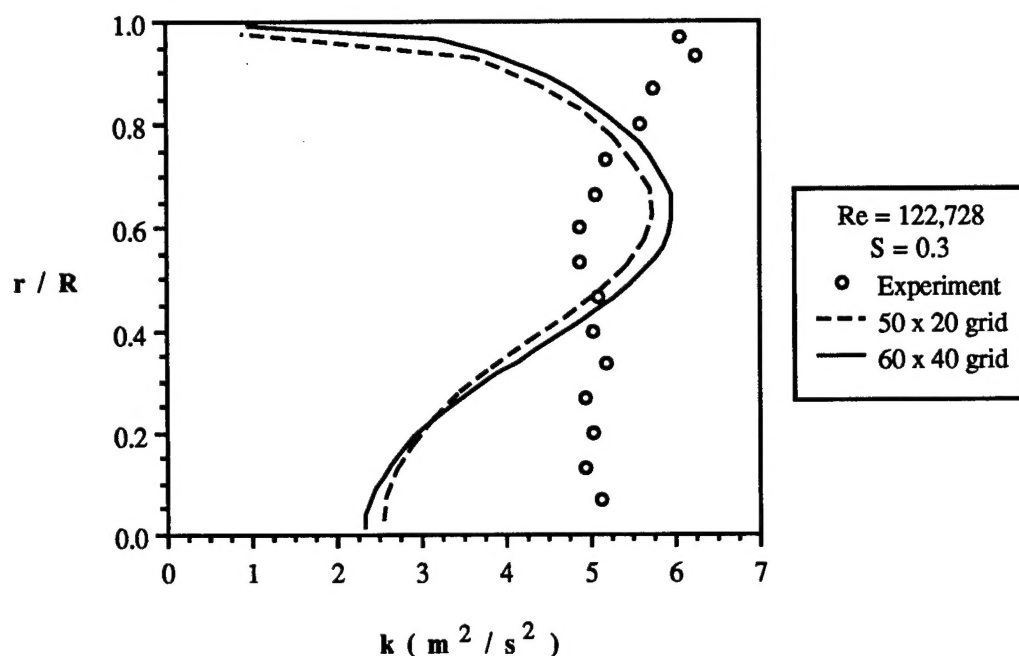results from Nejad, et. al., 1989.

Figure 65: Comparison of experimentally and numerically obtained
turbulent kinetic energy profiles for a turbulent swirling flow.
The profiles correspond to an axial location of x/H equal to 10.
Experimental results from Nejad, et. al., 1989.

121

Figure 66: Comparison of experimentally and numerically obtained turbulent kinetic energy profiles for a turbulent swirling flow. The profiles correspond to an axial location of x/H equal to 18. Experimental results from Nejad, et. al., 1989.
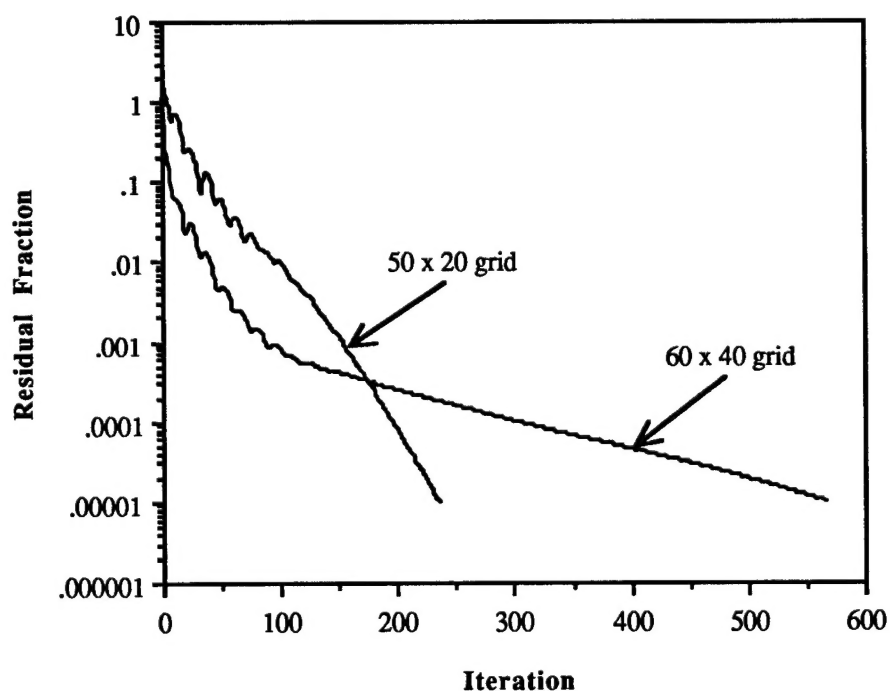

Figure 67: Convergence histories for the two calculations made of a turbulent swirling flow in an axisymmetric sudden expansion.

APPENDIX   A

The equations which are taken to govern laminar flow in axisymmetric geometries (r,z) are given:

$$\frac{\partial}{\partial z}(\rho u) + \frac{1}{r}\frac{\partial}{\partial r}(\rho rv) = 0 \tag{A.1}$$

$$\rho u \frac{\partial u}{\partial z} + \rho v \frac{\partial u}{\partial r} = -\frac{\partial P}{\partial z} + \frac{1}{r}\frac{\partial (r\tau_{rz})}{\partial r} + \frac{\partial \tau_{zz}}{\partial z} \tag{A.2}$$

$$\rho u \frac{\partial v}{\partial z} + \rho v \frac{\partial v}{\partial r} - \frac{\rho w^2}{r} = -\frac{\partial P}{\partial r} + \frac{1}{r}\frac{\partial (r\tau_{rr})}{\partial r} + \frac{\partial \tau_{rz}}{\partial z} - \frac{\tau_{\theta\theta}}{r} \tag{A.3}$$

$$\tau_{rr} = \mu \left[2 \frac{\partial v}{\partial r} - \frac{2}{3} \left(\frac{1}{r}\frac{(rv)}{\partial r} + \frac{\partial u}{\partial z} \right) \right] \tag{A.4}$$

$$\tau_{zz} = \mu \left[\frac{4}{3}\frac{\partial u}{\partial z} - \frac{2}{3}\frac{1}{r}\frac{\partial (rv)}{\partial r} \right] \tag{A.5}$$

$$\tau_{\theta\theta} = \mu \left[\frac{2v}{r} - \frac{2}{3} \left(\frac{1}{r}\frac{\partial (rv)}{\partial r} + \frac{\partial u}{\partial z} \right) \right] \tag{A.6}$$

$$\tau_{rz} = \mu \left[\frac{\partial u}{\partial r} + \frac{\partial v}{\partial z} \right] \tag{A.7}$$

$$\frac{\partial}{\partial z}(\rho u h_o) + \frac{1}{r}\frac{\partial}{\partial r}(\rho rv h_o) = \frac{\partial}{\partial z}\left[\frac{\mu}{Pr}\frac{\partial h_o}{\partial z} \right] + \frac{1}{r}\frac{\partial}{\partial r}\left[r \frac{\mu}{Pr}\frac{\partial h_o}{\partial r} \right] - \sum_{i=1}^{N} \dot{\omega}_i h_i^o \tag{A.8}$$

$$\frac{\partial}{\partial z}(\rho u Y_i) + \frac{1}{r}\frac{\partial}{\partial r}(\rho rv Y_i) = \frac{\partial}{\partial z}\left[\frac{\mu}{Sc}\frac{\partial Y_i}{\partial z} \right] + \frac{1}{r}\frac{\partial}{\partial r}\left[r \frac{\mu}{Sc}\frac{\partial Y_i}{\partial r} \right] + \dot{\omega}_i \tag{A.9}$$

123

APPENDIX B

The equations which are taken to govern turbulent flow in axisymmetric geometries (r,z) when an eddy viscosity model is used to close the system of equations are given:

$$\frac{\partial}{\partial z}(\bar{\rho}\tilde{u}) + \frac{1}{r}\frac{\partial}{\partial r}(\bar{\rho}r\tilde{v}) = 0 \tag{B.1}$$

$$\frac{\partial}{\partial z}(\bar{\rho}\tilde{u}\tilde{u}) + \frac{1}{r}\frac{\partial}{\partial r}(\bar{\rho}r\tilde{v}\tilde{u}) = -\frac{\partial \bar{P}}{\partial z} + \frac{\partial}{\partial z}\left[\Gamma_{eff}\frac{\partial \tilde{u}}{\partial z}\right] + \frac{1}{r}\frac{\partial}{\partial r}\left[r\Gamma_{eff}\frac{\partial \tilde{u}}{\partial r}\right] \tag{B.2}$$

$$\frac{\partial}{\partial z}(\bar{\rho}\tilde{u}\tilde{v}) + \frac{1}{r}\frac{\partial}{\partial r}(\bar{\rho}r\tilde{v}\tilde{v}) = -\frac{\partial \bar{P}}{\partial r} + \frac{\partial}{\partial z}\left[\Gamma_{eff}\frac{\partial \tilde{v}}{\partial z}\right] + \frac{1}{r}\frac{\partial}{\partial r}\left[r\Gamma_{eff}\frac{\partial \tilde{v}}{\partial r}\right] \tag{B.3}$$

$$- 2\Gamma_{eff}\frac{\tilde{v}}{r^2} + \frac{\bar{\rho}\tilde{w}^2}{r}$$

$$\frac{\partial}{\partial z}(\bar{\rho}\tilde{u}\tilde{h}_o) + \frac{1}{r}\frac{\partial}{\partial r}(\bar{\rho}r\tilde{v}\tilde{h}_o) = \frac{\partial}{\partial z}\left[\frac{\Gamma_{eff}}{Pr_T}\frac{\partial \tilde{h}_o}{\partial z}\right] + \frac{1}{r}\frac{\partial}{\partial r}\left[\frac{r\Gamma_{eff}}{Pr_T}\frac{\partial \tilde{h}_o}{\partial r}\right] - \sum_{i=1}^{N}\overline{\dot{\omega}_i\,h_i^o} \tag{B.4}$$

$$\frac{\partial}{\partial z}(\bar{\rho}\tilde{u}\tilde{Y}_i) + \frac{1}{r}\frac{\partial}{\partial r}(\bar{\rho}r\tilde{v}\tilde{Y}_i) = \frac{\partial}{\partial z}\left[\frac{\Gamma_{eff}}{Sc_T}\frac{\partial \tilde{Y}_i}{\partial z}\right] + \frac{1}{r}\frac{\partial}{\partial r}\left[\frac{r\Gamma_{eff}}{Sc_T}\frac{\partial \tilde{Y}_i}{\partial r}\right] + \overline{\dot{\omega}_i} \tag{B.5}$$

$$\frac{\partial}{\partial z}(\bar{\rho}\tilde{u}k) + \frac{1}{r}\frac{\partial}{\partial r}(\bar{\rho}r\tilde{v}k) = \frac{\partial}{\partial z}\left[\Gamma_{eff}\frac{\partial k}{\partial z}\right] + \frac{1}{r}\frac{\partial}{\partial r}\left[r\Gamma_{eff}\frac{\partial k}{\partial r}\right] + P_k - \bar{\rho}\varepsilon \tag{B.6}$$

$$\frac{\partial}{\partial z}(\bar{\rho}\tilde{u}\varepsilon) + \frac{1}{r}\frac{\partial}{\partial r}(\bar{\rho}r\tilde{v}\varepsilon) = \frac{\partial}{\partial z}\left[\Gamma_{eff}\frac{\partial \varepsilon}{\partial z}\right] + \frac{1}{r}\frac{\partial}{\partial r}\left[r\Gamma_{eff}\frac{\partial \varepsilon}{\partial r}\right] + \frac{\varepsilon}{k}(C_1 P_k - C_2\bar{\rho}\varepsilon) \tag{B.7}$$

$$\frac{\partial}{\partial z}(\bar{\rho}\tilde{u}\tilde{\phi}) + \frac{1}{r}\frac{\partial}{\partial r}(\bar{\rho}r\tilde{v}\tilde{\phi}) = \frac{\partial}{\partial z}\left[\Gamma_{eff}\frac{\partial \tilde{\phi}}{\partial z}\right] + \frac{1}{r}\frac{\partial}{\partial r}\left[r\Gamma_{eff}\frac{\partial \tilde{\phi}}{\partial r}\right] + S^{\phi}(z,r) \tag{B.8}$$

$$P_k = \mu_{eff}\left\{2\left[\left(\frac{\partial \tilde{u}}{\partial z}\right)^2 + \left(\frac{\partial \tilde{v}}{\partial r}\right)^2 + \left(\frac{\tilde{v}}{r}\right)^2\right] + \left[\frac{\partial \tilde{u}}{\partial r} + \frac{\partial \tilde{v}}{\partial z}\right]^2 + \left[r\frac{\partial}{\partial r}\left(\frac{\tilde{w}}{r}\right)\right]^2 + \left[\frac{\partial \tilde{w}}{\partial z}\right]^2\right\} \tag{B.9}$$

APPENDIX C

The general conservation equation in (r,z) coordinates is transformed to general curvilinear coordinates. The transformation results in the following governing equation and transformation metrics:

$$\frac{\partial}{\partial \xi}(\rho U \phi) + \frac{\partial}{\partial \eta}(\rho V \phi) = \frac{\partial}{\partial \xi}\left[\Gamma q_{11} \frac{\partial \phi}{\partial \xi}\right] + \frac{\partial}{\partial \eta}\left[\Gamma q_{22} \frac{\partial \phi}{\partial \eta}\right]$$
$$+ \frac{\partial}{\partial \xi}\left[\Gamma q_{12} \frac{\partial \phi}{\partial \eta}\right] + \frac{\partial}{\partial \eta}\left[\Gamma q_{21} \frac{\partial \phi}{\partial \xi}\right]$$
$$+ r |J| S^\phi (\xi,\eta) \tag{C.1}$$

$$U = r (u r_\eta - v z_\eta) \tag{C.2}$$

$$V = r (v z_\xi - u r_\xi) \tag{C.3}$$

$$q_{11} = \frac{r}{|J|} (r_\eta^2 + z_\eta^2) \tag{C.4}$$

$$q_{22} = \frac{r}{|J|} (r_\xi^2 + z_\xi^2) \tag{C.5}$$

$$q_{21} = q_{12} = - \frac{r}{|J|} (r_\xi r_\eta + z_\xi z_\eta) \tag{C.6}$$

$$|J| = (z_\xi r_\eta - z_\eta r_\xi) \tag{C.7}$$